Theory of High Speed Impact

(Summary Report, 3 November 1960 - 2 November 1961)

Technical Documentary Report No. APGC-TDR-62-20

MARCH 1962

DEPUTY FOR AEROSPACE

AIR PROVING GROUND CENTER
Air Force Systems Command
United States Air Force
Eglin Air Force Base, Florida

Project No. 9860 819485

(Prepared under Contract No. AF 08(635)-1713 by T. D. Riney, Space Sciences Laboratory, General Electric Co., Valley Forge Space Technology Center, King of Prussia, Pa.)

FOREWORD

This report was prepared under Air Force Contract No. AF 08(635)-1713, (U) "Theory of High Speed Impact". The work was administered under the direction of the Deputy for Aerospace, Ballistics Division, APGC, (PGWR) with Mr. A. G. Bilek as Project Engineer.

The contributions of Mr. P. R. Chernoff to the numerical analysis are gratefully acknowledged. The author also wishes to express his appreciation to Mr. M. H. Slud and Dr. F. W. Wendt for many interesting and helpful technical discussions. Thanks are also due to Mr. R. P. Supina for assistance in reducing the numerical results.

Catalog cards may be found at the back of this document.

ABSTRACT

Existing experimental results of hypervelocity impact tests have been gathered from various sources and the composite data are presented and discussed. The extrapolated results to higher velocities are seen to differ with the theoretical prediction from the perfect fluid model proposed by R. L. Bjork. Re-examination of his assumptions and the experimental results indicate the desirability of including the effects of the viscosity and the yield strength of the materials into the mathematical model. A visco-plastic model for hypervelocity impact is then formulated to meet these requirements. This is accomplished by introducing a viscosity factor μ_o and a yield stress τ_o into the perfect fluid equations.

The equations governing the visco-plastic model are then studied and the characteristic features of the theory are deduced. Certain dimensionless parameters are found which determine the relative importance of the inertial, viscous and plastic effects during the various stages of the hypervelocity cratering process.

To exhibit quantitatively the importance of including the viscous and plastic effects, a one-dimensional impact model was studied. In this study the values of μ_o and τ_o are varied since definitive data are available for neither parameter in the hypervelocity range. Two distinct finite difference schemes have been developed for performing the required calculations on an IBM 7090 computer. These are described in detail.

The results of the calculations are related to the qualitative model of crater formations that has evolved from experimental studies in which the actual cratering process has been monitored. It is concluded that the viscous and strength effects strongly affect the cavitation process which is the essential mechanism of crater formation. Finally, experiments are suggested which would provide the necessary data to verify and extend the theory.

PUBLICATION REVIEW

This technical documentary report has been reviewed and is approved.

MORRILL E. MARSTON
Colonel, USAF
Deputy for Aerospace

LIST OF SYMBOLS

P_c	crater depth measured from original target surface
D_c	crater diameter at original target surface
D_s	diameter of sphere with mass equal to projectile
D	strain-rate
D_{ik}	total strain-rate tensor
D^*_{ik}	distortional strain-rate tensor
τ_o	yield value of shear stress
τ_{ik}	components of stress tensor
τ^*_{ik}	components of distortional stress tensor
τ^2	von Mises flow statistic
δ_{ik}	Kronecker delta function
$\mu = \mu(D)$	strain-rate dependent viscosity coefficient
μ_o	proportionality constant (viscosity factor)
μ'	second coefficient of viscosity
$V\ (=1/\rho)$	specific volume of visco-plastic medium
V_c	crater volume below original target surface
V_p	projectile volume
ρ_p	mass density of projectile
ρ_t	mass density of target
ρ_o	mass density of undisturbed visco-plastic medium
ρ	density of visco-plastic medium
v_o	impact velocity of projectile
v	characteristic velocity of flow of visco-plastic medium
v*	value of v at which inertial and strength effects almost equal

LIST OF SYMBOLS (Continued)

K_i	proportionality factors between parameters of dynamically similar flows
B	Bingham number
R	Reynolds number
M	Mach number ($=v/c_o$)
M*	generalized Mach number
N	dimensionless energy number
(r, θ, z)	Eulerian cylindrical coordinates
$(\ )'$	prime denotes dimensionless value of quantity
$\bar{q} = (q_r, 0, q_z)$	velocity of flow of medium in Eulerian formulation
q	value of q_z in one dimensional model
q_i	initial velocity of flow at interface of impacting bodies
p	thermodynamic pressure
p_i	initial pressure at interface of impacting bodies
U	specific internal energy of medium
T	absolute temperature
z	Eulerian coordinate in one dimensional model
x	particle label in Lagrangian coordinates
X	instantaneous position of particle in Lagrangian coordinates
t	time
g	any dependent variable
g_j^n	value of g at time mesh n and space mesh j
Δx	size of space mesh
Δt	size of time mesh
ℓ	constant with dimensions of length

LIST OF SYMBOLS (Continued)

a	constant determining magnitude of artificial viscosity
Q	artificial viscosity term
S	real viscosity term
u	flow velocity of medium relative to shock wave
W	shock wave velocities
d	constants with dimensions of mass density
h_t	Brinnell hardness
ν	Poisson's ratio
E	Young's modulus
c_o	speed of sound in undisturbed medium
c	speed of sound in visco-plastic medium
$\Delta[\ ]$	delta denotes increment of quantity
$[\ ]_j^n$	value of quantity at time station n, space station j
$\tilde{[\ ]}_j^n(k)$	k-th approximation of quantity at time n, position j
K	number of iterations performed
J	position station chosen to be in front of disturbance
$\dot{[\ ]}$	first variation of quantity
$A_K, \ldots, F_k$	coefficients in Fourier representations
β	quantity defined in (B-16)
Λ	quantity defined in (B-16)
ϵ	quantity defined in (B-16)
γ	quantity defined in (B-16)
δ	quantity defined in (B-16)
ζ	quantity defined in (B-16)
G	amplification matrix
λ	eigenvalues of amplification matrix

TABLE OF CONTENTS

TABLE OF CONTENTS (Continued)

LIST OF ILLUSTRATIONS

LIST OF ILLUSTRATIONS (Continued)

LIST OF ILLUSTRATIONS (Continued)

INTRODUCTION

For satellites and for manned space flight, the presence of meteoritic material in space accounts for one of the important environmental hazards. The velocity of the meteoroids is estimated to range from 0.5 to 7.2 cm/microsecond.* A similar problem, potentially, is the damage that may be inflicted on a ballistic missile by high speed particles produced and directed by artificial means. For these reasons, increasing attention has been recently focused on the problems attendant to the collision of a projectile and a target in the hypervelocity regime. The ultimate objective of these studies is to determine the minimum hull thickness required to ensure that the space vehicle is not pierced. More explicitly, the dependence of the minimum thickness on the various parameters is the information sought.

Until quite recently, laboratory techniques were only capable of producing velocities of less than about 0.6 cm/microsecond. A great deal of data are available describing the craters formed at these lower speeds. In the past year a method has been developed for projecting hypervelocity pellets up to 2 cm/microsecond. At present, however, little data are available in this range. As an adjunct to such experiments, empirical formulas and cratering theories have been proposed to extrapolate the experimental results to cover the velocity range of interest. In the following both the data and the theories are reviewed and the conclusions used as a basis for the formulation of a visco-plastic model for hypervelocity impact which takes into account the viscosity and strength of the projectile and target materials as well as their compressibilities.

The visco-plastic model is proposed only for materials that behave in a ductile manner when impacted. The phenomenon is quite different for brittle materials such as rock. The survey of the experimental data is restricted to thick metal targets impacted at normal incidence. The use of a target which is essentially a semi-infinite body rules out geometrical complications such as reflected shock waves at free surfaces, bending, etc. The large majority of past investigations have been similarly restricted.

---

*The gram-centimeter-microsecond system of units is used throughout this report.

REVIEW OF EXISTING DATA AND THEORIES

When velocity limits of power propellant guns were reached experimenters provided the first hypervelocity impact data through the utilization of light gas (hydrogen, helium) projectors. The first light gas projector was developed and constructed at the New Mexico School of Mines by Dr. W. D. Crozier and Dr. William Hume. Most of the hypervelocity data presently available have been obtained by use of light gas guns. The upper limit reported as attained by them is about 0.6 cm/microseconds.

(a) Survey of Data

The data which will be presented have been abstracted from the reports of tests using both these high velocity, single particle impact techniques, References 1 through 14. The particle properties are therefore well defined. Our object is to analyze the data for characteristic features of the impact phenomenon; results are not to be included if the particular projectile and target material combination has been studied in a single series of tests.

Changes in the crater profile as the velocity is increased over the known range are illustrated by Figures 1 through 4. The ratio of the penetration to the diameter of the crater, P_c/D_c, is plotted for various projectile materials impacting massive targets of lead, copper, steel, and aluminum respectively. The low velocity scatter is associated with undeformed projectile penetration. At higher velocities, depending on the strength of the projectile and target, the projectile deforms plastically. As the impact velocity increases still further, these data show that for most projectile materials the crater profile parameter, P_c/D_c, approaches 0.5, the value corresponding to hemispherical craters.

For some material combinations the velocity at which the 0.5 level is attained, if attained at all, is seen to be quite high, especially for cases in which the yield strengths of the projectile and target are high. This is demonstrated by Figure 3, which shows that tungsten carbide and aluminum alloy projectiles impacting steel have not attained P_c/D_c = 0.5 for velocities up to 0.5 cm/microsecond. In the former the ratio is closer to about 0.6, while it is closer to 0.4 in the latter.

In Figures 5 through 8 the penetration parameter, P_c/D_s, has been plotted as a function of the impact velocity for results where projectile and target materials were the same. Here D_s denotes the diameter of a sphere having the same mass as the actual projectile. P_c again denotes the depth of a crater. The impact velocity is expressed in dimensionless terms through division by the velocity of sound in the undisturbed target material, v_o/c_o. When both projectile and target are of low strength the log-log plot of the data is seen to be well fitted by a straight line of slope 2/3, Figures 7 and 8. For materials of greater strength the slope at low velocities differs but appears to tend towards 2/3 at the higher velocities, Figures 5 and 6.

In Figures 9 through 12 the crater volume parameter, V_c/V_p, is plotted against the dimensionless velocity for the projectile and target materials corresponding to Figures 5 through 8 respectively. Here V_c and V_p denote the crater and projectile volumes respectively. A straight line of slop 2 is seen to be in excellent agreement with the plot on log-log paper in all cases, even at the lower velocities. This result is compatible with the variation of P_c/D_s with $(v_o/c_o)^{2/3}$ and with the tendency of the craters to approach a hemispherical shape as described above.

(b) Empirical Formulas

Nearly everyone who has obtained experimental results has developed empirical formulas that represent his observations to a fair degree of accuracy. The formulas are not based on rational theoretical grounds and generally are not valid for velocities and projectile-target material combinations outside the restricted regions covered by the tests. Recently, Bruce (Ref. 15) has fitted formulas to the composite firing results which are consistent with the assumptions that in the hypervelocity range $P_c/D_c = 0.5$, $P_c/D_s \sim (v_o/c_o)^{2/3}$ and $V_c/V_p \sim (v_o/c_o)^2$. His are probably one of the two most reliable sets of engineering formulas presently available, but even then extrapolation to other materials or to velocities greater than about 1.0 cm/microsecond is hazardous.

More recently, Herrmann and Jones (Ref. 16) have also gathered and analyzed the available data on cratering by high speed impact in semi-infinite targets. They found that the penetration in the high velocity region is best fitted by the dimensionless equation

(1) $\quad P_c/D_s = k\,(\rho_p/\rho_t)^{2/3}\,H$ where $H = \rho_t\, v_o^2/h_t$.

Here k is a constant near 0.36 for most materials; ρ_p and ρ_t are the densities of the projectile and target materials; h_t is the Brinnell Hardness of the target. The Brinnell Hardness is defined as the load applied to a spherical stylus divided by the area of the resultant depression, and thus has the dimensions of a stress.

There is an approximate dependence of indentation hardness on the shear yield stress, τ_o. The relation is approximately

(2) $h \cong 7.2\,\tau_o$.

It would therefore appear that the strength of the target material is an important factor in the cratering mechanism. In fact Herrmann and Jones tried various parameter combinations in which the material strength was neglected, and found that none could fit the composite experimental data.

(c) Previous Cratering Theories

A number of simple theories of hypervelocity impact have been proposed for the prediction of penetration (Refs. 17 through 23). Most of the theories show little agreement with the experimental data; this is not surprising since neither realistic compressibilities nor flow geometries are introduced into any of the derivations.

The only serious attempt to calculate the phenomenology of hypervelocity impact from basic physical equations has been made by Bjork (Ref. 24). He uses a hydrodynamical model and treats the rotationally symmetric case of two dimensional, unsteady, compressible flow in a semi-infinite target under normal impact by a cylindrical projectile of the same material. In setting up the mathematical model Bjork assumes that a) the elastic waves can be neglected since the stresses and particle velocities carried by these waves are much less than those caused by shock waves, b) the flow is strictly adiabatic, c) the strength of the target and projectile material is negligible, and d) the flow is inviscid.

The results of Bjork's calculations are summarized by the equations

(3)
$$\text{Al on Al}: \quad P_c/D_s = 2.09\,(v_o/c_o)^{1/3}$$
$$\text{Fe on Fe}: \quad P_c/D_s = 1\ 69\,(v_o/c_o)^{1/3}.$$

Within the numerical error of the computational procedure he found the craters to be hemispherical and so, from geometry alone,

(4) $V_c/V_p = 4\,(P_c/D_s)^3$.

Substitution of equation (3) into (4) yields

(5) $$\text{Al on Al}: \quad V_c/V_p = 36.5\,v_o/c_o$$
$$\text{Fe on Fe}: \quad V_c/V_p = 19.3\,v_o/c_o.$$

According to this model, therefore, the penetration at hypervelocities actually increases with about the one-third power of velocity rather than with the two-thirds power as extrapolation from the lower velocity tests would indicate.

Since densities and velocities are the primary variables in the perfect fluid model, equations (3) and (5) should apply equally well to other materials of equal density. The predicted curves for the penetration parameter and crater volume parameter are superimposed on the experimental plots of Figures 5, 6, and Figures 9, 10 respectively. The mismatch even at the higher velocities in the experimental range causes one to have reservations in using the model to predict results in the upper reaches of the 0.5 to 7.2 cm/microsecond range. Therefore, this leads to examination of his four basic assumptions. Since a) and b) are almost certainly justified attention is focused on c) and d).

(d) Viscous and Strength Effects

As to neglecting the strength of the material, for dynamic conditions where the duration of loading is very small (say in the order of microseconds) the dynamic yield strength may rise by several orders of magnitude. Although suggested by earlier workers (Refs. 25 and 26) and emphasized above, this dependence of the cratering process on the material strength has recently been directly illustrated by an experiment carried out at the Carnegie Institute of Technology (Ref. 13). The experiment consisted simply of firing steel pellets (0.18 gram, 0.5 cm/microsecond) into targets of lead, cadmium, zinc, and copper and observing the craters produced by the impact as the target temperature was varied over a wide range. The crater volume plotted against temperature showed abrupt changes at certain temperatures that are identified with similar discontinuities in tensile tests made on the metals as the temperature was varied. The critical temperatures are the points where certain metallurgical changes such as transition from brittle to ductile behavior or stress anneal occur.

That the viscosity of the target plays an important role in impact phenomenon may be seen from post mortem metallurgical examination of the microstructure surrounding a high velocity crater (Ref. 2). Practically no change in the shape of the grains in the material occurs under the crater where the strain rate is small. On the other hand, the grains are found to be elongated considerably along the sides of the crater where the strain rate is greatest. The distortion is caused by the shear stresses which result from the high strain rate. Bjork's inviscid model allows only for hydrostatic pressure, and thus does not take this effect into account. The viscosity is also important from the point of view that without considering it there is apparently no way of introducing anisotropic stresses into the flow. This must be done if a strength effect, which is clearly essential, is to be introduced.

VISCO-PLASTIC MODEL

In this section the problem will be considered anew in order to formulate a mathematical model which takes into account both the strength and viscosity of the materials involved.

(a) Bingham Model

When an ultra-high-speed projectile strikes a target a strain-rate which depends on the impact velocity is imposed on the projectile and target materials. The plastic deformation will be resisted not only by the static yield stress, but also by viscosity stresses with magnitudes dependent on the strain rate. Both these effects seem to be important. Such a plastic solid (exhibiting visco-plastic flow) is most simply represented by a Bingham model. The material is considered rigid if stressed below its yield strength, whereas above this value the material acts like a Newtonian viscous liquid; a schematic representation of such a material is given in Figure 13(a). In simple shearing flow, in which the velocity is q (y), and dq/dy is a constant D, this means that

$$
\begin{aligned}
&\tau - \tau_0 = \mu_0 D && (\tau \geqq \tau_0) \\
(6)\quad &\tau + \tau_0 = \mu_0 D && (\tau \leqq -\tau_0) \\
&D = 0 && (|\tau| < \tau_0),
\end{aligned}
$$

where τ_0 is the yield value of the shearing stress and μ_0 is a constant (if temperature dependence and pressure gradient effects are neglected) determining the magnitude of the strain-rate effect.

Now the usual definition of the viscosity of a liquid is based on Newton's assumption that the shear stress and the strain-rate are related according to

$$\tau = \mu D,$$

where the viscosity coefficient μ is a constant at constant temperature. When equations (6) are written in this form, the result is

$$(7)\quad \tau = \mu(D)\, D,$$

where the strain-rate dependent viscosity coefficient $\mu = \mu(D)$ is given by

$$
\begin{aligned}
(8)\quad \mu(D) &= \mu_0 + \frac{\tau_0}{|D|} && (|\tau| \geqq \tau_0) \\
&= \infty && (|\tau| < \tau_0).
\end{aligned}
$$

This dependence of μ on D is illustrated in Figure 13(b). The viscosity coefficient decreases with increased strain-rate.

The use of the Bingham model is proposed to bridge the transition from the plastic to the hydrodynamic regimes (Ref. 27). It is analogous to Malvern's model which seems to have successfully bridged the transition from the elastic to the plastic regime (Ref. 28). Malvern assumed that the strain-rate was directly proportional to the difference between the instantaneous stress and the static stress corresponding to the strain, so that for longitudinal stress in a slender rod the relation takes the form

$$(9)\quad \frac{\partial}{\partial t}[E\epsilon - \sigma] = \frac{E}{\eta}[\sigma - F(\epsilon)]$$

where E is the elastic modulus; σ and ϵ are the instantaneous values of longitudinal stress and strain; and $F(\epsilon)$ defines the static stress-strain curve. These quantities are depicted in Figure 14. As ϵ increases σ becomes negligible compared to $E\epsilon$, and $F(\epsilon)$ levels out and may be approximated by a constant σ_o. When very large strains are involved equation (9) may therefore be approximated by the relation

$$(10)\quad \sigma - \sigma_o \cong \eta\dot{\epsilon} \qquad (\sigma \geqq \sigma_o)$$

The similarity of equations (6) and (10) is obvious.

(b) Axisymmetric Stress to Strain-Rate Relation

In order to extend the idealized visco-plastic model to a material subjected to hypervelocity impact the stress vs. strain-rate relations (7) and (8) must be generalized. As formulated there, only the properties of the material in simple shear flow are defined; corresponding relations for three dimensional flow are required. The expressions will be somewhat simplified by assuming that the projectile is axisymmetric in geometry, and that it strikes a semi-infinite target normal to the axis of symmetry. Furthermore, the angular momentum of the projectile is assumed to be zero at impact.

Under these assumptions the only non-vanishing components of the stress tensor are the normal stresses τ_{rr}, $\tau_{\theta\theta}$, τ_{zz} and the shearing stress $\tau_{rz} = \tau_{zr}$. The tensor may be decomposed into two parts, a component producing distortion and a component producing only a volume change:

$$(11)\quad \tau_{ik} = (\tau_{ik} + p\delta_{ik}) - p\delta_{ik}$$
$$= \tau^*_{ik} - p\delta_{ik}$$

where δ_{ik} is the Kronecker delta and

$$(12)\quad \tau^*_{ik} = \tau_{ik} + p\delta_{ik}; \qquad p = -\frac{1}{3}\tau_{ii}.$$

τ^*_{ik} is associated with the internal friction of the medium and p is assumed equal to the hydrodynamic pressure.*

*This assumption is equivalent to setting the "second coefficient of viscosity" $\mu' = -2\mu/3$. See Ref. 29.

Flow is assumed to occur whenever the von Mises criterion is satisfied, i.e. whenever

$$(13)\quad \tau^2 \geqq \tau_o^2 \quad \text{where} \quad \tau^2 = \tau_{rz}^{*2} + \frac{1}{2}(\tau_{rr}^{*2} + \tau_{\theta\theta}^{*2} + \tau_{zz}^{*2}) .$$

τ^2 is a measure of the magnitude of the components of the distortion stress tensor, τ_{ik}^*.

The non-vanishing components of the strain-rate tensor are defined by

$$(14)\quad D_{rr} = 2\frac{\partial q_r}{\partial r} \qquad D_{\theta\theta} = \frac{2}{r} q_r \qquad D_{zz} = 2\frac{\partial q_z}{\partial z}$$

$$D_{rz} = D_{zr} = \frac{\partial q_r}{\partial z} + \frac{\partial q_z}{\partial r}$$

This tensor may be decomposed into a distortional strain-rate and a dilational strain-rate:

$$D_{ik} = D_{ik}^* - \frac{2}{3}\left(\frac{1}{\rho}\frac{d\rho}{dt}\right)\delta_{ik}.$$

Here $-(1/\rho)\, d\rho/dt$ is the volume strain rate, the factor 1/3 is required to obtain the linear strain rate, and the 2 enters because of our definition of D_{ii}. The continuity equation for compressible flow,

$$(15)\quad \frac{d\rho}{dt} + \rho \operatorname{div} \bar{q} = 0,$$

may be used to write the above equation in the form

$$(16)\quad D_{ik} = D_{ik}^* + \frac{2}{3} \operatorname{div} \bar{q}\ \delta_{ik}.$$

To generalize (7), the distortional stress and strain-rate components are related by

$$(17)\quad \tau_{ik}^* = \mu D_{ik}^* \qquad (\tau^2 \geqq \tau_o^2)$$

$$D_{ik}^* = 0 \qquad (\tau^2 < \tau_o^2)$$

where the dependence of μ on the distortional rate of strain must generalize (8) in a natural manner. Substituting (12) and (16) into (17) gives

$$(18) \qquad \tau_{ik} = -p\delta_{ik} + \mu D_{ik} - \frac{2}{3}\mu \operatorname{div} \bar{q}\, \delta_{ik}.$$

If μ were a constant, equation (18) would reduce to the classical stress to strain-rate relationship of the Navier-Stokes theory of hydrodynamics. On the other hand, if one does not assume that the mean normal stress is the thermodynamic pressure, (12), the relationship is complicated by the factor $-2\mu/3$ in the last term being replaced by the second coefficient of viscosity μ'.

Since the viscosity coefficient μ depends on the distortional strain-rate it must be a scalar function of the three invariants of the tensor D^{*}_{ik}, i.e. μ must be independent of the particular frame of reference. Now the first invariant is zero and the dependence on the third invariant is small. Therefore, the viscosity may be assumed to depend only on the second invariant:

$$(19) \qquad D^2 = D^{*2}_{rz} + \frac{1}{2}\left(D^{*2}_{rr} + D^{*2}_{\theta\theta} + D^{*2}_{zz}\right)$$

$$= D^2_{rz} + \frac{1}{2}\left(D^2_{rr} + D^2_{\theta\theta} + D^2_{zz}\right) - \frac{2}{3}(\operatorname{div} \bar{q})^2.$$

Thus, the natural generalization of the Bingham model to the case of axisymmetric flow is for the viscosity μ to depend on the rate of strain according to functional relation (8) with D given by (19):

$$(20) \qquad \begin{cases} \mu = \mu_o + \dfrac{\tau_o}{\left[D^2_{rz} + \frac{1}{2}\left(D^2_{rr} + D^2_{\theta\theta} + D^2_{zz}\right) - \frac{2}{3}(\operatorname{div} \bar{q})^2\right]^{1/2}} & (\tau^2 \geqq \tau_o^2) \\ \mu = \infty & (\tau^2 < \tau_o^2). \end{cases}$$

The generalization of the Bingham model to 3 dimensions has been formulated by Oldroyd (Ref. 30) for the case of rectangular coordinates.

(c) Formulation of Governing Equations

Now that we have the expression for the dependence of the viscosity on the strain-rate the principle of the conservation of momentum may be applied to write the two equations of motion corresponding to the Navier-Stokes equations for axially symmetric flow. The result is the same except for the non-constancy of μ. These two equations together with the continuity equation (15), which results from the conservation of matter, give three equations in the four dependent variables q_r, q_z, p, ρ. To write another equation some assumption that specifies the particular type of flow must be introduced. An assumption is made identical to that of Bjork, that no heat is transferred between neighboring particles of the material. This leads to the well known

energy equation of hydrodynamics (Ref. 31). This equation, however, introduces a fifth dependent variable, the internal energy per unit mass U. This difficulty is circumvented by assuming that an experimentally determined equation of state relates this thermodynamic parameter to the other state parameters p, ρ. A discussion of our choice for the equation of state is given later in the report.

The final five equations are as follows:

(21) $$\frac{d\rho}{dt} + \rho \operatorname{div} \bar{q} = 0$$ (Mass)

(22) $$\rho \frac{dq_r}{dt} = -\frac{\partial p}{\partial r} + \frac{\partial}{\partial r}\left[\mu(D)\, 2\left(\frac{\partial q_r}{\partial r} - \frac{2}{3} \operatorname{div} q\right)\right] + \frac{\partial}{\partial z}\left[\mu(D)\left(\frac{\partial q_z}{\partial r} + \frac{\partial q_r}{\partial z}\right)\right] + \frac{2\mu(D)}{r}\left(\frac{\partial q_r}{\partial r} - \frac{q_r}{r}\right)$$ (Radial Momentum)

(23) $$\rho \frac{dq_z}{dt} = -\frac{\partial p}{\partial r} + \frac{\partial}{\partial z}\left[\mu(D)\left(2\frac{\partial q_z}{\partial z} - \frac{2}{3} \operatorname{div} \bar{q}\right)\right] + \frac{1}{r}\frac{\partial}{\partial r}\left[r\mu(D)\left(\frac{\partial q_r}{\partial z} + \frac{\partial q_z}{\partial r}\right)\right]$$ (Axial Momentum)

(24) $$p = f(\rho, U)$$ (State)

(25) $$\rho\left[\frac{dU}{dt} + p\frac{d(1/\rho)}{dt}\right] = \mu(D)\, D^2.$$ (Energy)

The material time derivatives may be expanded according to the relation

$$\frac{d}{dt}(\ ) = \frac{\partial(\ )}{\partial t} + \bar{q} \cdot \operatorname{grad}(\ ),$$

and the divergence for the axially symmetric case is

$$\operatorname{div} \bar{q} = \frac{1}{r}\frac{\partial}{\partial r}(rq_r) + \frac{\partial}{\partial z} q_z.$$

STUDY OF GOVERNING EQUATIONS

The introduction of the effects of viscosity and strength into the perfect fluid equations has necessarily led to complication of the partial differential equations governing the flow. As the next logical step these equations will be studied qualitatively to determine the dimensionless parameters which control the relative importance of the inertial, viscous and strength effects

(a) Characteristic Numbers

Consider two distinct projectile-target systems, both having projectile and target geometrically similar. Choose the diameter, D_s, of the sphere with mass equal to that of the projectile as the characteristic length. We may set

$$D_{s2} = K_1 D_{s1}. \tag{26}$$

The same relation holds between all other pairs of corresponding points if cratering flows are dynamically similar:

$$r_2 = K_1 r_1 \qquad z_2 = K_1 z_1.$$

For two corresponding times t_2 and t_1 set

$$t_2 = K_2 t_1. \tag{27}$$

Since velocity means traveling a certain length in a certain time, the characteristic velocities (impact values) in the two systems are related according to

$$v_2 = \frac{K_1}{K_2} v_1 \tag{28}$$

and hence

$$q_{r2} = \frac{K_1}{K_2} q_{r1} \qquad q_{z2} = \frac{K_1}{K_2} q_{z1}.$$

Furthermore, we may set

$$\begin{aligned} &\rho_2 = K_3 \rho_1 \qquad p_2 = K_4 p_1 \qquad U_2 = K_5 U_1 \\ &\mu_{o2} = K_6 \mu_{o1} \qquad \tau_{o2} = K_7 \tau_{o1}. \end{aligned} \tag{29}$$

We now use relations (26) through (29) to express the magnitudes of the variables of the second cratering flow in terms of those of the first. This is

done in each of the equations governing the visco-plastic formulation. The K factors for the two terms in (21) are the same so that the continuity equations for the two flows are identical. The viscosity $\mu = \mu(D)$ which appears in the momentum and energy equations is homogeneous in K only if

$$(30) \qquad K_6 = K_2 K_7 \quad \text{or} \quad K_6 = K_1 K_7 \frac{K_2}{K_1}.$$

Then $\mu_2 = K_6 \mu_1$ and all terms in (22) and (23) have the same factor provided

$$(31) \qquad \frac{K_1 K_3}{K_2^2} = \frac{K_6}{K_1 K_2} = \frac{K_4}{K_1}.$$

The specific energy term (consisting of kinetic and internal energy components) in (25) is homogeneous in K only if $K_5 = K_4/K_3$ or, from (31),

$$(32) \qquad K_5 = \frac{K_1^2}{K_2^2}.$$

Then all the terms in the energy equation have the same factor provided

$$(33) \qquad \frac{K_3 K_5}{K_2} = \frac{K_6}{K_2^2}.$$

Upon substitution from (26), (27), and (29) the required K relations may be rewritten in dimensionless forms. Relation (30) is equivalent to

$$\frac{D_{s1}\, \tau_{o1}}{\mu_{o1}\, v_1} = \frac{D_{s2}\, \tau_{o2}}{\mu_{o2}\, v_2}.$$

Relations (31) are equivalent to

$$\frac{D_{s1}\, \rho_1\, v_1}{\mu_{o1}} = \frac{D_{s2}\, \rho_2\, v_2}{\mu_{o2}} \quad \text{and} \quad \frac{\rho_1 v_1^2}{p_1} = \frac{\rho_2 v_2^2}{p_2}.$$

Relation (32) is equivalent to

$$\frac{U_1}{v_1^2} = \frac{U_2}{v_2^2}$$

and relation (33) gives nothing new.

Necessary conditions for dynamic similarity of the two systems are that they have the same values for the dimensionless ratios, Reference 32

$$B_o = \frac{D_s \tau_o}{\mu_o v_o} \qquad R_o = \frac{D_s \rho_o v_o}{\mu_o}$$

(34)

$$M_\gamma^* = \frac{v_o}{\sqrt{p_o/\rho_o}} \qquad N_o = \frac{U_o}{v_o^2} .$$

Here the subscript o denotes that the quantity is evaluated in the undisturbed state. B_o and R_o are the familiar Bingham and Reynolds numbers which ordinarily arise separately in the theory of slow visco-plastic flow and the theory of viscous liquids respectively. Here both occur as the model includes the two types of flow. M* is the generalized Mach number which for an ideal gas may be decomposed into two factors, the ratio of specific heats and the ordinary Mach number M. It is interesting to note that if the characteristic pressure p_o is taken to be the Brinnell Hardness, see equation (1), then

$$M^* = \sqrt{H.}$$

The characteristic specific internal energy, U_o, may be taken to be the energy required to melt or vaporize a unit mass of the medium.

Since the governing equations also include the equation of state, equality of numbers (34) are not sufficient to ensure that two geometrically similar flows are dynamically similar. The equation of state does not lend itself to this type of investigation since it is an empirical formula.

(b) Relation to Perfect Fluid Model

The equations governing the flow can be written in dimensionless form by setting

$$r = Lr' \qquad z = Lz' \qquad \rho = \rho_o \rho'$$

$$q_r = v q_r' \qquad q_z = v q_z' \qquad U = v^2 U'$$

(35)

$$p = \rho_o v^2 p' \qquad t = L v^{-1} t' \qquad R = L \rho_o v \mu_o^{-1}$$

$$\mu_o = L \rho_o v R^{-1} \qquad \tau_o = \rho_o v^2 B R^{-1} \qquad B = L \tau_o (\mu_o v_o)^{-1},$$

where the dimensionless quantities are indicated by a prime. The governing equations then become

(36) $$\frac{d\rho'}{dt} + \rho' \operatorname{div}' \tilde{q}' = 0$$

$$R \left\{ \rho' \frac{dq_{r'}}{dt'} + \frac{\partial p'}{\partial r'} \right\} =$$

(37) $$\left\{ \frac{\partial}{\partial r'} \left(2 \frac{\partial q'_r}{\partial r'} - \frac{2}{3} \operatorname{div}' \tilde{q}' \right) + \frac{\partial}{\partial z'} \left(\frac{\partial q'_r}{\partial z'} + \frac{\partial q_{z'}}{\partial r'} \right) + \frac{2}{r'} \left(\frac{\partial q'_r}{\partial r'} - \frac{q'_r}{r'} \right) \right\}$$

$$+ B \left\{ \frac{\partial}{\partial r'} \frac{1}{|\overline{D}|} \left(2 \frac{\partial q'_r}{\partial r'} - \frac{2}{3} \operatorname{div}' \tilde{q}' \right) + \frac{\partial}{\partial z'} \frac{1}{|\overline{D}|} \left(\frac{\partial q'_r}{\partial z'} + \frac{\partial q'_z}{\partial r'} \right) \right.$$

$$\left. + \frac{2}{r'} \frac{1}{|\overline{D}|} \left(\frac{\partial q'_r}{\partial r'} - \frac{q'_r}{r'} \right) \right\}$$

$$R \left\{ \rho' \left(\frac{dq'_z}{dt'} + \frac{\partial p'}{\partial z'} \right) \right\} =$$

(38) $$\left\{ \frac{\partial}{\partial z'} \left(2 \frac{\partial q'_z}{\partial z'} - \frac{2}{3} \operatorname{div} \tilde{q}' \right) + \frac{1}{r'} \frac{\partial}{\partial r'} r' \left(\frac{\partial q'_r}{\partial z'} + \frac{\partial q'_z}{\partial r'} \right) \right\}$$

$$+ B \left\{ \frac{\partial}{\partial z'} \frac{1}{|\overline{D}'|} \left(2 \frac{\partial q'_z}{\partial z'} - \frac{2}{3} \operatorname{div}' \tilde{q}' \right) + \frac{1}{r'} \frac{\partial}{\partial r'} r' \frac{1}{|\overline{D}'|} \left(\frac{\partial q'_r}{\partial z'} + \frac{\partial q'_z}{\partial r'} \right) \right\}$$

(39) $$p' = \frac{1}{\rho_o v^2} f(\rho_o \rho', v^2 U')$$

(40) $$R \left\{ \rho' \frac{dU'}{dt'} + p' \operatorname{div}' \tilde{q}' \right\} = \left\{ D'^2 \right\} + B \left\{ |D'| \right\}$$

where

$$D'^2 = \left(\frac{\partial q'_r}{\partial z'} + \frac{\partial q'_z}{\partial r'} \right)^2 + 2 \left[\left(\frac{\partial q'_r}{\partial r'} \right)^2 + \left(\frac{1}{r'} q'_r \right)^2 + \left(\frac{\partial q'_z}{\partial z'} \right)^2 \right] - \left(\frac{2}{3} \operatorname{div}' \tilde{q}' \right)^2 .$$

The left side of (40) may also be written as

$$R\left\{\rho'\left[\frac{dU'}{dt'}+p'\frac{d\,(1/\rho')}{dt'}\right]\right\}$$

upon substitution from (36).

The quantities in the brackets in each of equations (37), (38), (40) will be of order unity at each point in space and time that L, v are truly representative values. If so, and if one of the three numbers R, 1, B is much greater than the other two, a single set of terms in each equation predominates, and the motion may be approximately described by equating the coefficient of the predominant number to zero For example, if $R \gg 1, B$, the equations (37), (38), (40) reduce to

$$\rho'\frac{dq'_r}{dt'}+\frac{\partial p'}{\partial r'}=0$$

$$\rho'\frac{dq'_z}{dt'}+\frac{\partial p'}{\partial z'}=0 \tag{41}$$

$$\rho'\frac{dU'}{dt'}+p'\,\mathrm{div}\,\vec{q}'=0,$$

respectively.

Actually, these combined with (36) and (39) are the perfect fluid equations, and are seen to be valid when the inequalities $R \gg 1, B$ hold, i.e. only when the inertial effect predominates. This will be the case during those parts of the cratering process when the characteristic velocity v appearing in R and B is high enough, i.e., by (35),

$$v \gg \text{maximum}\left(\sqrt{\tau_o/\rho_o},\ \mu_o/L\rho_o\right). \tag{42}$$

As the rate of flow decreases so does the characteristic velocity until eventually, when the flow ceases, $v = 0$. Clearly, in the late stages of flow the inequalities required for the perfect fluid approximation to be valid are reversed, i.e., $R \ll 1, B$. At other stages, two or possibly all three of the groups of terms may be equally important.

It is seen that the strength terms are insignificant during the early stages of flow but become predominant in the latter stages. The question arises as to the importance of the viscous terms. Clearly, they would always be negligible only if

$$\text{maximum}\,(R, B) \gg 1 \tag{43}$$

for the entire range of v, $(0, v_o)$. Since R and B are respectively, monotone

increasing and decreasing functions of v the left side of (43) is attained when R= B, i.e., when the flow velocity is given by

$$v^* = \sqrt{\tau_o/\rho_o} \ .$$

The required inequality for the viscous terms to be negligible throughout the cratering process therefore becomes

$$\mu_o \ll L\sqrt{\rho_o \tau_o} \quad . \tag{44}$$

At the instant of impact an exceedingly large strain-rate gradient is imposed at the surface of contact. The use for example, of the diameter of the projectile, D_s, for the representative length L cannot be justified; a much smaller value is actually required. Accordingly, the inequalities (42) and (44) are very restrictive. The viscosity is probably never really negligible in the time interval immediately after impact.

(c) Choice of Parameter Values

The principal difficulty in testing these conclusions, and a real difficulty in the application of the governing equations themselves, is in assuming the viscosity coefficients for structural materials such as steel, copper, or aluminum. The viscosity involved here has little relation to ordinary creep data. The choice of an appropriate value for the dynamic shear yield strength τ_o is nearly as troublesome. It is known to increase with increasing strain-rate, but values are not known in the hypervelocity impact range. Therefore, to check the philosophy used in the construction of the mathematical model exploratory calculations had to be performed in which the values of μ_o and τ_o were varied over several orders of magnitude and the impact velocity v_o was allowed to assume a set of values in the range of interest.

As a first step in choosing trial values for μ_o the visco-plastic formulation will be applied to the case of a long rod subjected to uniaxial loading (along z - axis). Then

$$D_{rz} = 0 \qquad D_{rr} = D_{\theta\theta} = -\frac{1}{2} D_{zz} \qquad \operatorname{div} \bar{q} = 0$$

and the viscosity coefficient, (20), reduces to

$$\mu = \mu_o + \frac{\tau_o}{\sqrt{3}\left|\frac{\partial q_z}{\partial z}\right|} \ .$$

Hence, by (12), the uniaxial stress and strain-rate are related according to

$$\tau_{zz} - \sqrt{3}\,\tau_o = 3\mu_o \frac{\partial q_z}{\partial z}$$

This relation compares with (10) upon setting

(45) $\mu_o \cong \eta/3.$

Now, Malvern (Ref. 28) has applied his model, (9), to experimental data obtained upon subjecting a long rod to a plastic wave. In this way values for η in the elastic-plastic transition region were determined. His values may be substituted into (45) to obtain approximate values of μ_o for the plastic-hydrodynamic transition region:

Steel: $\mu_o = 0.8$ gm cm^{-1} microsecond^{-1}

Copper: $\mu_o = 0.4$ gm cm^{-1} microsecond^{-1}.

Others have also obtained approximately the same values, Reference 33. Our calculations have all been for iron and μ_o is assumed to be within a factor of ten of 0.8.

For mild steel, Reiner (Ref. 34) quotes the static yield stress to be approximately

$$\tau_o = 10^{-2} \text{ gm cm}^{-1} \text{ microsecond}^{-2},$$

i.e. ten kilobars. For our calculations the dynamic yield stress is pertinent. The above value is assumed to be the lowest value likely, and τ_o is varied up to one hundred times as large, i.e. one megabar.

The various combinations of assumptions for μ_o, τ_o and impact velocity, v_o, are displayed in Table I. The choices of v_o (=0.5, 4, 7.5 cm/microsecond) represent the extremes and mean of the meteoroid velocity range. It will be desirable to have further results for $v_o = 1.0$ cm/microsecond. The values of the dimensionless parameters B_o and R_o are also listed for each combination of μ_o, τ_o, v_o. They are seen to vary widely with the choice of combinations.

TABLE I

Enumeration of parameter combinations considered for iron-iron impact. The units are in the gram-centimeter-microsecond system. $\rho_o = 7.8$ gm/cm^3, $D_s = 1$. In computing the required net size for the explicit scheme, a is chosen as 1.5, $l = 1.5\Delta x$.

No.	Parameters			Bingham No.	Reynolds No.	Stability Criteria		Net Size
	v_o	τ_o	μ_o	$B_o = \frac{D_s \tau_o}{U_o v_o}$	$R_o = \frac{D_s \rho_o v_o}{U_o}$	$\Delta t/(\Delta x)^2$	$\Delta t/\Delta x$	$\frac{\Delta x}{\Delta t} = 0.1$
1	0.5	0	0	-	∞	3.06	0.60	3.0×10^{-2}
2	0.5	0	8×10^{-2}	0	4.88 x 10	2.70		2.7 "
3	0.5	0	8×10^{-1}	0	4.88	1.38		1.4 "
4	0.5	0	8	0	4.88×10^{-1}	0.23		2.3×10^{-3}
5	0.5	10^{-2}	0	∞	∞	3.06	0.60	3.0×10^{-2}
6	0.5	10^{-2}	8×10^{-2}	2.5×10^{-1}	4.88 x 10	2.70		2.7 "
7	0.5	10^{-2}	8×10^{-1}	2.5×10^{-2}	4.88	1.38		1.4 "
8	0.5	10^{-2}	8	2.5×10^{-3}	4.88×10^{-1}	0.23		2.3×10^{-3}
9	0.5	10^{-1}	0	∞	∞	3.06	0.60	3.0×10^{-2}
10	0.5	10^{-1}	8×10^{-2}	2.5	4.88 x 10	2.70		2.7 "
11	0.5	10^{-1}	8×10^{-1}	2.5×10^{-1}	4.88	1.38		1.4 "
12	0.5	10^{-1}	8	2.5×10^{-2}	4.88×10^{-1}	0.23		2.3×10^{-3}
13	0.5	1	0	∞	∞	3.06	0.60	3.0×10^{-2}
14	0.5	1	8×10^{-2}	2.5 x 10	4.88 x 10	2.70		2.7 "
15	0.5	1	8×10^{-1}	2.5	4.88	1.38		1.4 "
16	0.5	1	8	2.5×10^{-1}	4.88×10^{-1}	0.23		2.3×10^{-3}
17	4	0	0	-	∞	0.21	0.44	2.1 "
18	4	0	8×10^{-2}	0	3.9×10^2	0.21		2.1 "
19	4	0	8×10^{-1}	0	3.9 x 10	0.18		1.8 "
20	4	0	8	0	3.9	0.085		8.5×10^{-4}
21	4	10^{-2}	0	∞	∞	0.21	0.44	2.1×10^{-3}
22	4	10^{-2}	8×10^{-2}	3.13×10^{-2}	3.9×10^2	0.21		2.1 "
23	4	10^{-2}	8×10^{-1}	3.13×10^{-3}	3.9 x 10	0.18		1.8 "
24	4	10^{-2}	8	3.13×10^{-4}	3.9	0.085		8.5×10^{-4}
25	4	10^{-1}	0	∞	∞	0.21	0.44	2.1×10^{-3}
26	4	10^{-1}	8×10^{-2}	3.13×10^{-1}	3.9×10^2	0.21		2.1 "
27	4	10^{-1}	8×10^{-1}	3.13×10^{-2}	3.9 x 10	0.18		1.8 "
28	4	10^{-1}	8	3.13×10^{-3}	3.9	0.085		8.5×10^{-4}
29	4	1	0	∞	∞	0.21	0.44	2.1×10^{-3}
30	4	1	8×10^{-2}	3.13	3.9×10^2	0.21		2.1 "
31	4	1	8×10^{-1}	3.13×10^{-1}	3.9 x 10	0.18		1.8 "
32	4	1	8	3.13×10^{-2}	3.9	0.085		8.5×10^{-4}
33	7.5	0	0	-	∞	0.093	0.40	9.3 "
34	7.5	0	8×10^{-2}	0	7.3×10^2	0.092		9.2 "
35	7.5	0	8×10^{-1}	0	7.3 x 10	0.086		8.6 "
36	7.5	0	8	0	7.3	0.051		5.1 "
37	7.5	10^{-2}	0	∞	∞	0.093	0.40	9.3 "
38	7.5	10^{-2}	8×10^{-2}	1.67×10^{-2}	7.3×10^2	0.092		9.2 "
39	7.5	10^{-2}	8×10^{-1}	1.67×10^{-3}	7.3 x 10	0.086		8.6 "
40	7.5	10^{-2}	8	1.67×10^{-4}	7.3	0.051		5.1 "
41	7.5	10^{-1}	0	∞	∞	0.093	0.40	9.3 "
42	7.5	10^{-1}	8×10^{-2}	1.67×10^{-1}	7.3×10^2	0.092		9.2 "
43	7.5	10^{-1}	8×10^{-1}	1.67×10^{-2}	7.3 x 10	0.086		8.6 "
44	7.5	10^{-1}	8	1.67×10^{-3}	7.3	0.051		5.1 "
45	7.5	1	0	∞	∞	0.093	0.40	9.3 "
46	7.5	1	8×10^{-2}	1.67	7.3×10^2	0.092		9.2 "
47	7.5	1	8×10^{-1}	1.67×10^{-1}	7.3 x 10	0.086		8.6 "
48	7.5	1	8	1.67×10^{-2}	7.3	0.051		5.1 "
49	1	0	0	-	∞	1.29	0.54	1.3×10^{-2}
50	1	0	8×10^{-2}	0	9.8 x 10	1.22		1.2 "
51	1	0	8×10^{-1}	0	9.8	0.80		0.8×10^{-3}
52	1	0	8	0	9.8×10^{-1}	0.18		1.8 "

ONE-DIMENSIONAL PROBLEM

For the exploratory calculations we have considered the one-dimensional impact of two semi-infinite bodies, Figure 15, and compared the results obtained with those given by the perfect fluid equations. This is a problem of "plane strain" and the problem of a long rod considered above is a problem of "plane stress".

(a) The Eulerian Formulation

The visco-plastic equations for one-dimensional flow can be deduced from the axisymmetric equations by equating to zero q_r and all derivatives with respect to r. Then, setting $q_z = q$, the viscosity coefficient reduces to

$$\mu = \mu_o + \sqrt{\frac{3}{4}} \frac{\tau_o}{\left|\frac{\partial q}{\partial z}\right|} \qquad (\tau^2 \geq \tau_o^2)$$

(46)

$$\mu = \infty \qquad (\tau^2 < \tau_o^2).$$

The components of the distortional stress tensor are, by (17),

$$(47) \qquad \tau_{rr}^* = \tau_{\theta\theta}^* = -\frac{2}{3}\mu \frac{\partial q}{\partial z} \qquad \tau_{zz}^* = \frac{4}{3}\mu \frac{\partial q}{\partial z} \qquad \tau_{rz}^* = 0,$$

and the von Mises flow statistic therefore reduces to

$$(48) \qquad \tau^2 = \frac{4}{3}\mu^2 \left(\frac{\partial q}{\partial z}\right)^2.$$

$$= \tau_o^2 + \frac{4}{\sqrt{3}} \mu_o \tau_o \left|\frac{\partial q}{\partial z}\right| + \frac{4}{3} \mu_o^2 \left(\frac{\partial q}{\partial z}\right)^2.$$

The system of equations governing the flow reduces to

$$(49) \qquad \frac{d\rho}{dt} + \rho \frac{\partial q}{\partial z} = 0$$

$$(50) \qquad \rho \frac{dq}{dt} = -\frac{\partial p}{\partial z} + \frac{4}{3} \mu_o \frac{\partial^2 q}{\partial z^2}$$

(51) $p = f(\rho, U)$

(52) $$\rho \frac{dU}{dt} + p \frac{\partial q}{\partial z} = \frac{4}{3} \mu_o \left(\frac{\partial q}{\partial z}\right)^2 + \sqrt{\frac{4}{3}}\, \tau_o \left|\frac{\partial q}{\partial z}\right|.$$

In writing (50) we have used the relationship

(53) $$\frac{\partial}{\partial z}\left(\frac{\partial q}{\partial z} \frac{1}{\left|\frac{\partial q}{\partial z}\right|}\right) = 0.$$

To show that this is the case is equivalent to showing that the velocity gradient, $\partial q/\partial z$, never changes from just above zero to just below zero. From (46), (47) we see that this situation cannot occur since, for example, τ_{zz}^* would have to change from just above $\sqrt{4/3}\ \tau_o$ to just below $-\sqrt{4/3}\ \tau_o$, involving an impossible discontinuity of stress.

(b) The Lagrangian Formulation

The one dimensional formulation above is in the Eulerian form. The Lagrangian form, however, gives more information (it keeps track of each material particle) and has the virtue that conservation of mass is automatic and exact, even in the finite difference approximations. Because of this inherent greater accuracy the Lagrangian form is often preferred for problems in one space variable.

In Lagrangian coordinates the motion is considered in terms of the instantaneous position X of a section which is a function of time and a space coordinate x which identifies the section. Here the Lagrangian coordinate x will be taken to be the initial position of the section at time zero. The velocity is then given by

(54) $$q = \frac{\partial X}{\partial t}.$$

The transformation from the Eulerian variables (z, t) to the Lagrangian variables (x, t) is accomplished by the relations

(55) $$\frac{dg}{dt} = \left(\frac{\partial g}{\partial t}\right)_x \qquad \frac{\partial g}{\partial z} = \frac{\rho}{\rho_o}\left(\frac{\partial g}{\partial x}\right)_t,$$

where g is any dependent variable. In writing the second of these we have used the fact that the conservation of mass implies

$$\frac{\partial X}{\partial x} = \frac{\rho_o}{\rho}.$$

In Lagrangian form the governing equations, corresponding to (49) through (52) respectively, are as follows:

$$(56) \qquad \frac{\partial q}{\partial x} = \frac{\partial}{\partial t}\left(\frac{\rho_o}{\rho}\right) \quad \text{or} \quad \frac{\partial X}{\partial x} = \frac{\rho_o}{\rho}$$

$$(57) \qquad \rho_o \frac{\partial q}{\partial t} = -\frac{\partial p}{\partial x} + \frac{4}{3}\mu_o \frac{\partial}{\partial x}\left(\frac{\rho}{\rho_o}\frac{\partial q}{\partial x}\right)$$

$$(58) \qquad p = f(\rho, U)$$

$$(59) \qquad \frac{\partial U}{\partial t} + p\frac{\partial}{\partial t}\left(\frac{1}{\rho}\right) = \frac{4}{3}\mu_o \frac{\rho}{\rho_o^2}\left(\frac{\partial q}{\partial x}\right)^2 + \sqrt{\frac{4}{3}}\frac{\tau_o}{\rho_o}\left|\frac{\partial q}{\partial x}\right|.$$

The viscosity coefficient becomes

$$(60) \qquad \mu = \mu_o + \sqrt{\frac{3}{4}}\frac{\rho_o}{\rho}\frac{\tau_o}{\left|\frac{\partial q}{\partial x}\right|} \qquad (\tau^2 \geq \tau_o^2)$$

$$\mu = \infty \qquad (\tau^2 < \tau_o^2).$$

The stress components become

$$(61) \qquad \tau_{rr} = \tau_{\theta\theta} = -p - \frac{2}{3}\mu_o \frac{\rho}{\rho_o}\frac{\partial q}{\partial x} - \frac{\tau_o}{\sqrt{3}}\,\text{sign}\left(\frac{\partial q}{\partial x}\right)$$

$$\tau_{zz} = -p + \frac{4}{3}\mu_o \frac{\rho}{\rho_o}\frac{\partial q}{\partial x} + \sqrt{\frac{4}{3}}\tau_o\,\text{sign}\left(\frac{\partial q}{\partial x}\right) \qquad \tau_{rz} = 0.$$

and

$$(62) \qquad \tau^2 = \frac{4}{3}\mu^2\frac{\rho^2}{\rho_o^2}\left(\frac{\partial q}{\partial x}\right)^2$$

$$= \tau_o^2 + \frac{4}{\sqrt{3}}\mu_o\tau_o\frac{\rho}{\rho_o}\left|\frac{\partial q}{\partial x}\right| + \frac{4}{3}\mu_o^2\left(\frac{\rho}{\rho_o}\right)^2\left(\frac{\partial q}{\partial x}\right)^2.$$

(c) Necessity of Numerical Solution

Analytical methods for solving the governing equations are not available, even for these one dimensional formulations. It was therefore necessary to resort to finite difference techniques for the computations. To cover the desired range of parameter combinations, listed in Table I, required the development of two separate computational schemes. The first is an explicit difference scheme based on the Lagrangian formulation. It allows the two impacting bodies to be of different materials, and places no restriction on μ_o. For large values of μ_o and v_o, however, it is advantageous to use an alternate implicit scheme based on the Eulerian formulation. The latter scheme then requires less machine time, but it is only valid for impact between bodies of identical material with $\mu_o > 0$. The two methods are therefore mutually complementary.

The next two sections describe these schemes in detail. They may be omitted by the more casual reader.

EXPLICIT DIFFERENCE SCHEME

The explicit difference scheme represents an extension of a method commonly employed for perfect fluids to allow for the additional terms which occur in the visco-plastic model.

(a) Artificial Viscosity

In a perfect fluid shock waves occur as moving surfaces across which ρ, U, p, q are all discontinuous. The differential equations (which makes no sense on such surfaces) must then be augmented by jump conditions which serve as internal moving boundary conditions and their occurrence vastly complicates the solution. To avoid these difficulties von Neumann and Richtmeyer (Reference 35) introduced a purely "artificial viscosity" which has a smoothing effect so that the discontinuity surface is replaced by a thin transition layer in which the dependent variables change rapidly, but not discontinuously. The purely artificial dissipative mechanism was chosen of such form and strength that the required smoothness is achieved without affecting the flow pattern.

In the equations which are being investigated here a true viscosity may or may not be present. Such a smoothing mechanism must be included if all the parameter combinations are to be considered. In fact, it was found necessary to include such a device for certain cases where μ_o is positive but small. The real viscosity terms are proportional to the strain-rate whereas the artificial viscosity (as will be shown in (64)) is quadratic in the strain-rate. The latter is therefore more effective in smoothing extremely strong shocks. On the other hand, the artificial viscosity, being quadratic, is extremely small in the smooth part of the flow between shocks, where one wishes the true viscosity coefficient to predominate.

When the Lagrangian equations are rewritten to incorporate the artificial viscosity terms, they become

$$\frac{\partial X}{\partial t} = q$$

$$\frac{\partial q}{\partial t} = -\frac{1}{\rho_o}\frac{\partial (p + Q + S)}{\partial x}$$

(63)

$$\frac{\partial U}{\partial t} = -(p + Q + S)\frac{\partial V}{\partial t} + \sqrt{\frac{4}{3}}\tau_o \left|\frac{\partial V}{\partial t}\right|$$

(63) $$V = \frac{1}{\rho_o} \frac{\partial X}{\partial x}$$

$$p = f(\frac{1}{V}, U) \equiv g(V, U),$$

where we have set the specific volume $\rho^{-1} = V$ and introduced the notations

$$S = -\frac{4}{3} \frac{\mu_o}{V} \frac{\partial V}{\partial t}$$

(64) $$Q = \begin{cases} \frac{(\rho_o \ell)^2}{V} \left(\frac{\partial V^2}{\partial t}\right) & \text{if } \partial q/\partial x < 0 \\ 0 & \text{if } \partial q/\partial x \geqq 0 . \end{cases}$$

Here ℓ is a constant having the dimensions of a length.

(b) Difference Relations

Let Δx and Δt be small increments of the variables x and t. Then the set of points in x, t-space given by $x = j\Delta x$, $t = n\Delta t$, where $j, n = 0, 1, 2, \cdots$ is called a net (or grid or lattice) whose mesh size is determined by Δx and Δt. The approximation to $g(x, t)$ at the point $(j\Delta x, n\Delta t)$ is denoted by $g(j\Delta x, n\Delta t)$ or simply by

(65) $$g_j^n = g(j\Delta x, n\Delta t) .$$

There will be a need to define some of the dependent variables at space mesh stations midway between those corresponding to integral values of j. The values at these substations are denoted by

(66) $$g_{j+1/2}^n = \frac{1}{2}(g_j^n + g_{j+1}^n) .$$

For space differences the following notation will be used

$$(\delta g)_j^n = g((j + 1/2)\Delta x, n\Delta t) - g((j - 1/2)\Delta x, n\Delta t)$$

(67) $$= g_{j+1/2}^n - g_{j-1/2}^n .$$

Many finite difference systems have been devised for problems involving perfect fluids, Reference 35. The one most used will be adjusted to accommodate formulation (63) and (64):

$$(68)\qquad \frac{X_j^{n+1} - X_j^n}{\Delta t} = q_j^{n+1}$$

$$(69)\qquad \frac{q_j^{n+1} - q_j^n}{\Delta t} = -\frac{1}{\rho_o}\,\frac{(\delta p)_j^n + (\delta Q)_j^n + (\delta S)_j^n}{\Delta x}$$

$$(70)\qquad V_{j+1/2}^{n+1} = \frac{1}{\rho_o}\,\frac{X_{j+1}^{n+1} - X_j^{n+1}}{\Delta x}$$

$$(71)\qquad \frac{U_{j+1/2}^{n+1} - U_{j+1/2}^n}{\Delta t} + \left[p_{j+1/2}^n + Q_{j+1/2}^{n+1} + S_{j+1/2}^{n+1}\right]\,\frac{V_{j+1/2}^{n+1} - V_{j+1/2}^n}{\Delta t}$$
$$= \sqrt{\frac{4}{3}}\;\tau_o\left|\frac{V_{j+1/2}^{n+1} - V_{j+1/2}^n}{\Delta t}\right|$$

$$(72)\qquad p_{j+1/2}^{n+1} = f\left(\frac{1}{V_{j+1/2}^{n+1}}\,,\ U_{j+1/2}^{n+1}\right) = g\left(V_{j+1/2}^{n+1}\,,\ U_{j+1/2}^{n+1}\right)$$

$$(73)\qquad S_{j+1/2}^n = -\frac{8}{3}\,\frac{\mu_o}{V_{j+1/2}^n + V_{j+1/2}^{n-1}}\,\frac{V_{j+1/2}^n - V_{j+1/2}^{n-1}}{\Delta t}$$

$$(74)\qquad Q_{j+1/2}^n = \begin{cases} \dfrac{2(a\rho_o\Delta x)^2}{V_{j+1/2}^n + V_{j+1/2}^{n-1}}\left(\dfrac{V_{j+1/2}^n - V_{j+1/2}^{n-1}}{\Delta t}\right)^2 & \text{if } V_{j+1/2}^n < V_{j+1/2}^{n-1} \\ 0 & \text{Otherwise} \end{cases}$$

In (74) we have set $\ell = a\Delta x$, where a is a dimensionless constant approximately 1.5 to 2.0.

Equations (68) through (74) are the formulas required to carry out the stepwise computations. One starts the calculation by obtaining initial values (i.e., for time $t = 0$ or $n = 0$) of all quantities at all stations (and substations $j + 1/2$). The values of the quantities for the instant of time corresponding to $n = 1$ are first obtained at all stations. These values are then substituted

into the equations to evaluate the quantities at all stations for the instant of time corresponding to n= 2, etc. The procedure used in going from the instant n to the instant n + 1 is as follows:

a) Compute q^{n+1} from (69)

b) Compute X^{n+1} from (68)

c) Compute V^{n+1} from (70)

d) Compute S^{n+1} from (73)

e) Compute Q^{n+1} from (74)

f) Compute U^{n+1} from (71)

g) Solve (72) for p^{n+1}.

In all these calculations the values at the substations $j+1/2$ are computed according to (67). A flow chart describing the step-by-step numerical procedure is given in Fig. 16.

(c) Initial and Boundary Conditions

To use the above scheme of calculation the initial values (i.e. at time $t=0$ and at all points of the mesh) of all the dependent variables must be known. At the instant of impact their values are known everywhere except at the interface between the impacting bodies. These initial boundary values may be approximated by applying the Rankine-Hugoniot relations to the abrupt pressure profiles which emanate from the impact interface.

The relations are derived from the conditions that mass, momentum and energy are conserved across the shocks. The corresponding equations are, Reference 36,

$$\rho_o u_o = \rho_1 u_1$$

$$\rho_o u_o^2 + p_o = \rho_1 u_1^2 + p_1 \tag{75}$$

$$1/2\, u_o^2 + U_o + p_o V_o = 1/2\, u_1^2 + U_1 + p_1 V_1 .$$

The equation of state of the material provides a fourth relationship. The subscripts "0" and "1" refer to material in front of and behind the shock wave respectively. Here u_i is the flow velocity of the material relative to the shock wave.

Figure 15a illustrates the impact situation in laboratory coordinates before impact and at the instant of impact. In Fig. 17a the nomenclature used to depict the situation just after impact is illustrated. Since the two bodies may be of different materials an additional subscript has been introduced to make this distinction. The initial data is represented schematically in Fig. 17b. In Appendix A there are presented the detailed algebraic manipulations necessary to obtain the initial boundary data when the impacting bodies are of different materials.

In the special case that the two impacting bodies are of the same material $d_1 = d_2 = d$ and (A-17), (A-18) reduce to the single equation

$$(76) \qquad \frac{v_o^2}{4} d = f\left(\frac{\rho_o}{1 - \rho_o/d}, \frac{v_o^2}{8}\right) .$$

Now (76) can easily be solved for d by a machine program, and the dependent variables subsequently evaluated by (A-9) through (A-16),

$$(77) \qquad \begin{aligned} p_i &= v_o^2 d/4 \qquad \rho_1/\rho_o = (1 - \rho_o/d)^{-1} \qquad q_i = v_o/2 \\ U &= v_o^2/8 \qquad W_1 = (v_o/2)\ (2 - \rho_1/\rho_o)\ (\rho_1/\rho_o - 1)^{-1} \\ W_2 &= (v_o/2)\ (\rho_1/\rho_o)\ (\rho_1/\rho_o - 1)^{-1} \end{aligned}$$

The calculations have been carried out for iron-iron, copper-copper, aluminum-aluminum, cadmium-cadmium, tin-tin and lead-lead impact. The results for p_i vs v_o, U vs v_o and ρ_1/ρ_o vs v_o are plotted in Figures 18, 19 and 20 respectively. In Figure 21 the corresponding Hugoniot curves p_i vs V_1 $(= 1/\rho_1)$ are plotted.

(d) Stability and Convergence

Having formulated the governing differential equations as well as the initial and boundary conditions in finite difference form, consider next the choice of space-mesh size Δx and time mesh size Δt. Suppose that Δx has been assigned a value sufficiently small to allow a satisfactory definition of the flow. If Δt is chosen too large the calculation will not converge but will oscillate with increasing amplitude as n increases. This phenomenon, called instability, has nothing to do with round-off error, but is a property of the difference system (68) through (74). In fact, the error would only be made worse by taking a smaller value of Δr, unless Δt is also suitably reduced.

In Appendix B a stability analysis of the explicit difference system is presented in some detail; the essential results are contained in (B-22) and (B-24).

To apply criterion (B-22) we recall that

$$\frac{\partial V}{\partial t} = \frac{1}{\rho_o} \frac{\partial q}{\partial x}$$

and approximate $\partial q/\partial x$ by $-v_o/2\Delta x$. Here $v_o/2$ represents the velocity of the interface as calculated from the Rankine-Hugoniot conditions. In our calculations we have chosen $\ell = a\,\Delta x$, $a = 1.5$, so that the criterion reduces to

$$(78) \qquad \frac{\Delta t}{(\Delta x)^2} \leqq \frac{\rho_o{}^2 V}{\frac{8}{3}\mu_o + 4.5\ \rho_o v_o\ \Delta x}$$

The value for $V = 1/\rho$ may be approximated by the Hugoniot curve for the particular material, Fig. 21.

Now, in regions away from the shock $p \gg Q + \sqrt{\frac{4}{3}}\ \tau_o$ and condition (B-24) becomes roughly

$$\frac{\Delta t}{\Delta x} \leqq \frac{\rho_o}{2\sqrt{2\ \left|\frac{\partial g}{\partial V} - p\frac{\partial g}{\partial U}\right|}}$$

The adiabatic sound speed c is equal to *

$$c = V\sqrt{\frac{\partial g}{\partial V} - p\frac{\partial g}{\partial U}} = c_o\ \sqrt{\rho_o\ V}\ .$$

Consequently, in regions other than those containing a shock,

$$(79) \qquad \frac{\Delta t}{\Delta x} \leqq \sqrt{\frac{\rho_o\ V}{8\ c_o{}^2}} \qquad (\mu_o = 0)$$

is the approximate stability criterion.

---

* In an adiabatic process $dU + p\,dV = 0$. Since $p = g(V, U)$ we may write $dp = dV\,\partial g/\partial V + dU\,\partial g/\partial U$. Elimination of dU between the two yields $dp = (\partial g/\partial V - p\partial g/\partial U)\,dV = V^2(p\partial g/\partial U - \partial g/\partial V)\,d\rho$, whence

$$c^2 = dp/d\rho = V^2(p\partial g/\partial U - \partial g/\partial V).$$

If the same size mesh is to be used throughout the flow the more severe restriction on Δt must be observed, i.e. stability criterion (78). Both stability criteria have been calculated for each of the parameter combinations considered. The results are listed in Table I along with the corresponding value of Δt for the choice $\Delta x = 0.1$ cm.

The above conclusions have been substantiated by a number of machine calculations; the results are displayed in Table II, (Reference 37). The calculated requirement on Δt is seen to be a conservative estimate in each case. It may be expected that the theoretical stability criterion is close to the required condition for all the parameter combinations. For the most severe case, $\Delta t = 5.1 \times 10^{-4}$, this means that approximately 10,000 cycles are required for a 5 microsec. run. If 70 space mesh points are required this means 700,000 point calculations which would require approximately 1.4 hours on the IBM 7090.

TABLE II

Summary of preliminary runs testing stability of explicit difference scheme applied to iron-iron impact. $a = 1.5\ \ell = 1.5\ \Delta x$, $\Delta x = 0.1$.

NO.	NET SIZE		RESULT
	Theory	Trial	
1	0.03	0.100	Unstable
1	0.03	0.050	Stable
1	0.03	0.065	Stable
2	0.027	0.05	Stable
3	0.014	0.02	Stable
4	0.0023	0.005	Unstable
4	0.0023	0.0025	Unstable
4	0.0023	0.002	Stable
13	0.03	0.05	Stable
17	0.0021	0.05	Unstable
17	0.0021	0.025	Unstable
17	0.0021	0.01	Unstable
17	0.0021	0.005	Stable

IMPLICIT DIFFERENCE SCHEME

In this section there is outlined an alternate computational scheme which has been developed to reduce the machine time required for those parameter combinations with large μ_o and v_o values. It is an implicit scheme based on Eulerian formulation, whereas the original scheme is explicit and is based on the Lagrangian formulation. The new scheme is only valid for impact between bodies of identical material with $\mu_o \neq o$. Therefore it does not supersede the explicit scheme, but serves as a desirable complement.

The difference scheme has been adopted upon the suggestion of Dr. Herbert Keller, Institute of Mathematical Sciences, New York University. In treating similar systems of equations, Dr. Keller has found the implicit scheme to be unconditionally stable. Thus, no restriction on Δt and Δx is involved, only the desired accuracy need be considered in choosing the increment sizes.

(a) Difference Equations

Since the two impacting bodies are identical the phenomena are symmetric about the center of mass coordinates (Fig. 15b). The calculations will be made only for body 2 where the fixed space coordinates are denoted by (Fig. 22a) $j=0, 1, 2, \ldots$ There $\partial q/\partial z \leq 0$ and, consequently, the Eulerian formulations of the governing equations, equations (49) through (52), reduce to

$$(80) \qquad \frac{\partial \rho}{\partial t} + \frac{\partial(\rho q)}{\partial z} = 0$$

$$(81) \qquad \frac{\partial q}{\partial t} + q \frac{\partial q}{\partial z} = \frac{1}{\rho}\left[-\frac{\partial p}{\partial z} + \frac{4}{3}\mu_o \frac{\partial^2 q}{\partial z^2}\right]$$

$$(82) \qquad \frac{\partial U}{\partial t} + q \frac{\partial U}{\partial z} = \frac{1}{\rho}\frac{\partial q}{\partial z}\left[-p + \frac{4}{3}\mu_o \frac{\partial q}{\partial z} - \sqrt{\frac{4}{3}}\,\tau_o\right]$$

$$(83) \qquad p = f(\rho, U).$$

A centered difference scheme is used to provide more accuracy. To illustrate the process the details will be carried out for equation (80). The scheme is centered at point $z=j\Delta z$, $t=(n+1/2)\,\Delta t$ as shown

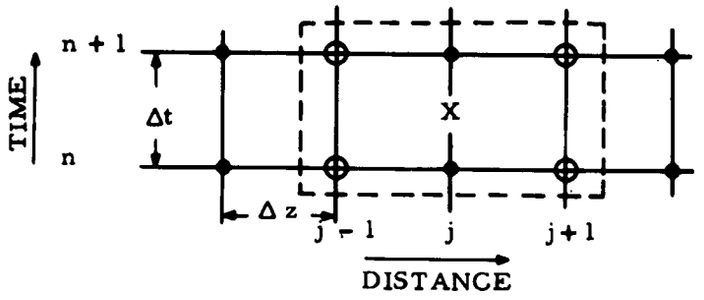

O points used in (80), (82)

● points used in (81)

X denotes center point

in the sketch. Equation (80) is replaced by

$$\frac{1}{2}\left\{\frac{\rho_{j-1}^{n+1}-\rho_{j-1}^{n}}{\Delta t}+\frac{\rho_{j+1}^{n+1}-\rho_{j+1}^{n}}{\Delta t}\right\}$$

$$+\frac{1}{2}\left\{\frac{(\rho q)_{j+1}^{n+1}-(\rho q)_{j-1}^{n+1}}{2\Delta z}+\frac{(\rho q)_{j+1}^{n}-(\rho q)_{j-1}^{n}}{2\Delta z}\right\}=0$$

Similar centered schemes may be written for (81) and (82). Upon simplification the system becomes

$$(84)\quad \begin{cases} \rho_{j-1}^{n+1}-\rho_{j+1}^{n+1}=\rho_{j-1}^{n}+\rho_{j+1}^{n} \\ +\frac{1}{2}\frac{\Delta t}{\Delta z}\left\{\left[(\rho q)_{j-1}^{n+1}+(\rho q)_{j-1}^{n}\right]-\left[(\rho q)_{j+1}^{n+1}+(\rho q)_{j+1}^{n}\right]\right\} \end{cases}$$

$$(85)\quad \begin{cases} q_j^{n+1}-q_j^{n}+\frac{1}{8}\frac{\Delta t}{\Delta z}\left(q_j^{n+1}+q_j^{n}\right)\left[q_{j+1}^{n+1}-q_{j-1}^{n+1}+q_{j+1}^{n}-q_{j-1}^{n}\right] \\ =\frac{1}{2}\frac{\Delta t}{\Delta z}\frac{1}{\rho_j^{n+1}+\rho_j^{n}}\left\{\left[p_{j+1}^{n+1}-p_{j-1}^{n+1}+p_{j+1}^{n}-p_{j-1}^{n}\right]\right. \\ \left.+\frac{8}{3}\frac{\mu_o}{\Delta z}\left[q_{j+1}^{n+1}-2q_j^{n+1}+q_{j-1}^{n+1}+q_{j+1}^{n}-2q_j^{n}+q_{j-1}^{n}\right]\right\} \end{cases}$$

$$U_{j-1}^{n+1} + U_{j+1}^{n+1} - \left[U_{j-1}^{n} + U_{j+1}^{n}\right]$$

$$+\frac{1}{8}\frac{\Delta t}{\Delta z}\left[q_{j-1}^{n+1} + q_{j+1}^{n+1} + q_{j+1}^{n} + q_{j-1}^{n}\right]\left[U_{j+1}^{n+1} - U_{j-1}^{n+1} + U_{j+1}^{n} - U_{j-1}^{n}\right]$$

$$(86) \quad = \frac{\Delta t}{\Delta z}\frac{q_{j+1}^{n+1} - q_{j-1}^{n+1} + q_{j+1}^{n} - q_{j-1}^{n}}{\rho_{j-1}^{n+1} + \rho_{j+1}^{n+1} + \rho_{j+1}^{n} + \rho_{j-1}^{n}}\left\{-2\sqrt{\frac{4}{3}}\tau_o\right.$$

$$\left. - \frac{1}{2}\left[p_{j-1}^{n+1} + p_{j+1}^{n+1} + p_{j+1}^{n} + p_{j-1}^{n}\right] + \frac{2}{3}\frac{\mu_o}{\Delta z}\left[q_{j+1}^{n+1} - q_{j-1}^{n+1} + q_{j+1}^{n} - q_{j-1}^{n}\right]\right\}$$

The required pressure values are computed from (83) according to

$$p_{j-1}^{n+1} = f\left(\rho_{j-1}^{n+1},\ U_{j-1}^{n+1}\right)$$

$$(87) \quad p_{j+1}^{n+1} = f\left(\rho_{j+1}^{n+1},\ U_{j+1}^{n+1}\right)$$

$$p_{j+1}^{n} = f\left(\rho_{j+1}^{n},\ U_{j+1}^{n}\right)$$

$$p_{j-1}^{n} = f\left(\rho_{j-1}^{n},\ U_{j-1}^{n}\right).$$

(b) Initial and Symmetry Conditions

The initial, $n = 0$, values of the dependent variables ρ, q, U, p are all known from the Rankine-Hugoniot equations (Fig. 22b). To determine their values at all other time intervals a method of computing the values at time $n + 1$ from those known at time n must be made available. An iteration technique will be devised for this purpose. The following relations, which follow from the symmetry of the problem, will be utilized:

$$(88) \quad \rho_{-j}^{n} = \rho_{j}^{n},\ q_{-j}^{n} = -q_{j}^{n} \ (\text{hence } q_{0}^{n} = 0)$$

$$U_{-j}^{n} = U_{j}^{n},\ p_{-j}^{n} = p_{j}^{n}.$$

(c) Iteration Procedure

To start the iteration let

$$(89) \qquad \tilde{q}^{\,n+1}_{j\,(0)} = q^{n}_{j}\,, \quad \tilde{U}^{n+1}_{j\,(0)} = U^{n}_{j}$$

be zero-order approximations to q_j^{n+1} and U_j^{n+1} respectively. Then the first-order approximations are calculated in the following sequence:*

(a-1) Substitute $q_j^{n+1} = \tilde{q}^{\,n+1}_{j\,(0)}$ into (84) and calculate $\tilde{\rho}^{\,n+1}_{j\,(1)}$ from the resulting two-term recurrence relation (n + 1 fixed, j varied):

$$\tilde{\rho}^{\,n+1}_{j-1(1)} + \tilde{\rho}^{\,n+1}_{j+1(1)} = \rho^{n}_{j-1} + \rho^{n}_{j+1} + \frac{1}{2}\frac{\Delta t}{\Delta z}\left\{\left[\tilde{\rho}^{\,n+1}_{j-1(1)}\ \tilde{q}^{\,n+1}_{j-1(0)} + (\rho q)^{n}_{j-1}\right]\right.$$

$$(90) \qquad \left. -\left[\tilde{\rho}^{\,n+1}_{j+1(1)}\ \tilde{q}^{\,n+1}_{j+1(0)} + (\rho q)^{n}_{j+1}\right]\right\}$$

Several methods of performing the calculations are discussed below in section (d).

(b-1) To obtain a trial value for p_j^{n+1} use (87) with $\rho_j^{n+1} = \tilde{\rho}^{\,n+1}_{j(1)}$ and $U_j^{n+1} = \tilde{U}^{n+1}_{j(0)}$:

$$(91) \qquad \tilde{p}^{\,n+1}_{j(1')} = f\left(\tilde{\rho}^{\,n+1}_{j\,(1)}\,,\ \tilde{U}^{n+1}_{j(0)}\right).$$

(c-1) To obtain a first-order approximation for U_j^{n+1} use (86) with q_j^{n+1}, ρ_j^{n+1}, p_j^{n+1} replaced by $\tilde{q}^{\,n+1}_{j\,(0)}$, $\tilde{\rho}^{\,n+1}_{j\,(1)}$, $\tilde{p}^{\,n+1}_{j\,(1')}$ respectively:

$$\tilde{U}^{\,n+1}_{j-1\,(1)} + \tilde{U}^{\,n+1}_{j+1\,(1)} - \left[U^{n}_{j-1} + U^{n}_{j+1}\right]$$

$$+ \frac{1}{8}\frac{\Delta t}{\Delta z}\left[\tilde{q}^{\,n+1}_{j-1(0)} + \tilde{q}^{\,n+1}_{j+1(0)} + q^{n}_{j+1} + q^{n}_{j-1}\right]\left[\tilde{U}^{\,n+1}_{j+1(1)} - \tilde{U}^{\,n+1}_{j-1(1)} + U^{n}_{j+1} - U^{n}_{j-1}\right]$$

$$(92) \qquad = \frac{\Delta t}{\Delta z}\,\frac{\tilde{q}^{\,n+1}_{j+1\,(0)} - \tilde{q}^{\,n+1}_{j-1(0)} + q^{n}_{j+1} - q^{n}_{j-1}}{\tilde{\rho}^{\,n+1}_{j-1(1)} + \tilde{\rho}^{\,n+1}_{j+1\,(1)} + \rho^{n}_{j+1} + \rho^{n}_{j-1}}\left\{ - 2\sqrt{\frac{4}{3}}\,\tau_o \right. \qquad \text{(continued)}$$

* This procedure is adopted upon the suggestion of Dr. Herbert Keller, Institute of Mathematical Sciences, New York University.

$$- \frac{1}{2}\left[\tilde{p}_{j-1(1')}^{n+1} + \tilde{p}_{j+1(1')}^{n+1} + p_{j+1}^{n} + p_{j-1}^{n}\right]$$

$$+ \frac{2}{3}\frac{\mu_o}{\Delta z}\left[\tilde{q}_{j+1(0)}^{n+1} - \tilde{q}_{j-1(0)}^{n+1} + q_{j+1}^{n} - q_{j-1}^{n}\right]\Bigg\} .$$

As with ρ, we have here a two-term linear recurrence relation for $\tilde{U}_{j(1)}^{n+1}$. Its solution is also discussed in section (d).

(d-1) A first-order approximation for p_j^{n+1} is now computed from (87) with $\rho_j^{n+1} = \tilde{\rho}_{j(1)}^{n+1}$ and $U_j^{n+1} = \tilde{U}_{j(1)}^{n+1}$

$$(93) \qquad \tilde{p}_{j(1)}^{n+1} = f\left(\tilde{\rho}_{j(1)}^{n+1}, \tilde{U}_{j(1)}^{n+1}\right) .$$

(e-1) To calculate a first-order approximation for q_j^{n+1} use (85) with $\rho_j^{n+1} = \tilde{\rho}_{j(1)}^{n+1}$, $p_j^{n+1} = \tilde{p}_{j(1)}^{n+1}$ and replace q_j^{n+1} in the difference expression for $q\ \partial q/\partial z$ by $\tilde{q}_{j(0)}^{n}$. The latter substitution linearizes the equation for $\tilde{q}_{j(1)}^{n+1}$, giving

$$\tilde{q}_{j(1)}^{n+1} - q_j^n + \frac{1}{8}\frac{\Delta t}{\Delta z}\left(\tilde{q}_{j(0)}^{n+1} + q_j^n\right)\left[\tilde{q}_{j+1(0)}^{n+1} - \tilde{q}_{j-1(0)}^{n+1} + q_{j+1}^{n} - q_{j-1}^{n}\right]$$

$$(94) \qquad = \frac{1}{2}\frac{\Delta t}{\Delta z}\frac{1}{\tilde{\rho}_{j(1)}^{n+1} - \rho_j^n}\Bigg\{\left[\tilde{p}_{j+1(1)}^{n+1} - \tilde{p}_{j-1(1)}^{n+1} + p_{j+1}^{n} - p_{j-1}^{n}\right]$$

$$+ \frac{8}{3}\frac{\mu_o}{\Delta z}\left[\tilde{q}_{j+1(1)}^{n+1} - 2\tilde{q}_{j(1)}^{n+1} + \tilde{q}_{j-1(1)}^{n+1} + q_{j+1}^{n} - 2q_j^n + q_{j-1}^{n}\right]\Bigg\} .$$

This is a three-term linear recurrence relation for $\tilde{q}_{j(1)}^{n+1}$ ($n+1$ fixed, j varied); a method of solution is discussed below in section (e).

The second-order approximations are calculated by merely repeating the iteration process: (a-2), (b-2), ..., (e-2). The resulting equations differ from the corresponding equations of the first iteration only in that the subscripts (1), (2) replace the subscripts (0), (1) respectively.

In general, to proceed from the k-order approximation to the (k+1) - order approximation we go through the above iteration process (with subscripts (0), (1) replaced by k and k+1 respectively). The process is repeated until a reasonable convergence criterion is satisfied. Usually, only a few cycles are required in such schemes.

Assume that it has been decided that K iterations are sufficient. Then set

$$\rho_j^{n+1} = \tilde{\rho}_j^{n+1}{}_{(K)}, \quad q_j^{n+1} = \tilde{q}_j^{n+1}{}_{(K)}, \quad U_j^{n+1} = \tilde{U}_j^{n+1}{}_{(K)}, \quad p_j^{n+1} = \tilde{p}_j^{n+1}{}_{(K)},$$

and proceed to the n + 2 time step. A flow chart describing the numerical procedure is given in Fig. 23.

(d) Two-Term Recurrence Relations

It is a consequence of the symmetry relations (88) that when j=0 the two-term recurrence relation (a-1) simplifies and yields the explicit formula

$$(95) \qquad \tilde{\rho}_{1\,(1)}^{n+1} = \rho_1^n \, \frac{1 - \frac{1}{2}\frac{\Delta t}{\Delta z} q_1^n}{1 + \frac{1}{2}\frac{\Delta t}{\Delta z} \tilde{q}_{1\,(0)}^{n+1}} .$$

Now (a-1) may be used to compute $\tilde{\rho}_j^{n+1}{}_{(1)}$ at all the odd j space-mesh points:

$$(96) \qquad \tilde{\rho}_{j+2\,(1)}^{n+1} \left[1 + \frac{1}{2}\frac{\Delta t}{\Delta z} \tilde{q}_{j+2(0)}^{n+1}\right] + \tilde{\rho}_{j(1)}^{n+1} \left[1 - \frac{1}{2}\frac{\Delta t}{\Delta z} q_{j(1)}^{n+1}\right]$$

$$= \rho_{j+2}^n \left[1 - \frac{1}{2}\frac{\Delta t}{\Delta z} q_{j+2}^n\right] + \rho_j^n \left[1 + \frac{1}{2}\frac{\Delta t}{\Delta z} q_j^n\right]$$

Thus, set j = 1 and compute $\tilde{\rho}_3^{n+1}{}_{(1)}$ in terms of $\tilde{\rho}_1^{n+1}{}_{(1)}$, set j = 3 and compute $\tilde{\rho}_5^{n+1}{}_{(1)}$ in terms of $\tilde{\rho}_{3\,(1)}^{n+1}$, etc.

The $\tilde{\rho}_j^{n+1}{}_{(1)}$ at even j are determined by the continuity of ρ ——— for sufficiently large j, $\rho_j^{n+1} = \rho_0$ (the density of the undisturbed medium, which has not yet been reached by the shock wave). Let J denote such a large even integer at time $t = (n+1)\,\Delta t$. Then $\tilde{\rho}_{J\,(1)}^{n+1} = \rho_0$ and the recursion formula is used to calculate from right to left. Thus, set j = J - 2 and compute $\tilde{\rho}_{J-2\,(1)}^{n+1}$ in terms of $\tilde{\rho}_J^{n+1}{}_{(1)}$, set j = J - 4 and compute $\tilde{\rho}_{J-4\,(1)}^{n+1}$ in terms of $\tilde{\rho}_{J-2\,(1)}^{n+1}$, etc.

A suitable value for J may be found by first making the calculations for the odd valued mesh points until $\tilde{\rho}_j^{n+1}{}_{(1)}$ has decreased to the value ρ_0. This value is then taken to be J - 1. This left-to-right-to-left technique is depicted in the sketch.

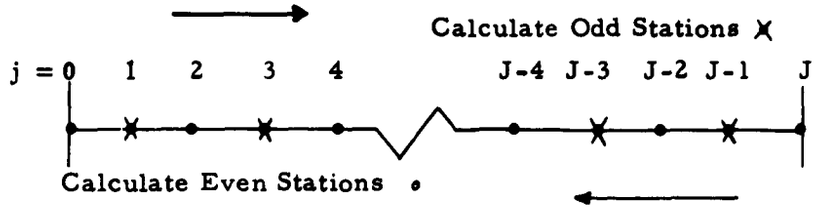

Alternatively, the choice for J may be made from a knowledge of the propagation velocity of the disturbance. Then the calculations for both the odd and the even stations may be performed from right-to-left. The advantage of this procedure is that equation (95) may then be reserved to check the calculations.

The remarks made above are also applicable to the two-term linear recurrence relation for $\tilde{U}_j^{\,n+1}_{(1)}$. Here the symmetry relations together with (92), with j=0, yield the explicit equation

$$(97)\qquad \tilde{U}_1^{\,n+1}_{(1)} = U_1^{\,n} + \frac{\Delta t}{\Delta z}\,\frac{\tilde{q}_{1\,(0)}^{\,n+1} + q_1^{\,n}}{\tilde{\rho}_1^{\,n+1}_{(1)} + \rho_1^{\,n}}\left\{-\sqrt{\frac{4}{3}}\,\tau_o\right.$$

$$\left. -\frac{1}{2}\left[\tilde{p}_{1\,(1')}^{\,n+1} + p_1^{\,n}\right] + \frac{2}{3}\,\frac{\mu_o}{\Delta z}\left[\tilde{q}_1^{\,n+1}_{(0)} + q_1^{\,n}\right]\right\}.$$

By replacing the word "density" by "specific internal energy" the remainder of the discussion on solving the recurrence relation also carries over.

(e) Three-Term Recurrence Relation

Relation (94) may be rewritten in the form

$$(98)\qquad -A_j\,\tilde{q}_{j+1\,(1)}^{\,n+1} + B_j\,\tilde{q}_{j\,(1)}^{\,n+1} - C_j\,\tilde{q}_{j-1\,(1)}^{\,n+1} = D_j$$

where Aj, Bj, Cj, Dj are known quantities:

$$A_j = \frac{4}{3}\,\mu_o\,\frac{\Delta t}{(\Delta z)^2}\,\frac{1}{\tilde{\rho}_j^{\,n+1}_{(1)} + \rho_j^{\,n}}$$

$$(99)\qquad B_j = 1 + 2A_j \qquad C_j = A_j$$

$$D_j = q_j^n - \frac{1}{8}\frac{\Delta t}{\Delta z}\left(\tilde{q}_{j\,(0)}^{\,n+1} + q_j^n\right)\left[\tilde{q}_{j+1\,(0)}^{\,n+1} - \tilde{q}_{j-1\,(0)}^{\,n+1} + q_{j+1}^n - q_{j-1}^n\right]$$

$$(100)\qquad + \frac{1}{2}\frac{\Delta t}{\Delta z}\frac{1}{\tilde{\rho}_{j\,(1)}^{\,n+1} + \rho_j^n}\left\{\left[\tilde{p}_{j+1\,(1)}^{\,n+1} - \tilde{p}_{j-1\,(1)}^{\,n+1} + p_{j+1}^{n+1} - p_{j-1}^n\right]\right.$$

$$\left. + \frac{8}{3}\frac{\mu_o}{\Delta z}\left[q_{j+1}^n - 2q_j^n + q_{j-1}^n\right]\right\}$$

A method for solving such a three-term linear recurrence relation which is particularly suitable for machine calculations is taken from Richtmyer, (Reference 35, p. 101)

The required inequalities $A_j>0$, $B_j>0$, $C_j>0$ and $B_j>A_j + C_j$ are all seen to be satisfied. The only other requirement is that q_j^{n+1} be specified at the left and right hand boundaries of the space mesh, j=0 and j=J:

$$(101)\qquad \tilde{q}_{0(1)}^{n+1} = 0 \qquad \tilde{q}_{J\,(1)}^{n+1} = -v_o/2\ .$$

NUMERICAL RESULTS

The various combinations of assumptions for μ_o, τ_o and v_o for which calculations have been made are displayed in Table I. In computing the values for dimensionless parameters, B_o and R_o, shown there the characteristic length is taken as unity. This choice is meaningful only after a stable wave has been established. In Figures 24 through 35 the results of the calculations are illustrated by pressure profiles for a number of typical parameter combinations. Some additional profile plots have been presented elsewhere (Reference 38).

To check the accuracy of the program the calculations for cases No. 1 ($v_o = 0.5$, $\tau_o = 0$, $\mu_o = 0$) and No. 49 ($v_o = 1.0$, $\tau_o = 0$, $\mu_o = 0$) have been examined in detail. The computed pressure profiles are depicted in Figures 24 and 34. The figures show that a stable shock front is quickly established. For comparison, the Rankine-Hugoniot solutions, applicable since here $\mu_o = \tau_o = 0$, are also shown at t= 1 and t= 5 microseconds. The other calculated dependent variables behind the stable shock may also be compared with the corresponding Rankine-Hugoniot values for those cases where $\mu_o = \tau_o = 0$. This is done in Table III for cases No. 17 ($v_o = 4.0$, $\tau_o = 0$, $\mu_o = 0$) and No. 33 ($v_o = 7.5$, $\tau_o = 0$, $\mu_o = 0$) as well as Nos. 1 and 49. The computed quantities represent mean values about which there are small oscillations at the various mesh points behind the front. The agreement is seen to be quite satisfactory.

The effect of viscosity on the amplitude and duration of the transient pressure profile which occurs immediately after impact is illustrated by comparing Figures 24a, 25a, 26a and 27. For all these cases, Nos. 1, 2, 3 and 4 respectively, the impact velocity and yield strength are the same ($v_o = 0.5$, $\tau_o = 0$). When $\mu_o = 0$ (No. 1) the interfacial pressure builds up to the final stable profile amplitude. For $\mu_o > 0$, however, the material near the interface is seen to be subjected to very large pressures in the first few tenths of microseconds. Subsequently, the interfacial pressure decreases from the original higher magnitude to the final stable profile amplitude. For $\mu_o = 0.08$ (No. 2) the duration of the overshoot is less than 0.4 microsecond; for $\mu_o = 0.8$ (No. 3) the duration is less than 0.8 microsecond; for $\mu_o = 8.0$ the duration of the overshoot persists for 5 microseconds. The amplitude of the transient pressure pulse also increases with an increase in μ_o.

The effect of viscosity on the characteristics of the stable pressure profile is illustrated by comparing Figures 24b, 25b, 26b and 27. These again correspond to cases Nos. 1, 2, 3 and 4 respectively. When $\mu_o = 0$ and $\mu_o = 0.08$ the thickness of the stable profile is about 0.2 cm. This is due to the artificial viscosity term. But for μ_o the thickness becomes 0.7 cm

TABLE III

Rankine-Hugoniot values compared with finite-difference calculations for one-dimensional iron-iron impact ($\mu_o = \tau_o = 0$). VP denotes velocity of stable profile relative to the interface.

		p	$1/\rho$	U	VP
Case 1 ($v_o = .5$)	Hugoniot	1.565	0.0873	0.0312	0.5466
	Computed	1.541	0.0867	0.0265	0.534
Case 49 ($v_o = 1$)	Hugoniot	4.646	0.0734	0.125	0.682
	Computed	4.601	0.0734	0.122	0.673
Case 17 ($v_o = 4$)	Hugoniot	49.62	.04662	2.0	1.157
	Computed	48.5927	.046869	2.02275	1.159
Case 33 ($v_o = 7.5$)	Hugoniot	154.2	.03601	7.031	1.481
	Computed	153.6917	.036368	7.1429	1.462

and when $\mu_o = 8.0$ it is greater than 5 cm. In the latter case, R_o & $B_o < 1$ and it might be anticipated that the viscous terms would predominate. The amplitude and velocity are only slightly increased by increasing μ_o. The time required for the stable profile to be established varies from less than 2 microseconds for $\mu_o = 0$ to approximately 10 microseconds for $\mu_o = 8.0$.

The effect of impact velocity is illustrated by comparing Figures 27, 35 and 31. These correspond to cases No. 4 ($v_o = 0.5, \tau_o = 0, \mu_o = 8$), No. 52 ($v_o = 1.0, \tau_o = 0, \mu_o = 8$) and No. 20 ($v_o = 4.0, \tau_o = 0, \mu_o = 8$) respectively. The duration of the transient pressure pulse is observed to decrease from about 5 microseconds for $v_o = 0.5$ to about 1 microsecond at $v_o = 1.0$, to less than 0.6 microsecond at $v_o = 4.0$. The stable profile becomes steeper as the impact velocity is increased. Naturally the amplitude and velocity of the wave are increased when v_o is increased.

To illustrate the effects of varying μ_o and v_o, results for cases where $\tau_o = 0$ have been cited, i.e. results for viscous liquids; the same effects are produced if τ_o is held equal to some reasonable positive value. To understand the behavior of such a visco-plastic medium refer to equation (62) and observe that in front of the disturbance $\partial q/\partial x = 0$, in the disturbance $\partial q/\partial x < 0$ and, finally $\partial q/\partial x$ drops back to zero after the disturbance passes. Consequently, $\tau^2 > \tau_o^2$ in the disturbance, but τ^2 drops to τ_o^2 after it passes. This means, in terms of our visco-plastic model, that there is flow only in that part of the medium through which the disturbance is currently passing; it again becomes rigid behind the disturbance. This phenomenon is illustrated in Figure 36 where the value of τ^2 (which is a measure of the distortion of the medium) is shown at various time intervals for two typical parameter combinations (Nos. 14 and 15). At each instant $\tau^2 > \tau_o^2$ is seen only in a finite region which represents the current position of the disturbance. Only in this moving region of disturbance does the medium behave as a viscous liquid. The region is more spread out the greater the value of μ_o.

Comparison of Figures 26b, 28 and 29 (cases Nos. 3, 7, 11 respectively) shows that even with an impact velocity as low as $v_o = 0.5$ cm/microsecond there is little change effected on the stable profile by inclusion of the yield stress if it is as low as $\tau_o = 0.01$ or $\tau_o = 0.1$. Only small increases in the pressure and in the disturbance velocity are apparent. This might be expected since for all these parameter combinations the ratios $B_o : R_o$ and $1 : R_o$ are small, i.e., the inertial terms predominate. A condition to keep in mind is that in an actual cratering process the flow velocity must always decrease to the point where τ_o is important.

On the other hand, comparison of Figure 26 (case No. 3) with Figure 30 (case No. 15) shows that both the amplitude and the velocity of the pressure pulse are significantly increased by the inclusion of the strength term if it is as large as $\tau_o = 1.0$. The shape of the pulse, however, is apparently not strongly affected, nor is the time required for the profile to be stabilized. For these cases the inertial and strength terms are both important, $R_o : B_o = 1.97$.

The characteristics of the stable profiles for all the various cases are depicted in Figures 37, 38 and 39. There p denotes the pressure behind the disturbance; ΔP and VP denote the thickness and velocity (relative to the interface) of the stable pressure profile, respectively.

REMARKS ON THE EQUATION OF STATE

In our model the medium is considered to act as a viscous liquid rather than a solid, provided $\tau^2 > \tau_o^2$. It is therefore consistent with ordinary viscous fluid theory that the equation of state be given in terms of a hydraulic pressure p, equal for all directions. We have, as usual, taken $p = -(\tau_{rr} + \tau_{\theta\theta} + r_{zz})/3$ as the thermodynamic pressure.

The particular equation of state employed in the calculations, $p = f(\rho, U)$, was determined by the Los Alamos group from measurements on pressure pulses induced by high explosive. The method is indirect in that the observed quantities are the pulse velocity and the free-surface velocity produced by normal reflection of the pulse from a free boundary. Pressure (strictly, stress normal to the wave front, $-\tau_{zz}$) and corresponding values of internal energy and density were computed from these measurements by means of the Rankine-Hugoniot relations. An equation of state based on the assumption that $\mu_o = \tau_o = 0$ has thus been employed to calculate the behavior of a model for the material which assumes that these parameters are not zero. This certainly leads to errors but they are of second order and would not be expected to mask the effect of including the viscous and plastic terms in the other equations governing the model. The results have borne this out since, as physical reasoning would imply, μ_o chiefly affects the shape of the stable disturbance and τ_o has its main effect on its amplitude. At lower velocities, τ_o would also affect the shape.

Other remarks on the equation of state are also relevant. In converting the measured velocities to pressure-energy-density states it was tacitly assumed that a stable, abrupt disturbance was obtained. Verification by direct measurement of the pressure profile has not been possible, and justification for the assumptions is based on the reasonable agreement with extrapolation of hydrostatic data. This should not be construed as proof that the viscosity and strength effects are negligible, however, since even with viscosity factors as large as $\mu_o = 0.8$ and yield stress as great as $\tau_o = 0.1$, when $v_o = .5$, the differences in the velocity and amplitude of the stable pressure would be difficult to observe by such measurements.

The fact that $-\tau_{zz}$ and not p is the actual pressure reflected from the free surface in the experiments may not greatly affect the equation of state calculations since the shape, velocity, and amplitude of the stable p and $-\tau_{zz}$ profiles are nearly identical. To see this compare Figures 26b, 27 and 30b with Figures 40, 41 and 42 respectively; these show the two corresponding profiles for three typical cases, Nos. 3, 4, 15.

Prior to the establishment of a stable profile, however, the components of the deformation stress tensor, of which $\tau_{zz} + p$ is one, are not small. At

the instant of impact between the two bodies a very large velocity gradient is imposed on the material near the interface. As the front of the disturbance propagates into the body the gradient at the interface decreases, and the gradient at the front of the disturbance also decreases because of the smearing action of the viscosity. From (48) is seen that the von Mises statistic, τ^2, which is a measure of the magnitude of the components of the deformation stress tensor, must act similarly. Thus when viscosity is present the material near the interface is subjected to a much greater distortion than material away from the interface. This is illustrated in Figure 36 by the envelopes of the τ^2 distributions.

These latter observations are consistent with experimental evidence that internal structural changes in a metal can be related to the distribution of stress that existed in an impulsively loaded body by plotting contours of equal hardness on sections of the body, Ref. 39. Contours were found to coincide with the isochromatics obtained in photoelastic studies, i.e., the contours lie along lines of maximum shear stress. Recent microhardness studies of one dimensional impacting plates have shown that indeed the microhardness near the impact interface is maximum, the value decreasing rapidly outside the interfacial zone, Ref. 40.

CONCLUSIONS

A visco-plastic model for hypervelocity impact has been proposed which takes into account the inertial, viscous, and plastic effects. This was accomplished by introducing a viscosity factor μ_o and a dynamic yield stress τ_o into the perfect fluid equations. From an examination of the resulting system of equations several dimensionless parameters were found which control the relative importance of the three effects at the various stages of the cratering process. The inertial effect was found to be important throughout the early stages while the strength of the medium is dominant during the final stages. Immediately after impact the viscous effect is very large in the zone near the contact interface. Its magnitude decreases as the strain-rate gradient decreases, but it may remain important throughout the flow process. The viscosity also has the important function of introducing anisotropic stresses into the flow which are essential if the strength effect is to be included.

In the absence of definitive data for μ_o and τ_o in the hypervelocity impact regime, computations were performed on a one-dimensional model in which the values of these two parameters were varied. The above qualitative conclusions were verified. Specifically, the following was found.

1) The assumption $\mu_o > 0$ results in large initial values for the pressure and deformation in a zone near the impact interface. As μ_o is increased the effect becomes greater and the disturbance propagates a greater distance before reducing to its stabilized shape and amplitude. For impact velocity $v_o = 0.5$ cm/μsec., the time the disturbance propagates before a stable profile is obtained varies from about 2 to 3 microseconds for $\mu_o = .08$ to more than 10 microseconds for $\mu_o = 8$. The required time is less the greater the impact velocity; the value of τ_o has little effect.

2) The amplitude and velocity of the stable pressure profile are only slightly increased as μ_o is increased, but its width (shape) is significantly larger. Increasing the yield strength has little effect on the shape of the stable pressure wave; it significantly increases its amplitude and velocity only if τ_o is as large as one megabar. The latter conclusion is valid for particle velocities of 0.25, 0.5 cm/microsecond and larger. At lower velocities τ_o has a more significant effect on the viscosity coefficient, see (8), and thus more effect on the pressure wave.

These conclusions may be related to the qualitative model of crater formation that has evolved from experimental studies in which the actual cratering process has been monitored, Ref. 41. The discovery was made that though only five to ten microseconds are required to use up the projectile, the crater continues to enlarge for several hundred microseconds. The mechanism of crater formation is therefore essentially one of cavitation, the size and shape of the final crater being determined by (a) the shape and amplitude of the pressure wave established during the first five to ten microseconds by the action of the projectile on the target, and (b) the resistance of the target material to flow. (c) The flow continues until the amplitude of the wave decreases below the intrinsic yield strength of the material.

The calculations presented in this paper show that the shape and amplitude of the pressure wave, (a), are in turn strongly dependent on the viscosity of the medium. This is especially true during the first microsecond after impact when the strain-rate gradient is largest. Also, the resistance of the target material to flow, (b), depends on the viscosity factor μ_o and, to a lesser degree, on the strength factor τ_o; the viscosity coefficient becomes larger and more dependent on τ_o at the smaller strain-rates. Finally, (c), the strength factor τ_o controls the instant when the flow ceases.

Thus, buth μ_o and τ_o are important in determining how long the crater continues to expand. This may explain why a crater in Lucite stops expanding earlier than one in aluminum despite the relative magnitudes of their yield strengths.

To establish the validity of this hypothesis will require experimental data which are currently not available. The necessary definitive experiments for the evaluation of μ_o and τ_o should be performed. They are likely to be one-dimensional in character. The dependence of both on the temperature of the medium should be studied, since this effect must eventually be incorporated into the refined visco-plastic model. Meanwhile, the theoretical program may be pursued by developing a numerical scheme for the calculation of the visco-plastic model under axial symmetric impact conditions.

BIBLIOGRAPHY

1. Summers, J. L., "Investigation of High-Speed Impact: Regions of Impact and Impact at Oblique Angles", NASA TN D-94, October, 1959.

2. Maiden, C. J., Tardif, H. P., and Charest, J., "An Investigation of Spalling and Crater Formation by Hypervelocity Projectiles", Canadian Armament Research and Development Establishment Technical Memorandum AB - 62, May, 1960.

3. Kineke, J. H., Jr., "An Experimental Study of Crater Formation in Lead", Proceedings of Third Symposium on Hypervelocity Impact, Armour Research Foundation Publication by F. Genevese, Vol. 1, February, 1959.

4. Atkins, W. W., "Hypervelocity Penetration Studies", Proceedings of Fourth Symposium on Hypervelocity Impact, Eglin Air Force Base, Florida, Vol. 1, September, 1960.

5. Atkins, W. W., "Hypervelocity Penetration Studies", Proceedings of Third Symposium on Hypervelocity Impact, Armour Research Foundation Publication by F. Genevese, Vol. 1, Pages 199-211, February, 1959.

6. Kineke, J. H., Jr., "An Experimental Study of Crater Formation in Metallic Targets", Proceedings of the Fourth Symposium on Hypervelocity Impact, Eglin Air Force Base, Florida, Vol. 1, September, 1960.

7. Collins, R. D., Jr., and Kinard, W. H., "The Dependency of Penetration on the Momentum Per Unit Area of the Impacting Projectile and the Resistance of Materials to Penetration", NASA TN D-238, May, 1960.

8. Culp, F. L., "Volume-Energy Relation for Craters Formed by High Velocity Projectiles", Proceedings of Third Symposium on Hypervelocity Impact, Armour Research Foundation Publication by F. Genevese, Vol. 1, Pages 141-155, February, 1959.

9. Partridge, W. S., "High Velocity Impact Studies at the University of Utah", Proceedings of the Second Hypervelocity and Impact Effects Symposium, Publication edited by Mannix, W. C., Atkins, W. W., and Clark, R. E., Vol. 1, Pages 93-107, December, 1957.

10. Van Fleet, H. B., Partridge, W. S., and Cannon, E. T., "The Anomalous Behavior of Lead-to-Lead Impact", Proceedings of the Third Symposium on Hypervelocity Impact, Armour Research Foundation Publication by F. Genevese, Vol. 1, Pages 115-135, February, 1959.

11. Van Fleet, H. B., Whited, C. R., and Partridge, W. S., "High Velocity Impact Craters in Lead-Tin Alloys", University of Utah Technical Report No. OSR-13, January, 1958.

12. Ferguson, W.J., and McKinney, K.R., "The Influence of Temperature Elevation on the Penetration of Missiles into Copper Targets", NRL Report 5407, November 19, 1959.

13. Allison, F.E., Becker, K.R., and Vitali, R., "Effects of Target Temperature and Hypervelocity Cratering", Carnegie Inst. Tech., Eighteenth Quarterly Report, Contract No. DA-36-061-ORD-513, April 30, 1960.

14. Kronman, S., and Kineke, J.H., Jr., "Explosive Devices for Projecting Hypervelocity Pellets up to 21.0 km/sec.", Presented at Fifth Symposium on Hypervelocity Impact, Denver, Colorado, October 30, 1961.

15. Bruce, E.P., "Review and Analysis of Hypervelocity Impact Data", General Electric MSVD, Final Report, Contract No. AF-04(647)-269, September 29, 1960.

16. Herrmann, W., and Jones, A.H., "Correlation of Hypervelocity Impact Data", Paper presented at the Fifth Symposium on Hypervelocity Impact in Denver, Colorado, October 31, 1961.

17. Grimminger, G., "Probability that a Meteorite Will Hit or Penetrate a Body Situated in the Vicinity of the Earth", Journal of Applied Physics, Vol. 19, p. 947, 1948.

18. Bohn, J. L., and Fuchs, J. P., "High Velocity Impact Studies Directed Towards the Determination of the Spatial Density, Mass and Velocity of Micrometeorites at High Altitudes", Contract No. AF 19(604)-1894, Scientific Report No. 1, ASTIA AD 243106.

19. Opik, E., "Researches on the Physical Theory of Meteor Phenomena: I Theory of the Formation of Meteor Craters", Acta et Comm. Univ. Tartuensis, 1936.

20. Whipple, F.L. "Vistas in Astronautics 1958: The Meteoric Risk to Space Vehicles", Pergamon Press, N.Y. (1958), pp 115-124.

21. Langton, N.H., "The Thermal Dissipation of Meteorites by a Bumper System", Bericht über den V. Internationalen Astronautischen Kongres, August, 1954.

22. Birkhoff, G., MacDougall, D.P., Pugh, E.M., and Taylor, G.I., "Explosives with Lined Cavities", Journal of Applied Physics, Vol. 19, Pages 563-582, 1948.

23. Rostoker, N., "The Formation of Craters by High Speed Particles", Meteoritics, Vol. 1, p. 11, 1953.

24. Bjork, R.L., "Effects of a Meteoroid Impact on Steel and Aluminum in Space", Technical Report P-1662, Rand Corporation, Eng. Division, Dec. 16, 1958.

25. Eichelberger, R.J., "Re-examination of Theories of Jet Formation and Target Penetration by Lined Cavity Charges", Carnegie Inst. of Tech., Dept. of Physics, CIL.

26. Palmer, E.P., and Grow, R.W., "Penetration and Cratering Studies", University of Utah, Eighth Quarterly Report, Contract No. AF-04(647)-176, February 29, 1960.

27. Riney, T.D., "A Visco-Plastic Model for Hypervelocity Impact" General Electric Company, First Quarterly Report, Contract AF 08(635)-1713, November 3, 1960-February 3, 1961, (APGC-TN-61-16).

28. Malvern, L.E., "The Propagation of Longitudinal Waves of Plastic Deformation in a Bar of Material Exhibiting a Strain-Rate Effect", Journal of Applied Physics, Vol. 18, p. 203, 1951.

29. Oswatitsch, K., Gas Dynamics, translated by Kuerti, G., Academic Press, Inc., New York (1956), p. 185.

30. Oldroyd, J.G., "A Rational Formulation of the Equations of Plastic Flow for a Bingham Solid", Proc. Cambridge Phil. Soc., vol. 43 (1947) pp. 100-105.

31. Pai, S.I., Viscous Flow Theory, vol. I., van Nostrand, Inc., Princeton, N.J. (1956), Chap. III.

32. Riney, T.D., "Study of Equations Governing the Visco-Plastic Model", General Electric Company, Second Quarterly Report, Contract AF 08 (635) - 1713, February 3, 1961 - May 3, 1961, (APGC-TN-61-30).

33. Turnbow, J.W., and Ripperger, E.A., "Strain-Rate Effects vs Stress-Strain Characteristics of Aluminum and Copper", Proceedings of Fourth Midwestern Conference on Solid Mechanics, Univ. of Texas Publication (1959), p. 415.

34. Reiner, M., Encyclopedia of Physics, Vol. 6, Elasticity and Plasticity, Springer-Verlag, 1958.

35. Richtmyer, R.D., Difference Methods for Initial-Value Problems, Interscience Publishers, Inc., New York, N.Y. (1957), Chap. X.

36. Courant, R., and Friedrichs, K.O., Supersonic Flow and Shock Waves, Interscience Publishers, Inc., New York, N.Y. (1948), Section 54.

37. Riney, T.D., "Numerical Investigation of One-Dimensional Visco-Plastic Model," General Electric Company, Third Quarterly Report, Contract AF 08 (635) - 1713, May 3, 1961 - September 3, 1961.

38. Riney, T.D., and Chernoff, P.R., "Inertial, Viscous, and Plastic Effects in High Speed Impact", Paper presented at the Fifth Symposium on Hypervelocity Impact in Denver, Colorado, October 31, 1961.

39. Rinehart, J.S., "Some Experimental Indications of the Stresses Produced in a Body by an Exploding Charge," Jor. Appl. Phys., Vol. 22, 1951.

40. Katz, S. and R.E. Peterson, "Study of Shock Propagation in Ferrous Metals," Poulter Laboratories, Technical Report 010-55, Stanford Research Institute, December 20, 1955.

41. Eichelberger, R.J. and J.W. Gehring, "Effects of Meteoroid Impacts on Space Vehicles," ARS Space Flight Report to the Nation, New York, October 9, 1961.

APPENDIX A

In Fig. 16a the notations used to describe the wave fronts in the impacting materials are depicted. The particle velocities q_{mk} and wave velocities W_m are with respect to fixed laboratory coordinates. The pressure and particle velocity must be continuous across the interface so that

$$p_{11} = p_{21} = p_i \qquad u_{10} = v_o + W_1 \qquad u_{20} = -W_2$$

$$q_{11} = q_{21} = q_i \qquad u_{11} = q_i + W_1 \qquad u_{21} = q_i - W_2$$

and application of equations (75) to the two discontinuity surfaces yields

(A-1) $$\rho_{10}(v_o + W_1) = \rho_{11}(q_i + W_1)$$

(A-2) $$\rho_{10}(v_o + W_2)^2 = \rho_{11}(q_i + W_1)^2 + p_i$$

(A-3) $$\tfrac{1}{2}(v_o + W_1)^2 = \tfrac{1}{2}(q_i + W_1)^2 + U_1 + p_i/\rho_{11}$$

(A-4) $$-\rho_{20} W_2 = \rho_{21}(q_i - W_2)$$

(A-5) $$\rho_{20} W_2^2 = \rho_{21}(q_i - W_2)^2 + p_i$$

(A-6) $$\tfrac{1}{2} W_2^2 = \tfrac{1}{2}(q_i - W_2)^2 + U_2 + p_i/\rho_{21}.$$

To these six equations in the eight unknowns p_i, q_i, W_1, W_2, ρ_{11}, ρ_{21}, U_1, and U_2 we may append two more,

(A-7) $$p_i = f_1(\rho_{11}, U_1)$$

(A-8) $$p_i = f_2(\rho_{21}, U_2),$$

the equations of state for the two materials.

Equations (A-1), (A-3) may be solved for W_1, W_2 and substituted into the remaining six. The new equations corresponding to (A-2), (A-5) may then be solved for p_i, q_i. These manipulations give the following relations:

(A-9) $$W_1 = (v_o - q_i \rho_{11}/\rho_{10})\ (\rho_{11}/\rho_{10} - 1)^{-1}$$

(A-10) $W_2 = (q_i \rho_{21}/\rho_{20})\ (\rho_{21}/\rho_{20}-1)^{-1}$

(A-11) $\rho_{11}/\rho_{10} = (1 - \rho_{10}/d_1)^{-1}$ where $d_1 \equiv \rho_{11}\ (\rho_{11}/\rho_{10}-1)^{-1}$

(A-12) $\rho_{21}/\rho_{20} = (1 - \rho_{20}/d_2)^{-1}$ where $d_2 \equiv \rho_{21}\ (\rho_{21}/\rho_{20}-1)^{-1}$

(A-13) $q_i = v_o \sqrt{d_1} \left(\sqrt{d_1} + \sqrt{d_2}\right)^{-1}$

(A-14) $p_i = v_o^2\ d_1\ d_2 \left(\sqrt{d_1} + \sqrt{d_2}\right)^{-2}$.

Equations (A-3), (A-6) may be solved for U_1, U_2 and the above relations used to give

(A-15) $U_1 = \frac{1}{2}\ v_o^2\ d_2 \left(\sqrt{d_1} + \sqrt{d_2}\right)^{-2}$

(A-16) $U_2 = \frac{1}{2}\ v_o^2\ d_1 \left(\sqrt{d_1} + \sqrt{d_2}\right)^{-2}$.

If (A-11), (A-12), (A-15) and (A-16) are substituted into (A-7), (A-8) there finally result two equations in the two unknowns d_1, d_2:

(A-17) $$v_o^2 \frac{d_1\ d_2}{\left(\sqrt{d_1} + \sqrt{d_2}\right)^2} = f_1 \left(\frac{\rho_{10}}{1 - \rho_{10}/d_2}, \frac{v_o^2}{2} \frac{d_2}{\left(\sqrt{d_1} + \sqrt{d_2}\right)^2} \right)$$

(A-18) $$v_o^2 \frac{d_1\ d_2}{\left(\sqrt{d_1} + \sqrt{d_2}\right)^2} = f_2 \left(\frac{\rho_{20}}{1 - \rho_{20}/d_2}, \frac{v_o^2}{2} \frac{d_1}{\left(\sqrt{d_1} + \sqrt{d_2}\right)^2} \right).$$

Once d_1 and d_2 have been determined the quantities q_i, p_i, ρ_{11}, ρ_{21}, U_1, U_2 may be computed from equations (A-11) through (A-16). The required initial data are then available for the finite-difference calculations as displayed in Fig. 16b.

Since the functions f_1, f_2 are too cumbersome for explicit solution for d_1 or d_2 to be practical, a numerical method must be used. One such method of successive approximation is as follows:

a) Guess a value for d_1, e.g. $d_1^{(1)}$.

b) Substitute $d_1^{(1)}$ into (A-17) and compute the corresponding estimate of d_2, say $d_2^{(1)}$, by trial-and-error.

c) Substitute $d_1^{(1)}$, $d_2^{(1)}$ into the two sides of (A-18).

(i) If equality holds $d_1 = d_1^{(1)}$, $d_2 = d_2^{(1)}$ and process is completed.

(ii) If equality does not hold $d_1 \neq d_1^{(1)}$, $d_2 \neq d_2^{(1)}$ and a second guess for d_1, say $d_1^{(2)}$, must be made and the process repeated, etc.

The method is simple but involves extensive calculations. A program has therefore been written to carry out the computations on a high speed digital computer.

APPENDIX B

The explicit difference equations are given by (68) through (74) of the Second Quarterly Report. They are as follows:

$$q_j^{n+1} = q_j^n - \frac{\Delta t}{\rho_o \Delta x}\left[p_{j+1/2}^n - p_{j-1/2}^n + Q_{j+1/2}^n - Q_{j-1/2}^n + S_{j+1/2}^n - S_{j-1/2}^n\right]$$

$$V_{j+1/2}^{n+1} = V_{j+1/2}^n + \frac{\Delta t}{\rho_o \Delta x}\left[q_{j+1}^{n+1} - q_j^{n+1}\right]$$

$$S_{j+1/2}^{n+1} = -\frac{8}{3}\frac{\mu_o}{\Delta t}\,\frac{1}{V_{j+1/2}^{n+1} + V_{j+1/2}^n}\left[V_{j+1/2}^{n+1} - V_{j+1/2}^n\right]$$

$$U_{j+1/2}^{n+1} = U_{j+1/2}^n - \left[V_{j+1/2}^{n+1} - V_{j+1/2}^n\right]\left[p_{j+1/2}^n + Q_{j+1/2}^{n+1} + S_{j+1/2}^{n+1}\right]$$

$$- \sqrt{\frac{4}{3}}\,\tau_o\left[V_{j+1/2}^{n+1} - V_{j+1/2}^n\right] \qquad \text{(B-1)}$$

$$Q_{j+1/2}^{n+1} = \frac{2(\rho_o \ell)^2}{(\Delta t \ell)^2}\,\frac{1}{V_{j+1/2}^{n+1} + V_{j+1/2}^n}\left[V_{j+1/2}^{n+1} - V_{j+1/2}^n\right]^2$$

$$p_{j+1/2}^{n+1} = g\left(V_{j+1/2}^{n+1},\ U_{j+1/2}^{n+1}\right)$$

where we have eliminated X from (68) and (70) to obtain the second equation and the equation of state is rewritten as $p = f(V^{-1}, U) \equiv g(V, U)$. Here ℓ is a parameter with dimension of length which essentially determines the magnitude of the pseudo-viscosity.

The analysis of the stability of this system follows the method outlined by Richtmyer (Reference 35). The equations of first variation of (B-1) will be obtained in which quantities of the second and higher order are dropped. This will give us linear equations for the first order variations $\dot{q}$, $\dot{V}$, $\dot{S}$, $\dot{U}$, $\dot{Q}$, $\dot{p}$ (the dot does <u>not</u> indicate time derivatives) in which the zero order quantities appear as coefficients. The equations obtained are

$$\dot{q}_j^{n+1} = \dot{q}_j^n - \frac{\Delta t}{\rho_o \Delta x}\left[\dot{p}_{j+1/2}^n - \dot{p}_{i-1/2}^n + \dot{Q}_{j+1/2}^n - \dot{Q}_{j-1/2}^n + \dot{S}_{j+1/2}^n - \dot{S}_{j-1/2}^n\right]$$

$$\dot{V}_{j+1/2}^{n+1} = \dot{V}_{j+1/2}^n + \frac{\Delta t}{\rho_o \Delta x}\left[\dot{q}_{j+1}^{n+1} - \dot{q}_j^{n+1}\right]$$

$$\dot{S}_{j+1/2}^{n+1} = -\frac{4}{3}\frac{\mu_o}{\Delta t}\frac{1}{V}\left[\dot{V}_{j+1/2}^{n+1} - \dot{V}_{j+1/2}^n\right]$$

(B-2)
$$\dot{U}_{j+1/2}^{n+1} = \dot{U}_{j+1/2}^n - \left(p+Q+S+\sqrt{\frac{4}{3}}\,\tau_o\right)\left[\dot{V}_{j+1/2}^{n+1} - \dot{V}_{j+1/2}^n\right]$$

$$\dot{Q}_{j+1/2}^{n+1} = -\frac{(\rho_o \ell)^2}{2V^2}\left(\frac{\partial V}{\partial t}\right)^2\left[\dot{V}_{j+1/2}^{n+1} + \dot{V}_{j+1/2}^n\right] + \frac{2(\rho_o \ell)^2}{V\,\Delta t}\frac{\partial V}{\partial t}\left[\dot{V}_{j+1/2}^{n+1} - \dot{V}_{j+1/2}^n\right]$$

$$\dot{p}_{j+1/2}^{n+1} = \frac{\partial g}{\partial V}\dot{V}_{j+1/2}^{n+1} + \frac{\partial g}{\partial U}\dot{U}_{j+1/2}^{n+1}$$

The zero order quantities are considered constants and, consequently, superscripts and subscripts denoting net points are omitted from them.

The first order quantities are assumed to have the Fourier representations

(B-3)
$$\dot{q}_j^n = \sum_k A_k^n e^{ikx} \qquad \dot{V}_j^n = \sum_k B_k^n e^{ikx}$$

$$\dot{S}_j^n = \sum_k C_k^n e^{ikx} \qquad \dot{U}_j^n = \sum_k D_k^n e^{ikx}$$

$$\dot{Q}_j^n = \sum_k E_k^n e^{ikx} \qquad \dot{p}_j^n = \sum_k F_k^n e^{ikx}$$

where $x = j\Delta x$. The von Neuman stability criterion is, essentially, that the coefficients $A_k^n, \ldots, F_k^n$ remain bounded as the calculations proceed from $t = n\Delta t$ to $t = (n+1)\Delta t$, $t = (n+2)\Delta t$, etc. To investigate this substitute representations (B-3) into (B-2) and set like harmonics equal to zero to obtain the relations

$$(B\text{-}4) \qquad A_k^{n+1} = A_k^n - i\beta\Delta t \left(F_k^n + E_k^n + C_k^n\right)$$

$$(B\text{-}5) \qquad B_k^{n+1} = B_k^n + i\beta\Delta t\, A_k^{n+1}$$

$$(B\text{-}6) \qquad C_k^{n+1} = -\frac{4}{3}\frac{\mu_o}{V\Delta t}\left[B_k^{n+1} - B_k^n\right]$$

$$(B\text{-}7) \qquad D_k^{n+1} = D_k^n - \left(p+Q+S+\sqrt{\frac{4}{3}}\,\tau_o\right)\left[B_k^{n+1} - B_k^n\right]$$

$$(B\text{-}8) \qquad E_k^{n+1} = -\frac{(\rho_o \ell)^2}{2V^2}\left(\frac{\partial V}{\partial t}\right)^2\left[B_k^{n+1} + B_k^n\right] + \frac{2(\rho_o \ell)^2}{V\Delta t}\frac{\partial V}{\partial t}\left[B_k^{n+1} - B_k^n\right]$$

$$(B\text{-}9) \qquad F_k^{n+1} = \frac{\partial g}{\partial V} B_k^{n+1} + \frac{\partial g}{\partial U} D_k^{n+1}$$

where

$$(B\text{-}10) \qquad \beta = \frac{2\sin(k\Delta x/2)}{\rho_o \Delta x}$$

Relations (B-5), (B-6) may be combined to yield

$$C_k^n = -\frac{4}{3}\frac{\mu_o}{V} i\beta A_k^n$$

This may be substituted into (B-4) to obtain

$$(B\text{-}11) \qquad A_k^{n+1} = \left(1 - \frac{4}{3}\frac{\mu_o}{V}\beta^2\Delta t\right) A_k^n - i\beta\Delta t\left[E_k^n + F_k^n\right]$$

If (B-11) is substituted into (B-5) the result is

$$(B\text{-}12) \qquad B_k^{n+1} = B_k^n + i\beta\Delta t\left(1 - \frac{4}{3}\frac{\mu_o}{V}\beta^2\Delta t\right) A_k^n + \beta^2(\Delta t)^2\left[E_k^n + F_k^n\right]$$

Now (B-12) may be used to eliminate B_k^{n+1} from (B-7) and (B-8) with the results

$$(B\text{-}13) \qquad D_k^{n+1} = D_k^n - \left(p+Q+S+\sqrt{\frac{4}{3}}\,\tau_o\right)\left[i\beta\Delta t\left(1 - \frac{4}{3}\frac{\mu_o}{V}\beta^2\Delta t\right) A_k^n + \beta^2(\Delta t)^2\left(E_k^n + F_k^n\right)\right]$$

$$E_k^{n+1} = -\frac{(\rho_o \ell)^2}{2V^2}\left(\frac{\partial V}{\partial t}\right)^2\left[2B_k^n + i\beta\Delta t\left(1-\frac{4}{3}\frac{\mu_o}{V}\beta^2\Delta t\right)A_k^n + \beta^2(\Delta t)^2\left(E_k^n + F_k^n\right)\right]$$

$$+\frac{2(\rho_o \ell)^2}{V\Delta t}\frac{\partial V}{\partial t}\left[i\beta\Delta t\left(1-\frac{4}{3}\frac{\mu_o}{V}\beta^2\Delta t\right)A_k^n + \beta^2(\Delta t)^2\left(E_k^n + F_k^n\right)\right] \qquad \text{(B-14)}$$

Finally, substitution of (B-12), (B-14) into (B-9) yields

$$F_k^{n+1} = \frac{\partial g}{\partial V}\left\{B_k^n + i\beta\Delta t\left(1-\frac{4}{3}\frac{\mu_o}{V}\beta^2\Delta t\right)A_k^n + \beta^2(\Delta t)^2\left(E_k^n + F_k^n\right)\right\}$$

$$+\frac{\partial g}{\partial U}\left\{D_k^n - \left(p+Q+S+\sqrt{\frac{4}{3}}\tau_o\right)\left[i\beta\Delta t\left(1-\frac{4}{3}\frac{\mu_o}{V}\beta^2\Delta t\right)A_k^n + \beta^2(\Delta t)^2\left(E_k^n + F_k^n\right)\right]\right\} \qquad \text{(B-15)}$$

Upon introduction of the notations

$$\beta = \frac{2\sin(k\Delta x/2)}{\rho_o \Delta x} \qquad \gamma = 1-\frac{4}{3}\frac{\mu_o}{V}\beta^2\Delta t$$

$$\Lambda = p+Q+S+\sqrt{\frac{4}{3}}\tau_o \qquad \delta = \frac{\partial g}{\partial V} - \Lambda\frac{\partial g}{\partial U} \qquad \text{(B-16)}$$

$$\epsilon = \frac{1}{2V}\frac{\partial V}{\partial t} \qquad \zeta = \frac{(\rho_o \ell)^2}{V}\frac{\partial V}{\partial t}$$

the relations (B-11) through (B-15) may be written in the matrix form

$$Y^{n+1} = G\,Y^n \qquad \text{(B-17)}$$

where

$$Y^n = \begin{bmatrix} A_k^n \\ B_k^n \\ D_k^n \\ E_k^n \\ F_k^n \end{bmatrix} \qquad Y^{n+1} = \begin{bmatrix} A_k^{n+1} \\ B_k^{n+1} \\ D_k^{n+1} \\ E_k^{n+1} \\ F_k^{n+1} \end{bmatrix}$$

and the "amplification matrix", which depends on μ_o and τ_o, is given by

$$(B\text{-}18) \qquad G = \begin{bmatrix} \gamma & 0 & 0 & -i\beta\Delta t & -i\beta\Delta t \\ i\beta\gamma\Delta t & 1 & 0 & \beta^2(\Delta t)^2 & \beta^2(\Delta t)^2 \\ -i\beta\gamma\Lambda\Delta t & 0 & 1 & -\beta^2\Lambda(\Delta t)^2 & -\beta^2\Lambda(\Delta t)^2 \\ i\beta\gamma\zeta\Delta t\left(\frac{2}{\Delta t}-\epsilon\right) & -2\epsilon\zeta & 0 & \beta^2\zeta(\Delta t)^2\left(\frac{2}{\Delta t}-\epsilon\right) & \beta^2\zeta(\Delta t)^2\left(\frac{2}{\Delta t}-\epsilon\right) \\ i\beta\gamma\delta\Delta t & \frac{\partial g}{\partial V} & \frac{\partial g}{\partial U} & \beta^2\delta(\Delta t)^2 & \beta^2\delta(\Delta t)^2 \end{bmatrix}$$

Now, expansion of the determinant $|G - \lambda I|$ and setting the result equal to zero shows that the eigenvalues, λ, of G satisfy the equation

$$(B\text{-}19) \qquad \lambda^2(\lambda-1)\left\{(\lambda-1)^2-(\lambda-1)\beta^2\Delta t\left[\delta\Delta t + \zeta(2-\epsilon\Delta t) - \frac{4}{3}\frac{\mu_o}{V}\right] + \beta^2(\Delta t)^2(2\epsilon\zeta-\delta)\right\} = 0$$

If ℓ = constant and $\Delta t/(\Delta x)^2 = O(1)$ as $\Delta t,\ \Delta x \longrightarrow 0$, then $\beta^2\Delta t = O(1)$ and the secular equation reduces to

$$(B\text{-}20) \qquad \lambda^2(\lambda-1)^2\left\{\lambda-1-\beta^2\Delta t\left[2\zeta - \frac{4}{3}\frac{\mu_o}{V}\right] - O(\Delta t)\right\}$$

Thus, the von Neuman requirement for stability

$$(B\text{-}21) \qquad |\lambda_m| \leq 1 + O(\Delta t)$$

is satisfied provided

$$\beta^2\Delta t\left[\frac{2}{3}\frac{\mu_o}{V} + \frac{(\rho_o\ell)^2}{V}\left|\frac{\partial V}{\partial t}\right|\right] \leq 1$$

where we have used the fact that $\partial V/\partial t < 0$. The inequality will hold provided

$$(B\text{-}22) \qquad \frac{\Delta t}{(\Delta x)^2} \leq \frac{\rho_o^2 V}{\frac{8}{3}\mu_o + 4(\rho_o\ell)^2\left|\frac{\partial V}{\partial t}\right|}$$

It may be noted from (B-22) that in the limit as the viscosity tends to zero the stability criterion reduces to

$$(B\text{-}23) \qquad \frac{\Delta t}{(\Delta x)^2} \leq \frac{V}{4\ell^2\left|\frac{\partial V}{\partial t}\right|} \qquad (\mu_o = 0)$$

which is the value given by Richtmyer (Ref. 35, p. 220) for this case.

In the case $\mu_o = 0$ it is also possible to derive a stability criterion from (B-19) and (B-21) under the condition that $\ell = a\,\Delta x$, where a is some constant, instead of holding ℓ constant. Then the restriction is found to be relaxed to

$$\text{(B-24)} \qquad \frac{\Delta t}{\Delta x} \leq \frac{\rho_o}{2\sqrt{2\left|\frac{\partial g}{\partial V} - \left(p+Q+\sqrt{\frac{4}{3}}\,\tau_o\right)\frac{\partial g}{\partial U}\right|}}$$

Criterion (B-23) holds in the region of the shock, and criterion (B-24) is valid in regions away from the shock. However, if true viscosity is present ($\mu_o \neq 0$) then we must always have $\Delta t/(\Delta x)^2 = O(1)$ for stability; if $\Delta t/\Delta x = O(1)$ one of the eigenvalues goes to infinity. This results since in this case the μ_o term in (B-19) does not have a factor of order $(\Delta x)^2$ but of order unity.

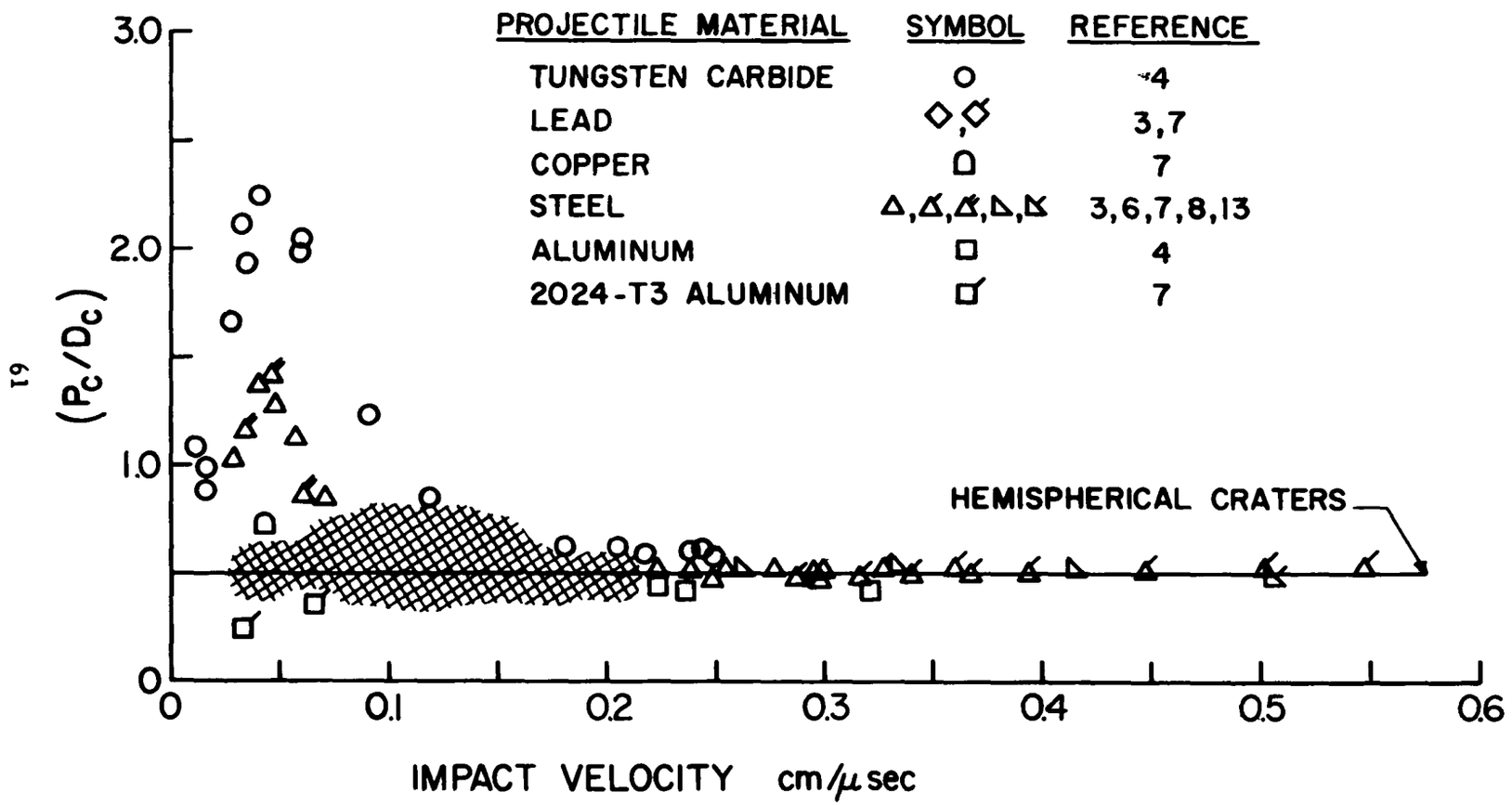

Figure 1 Crater profile vs impact velocity for lead target and various projectile materials.

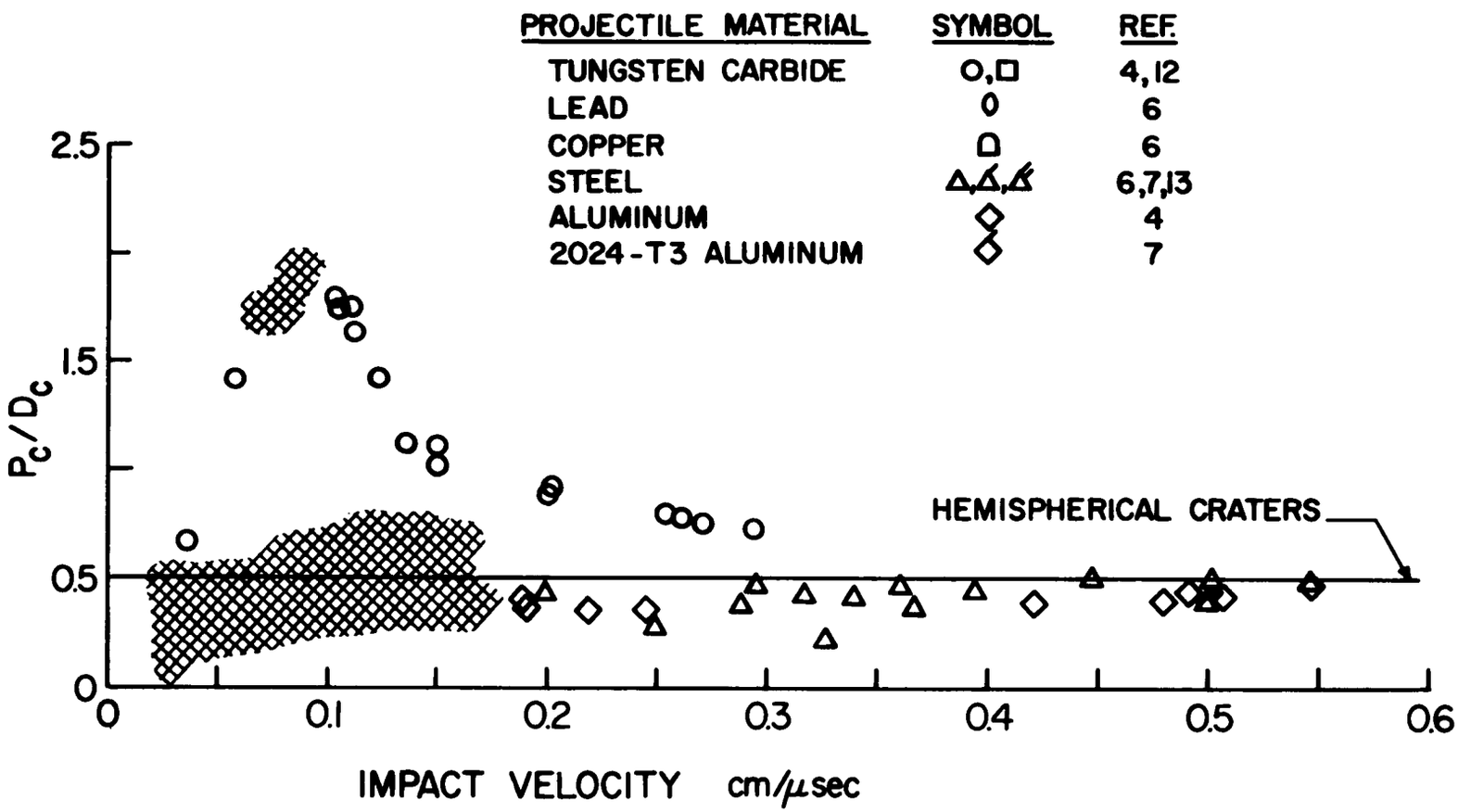

Figure 2 Crater profile vs impact velocity for copper target and various projectile materials.

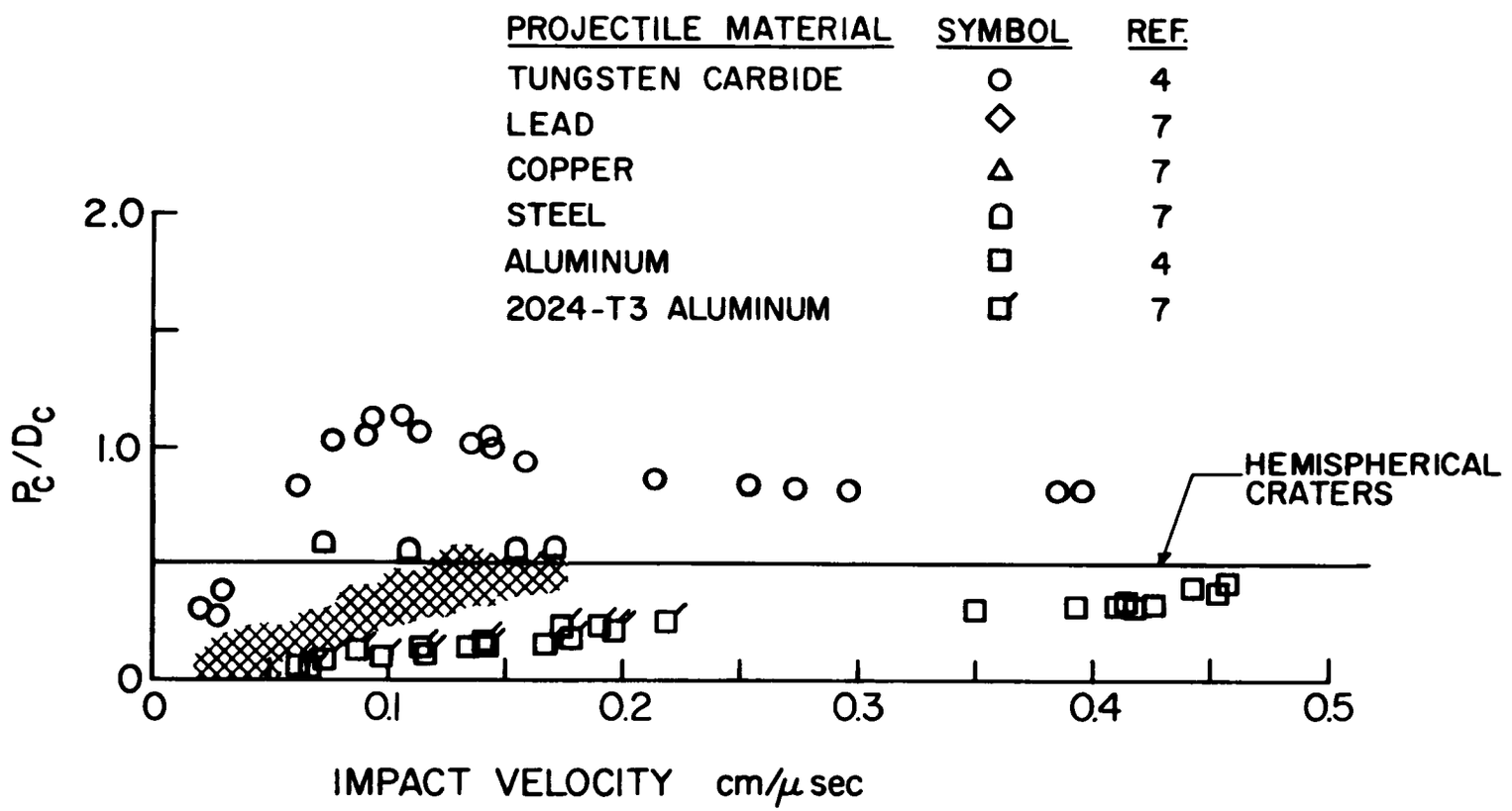

Figure 3 Crater profile vs impact velocity for steel target and various projectile materials.

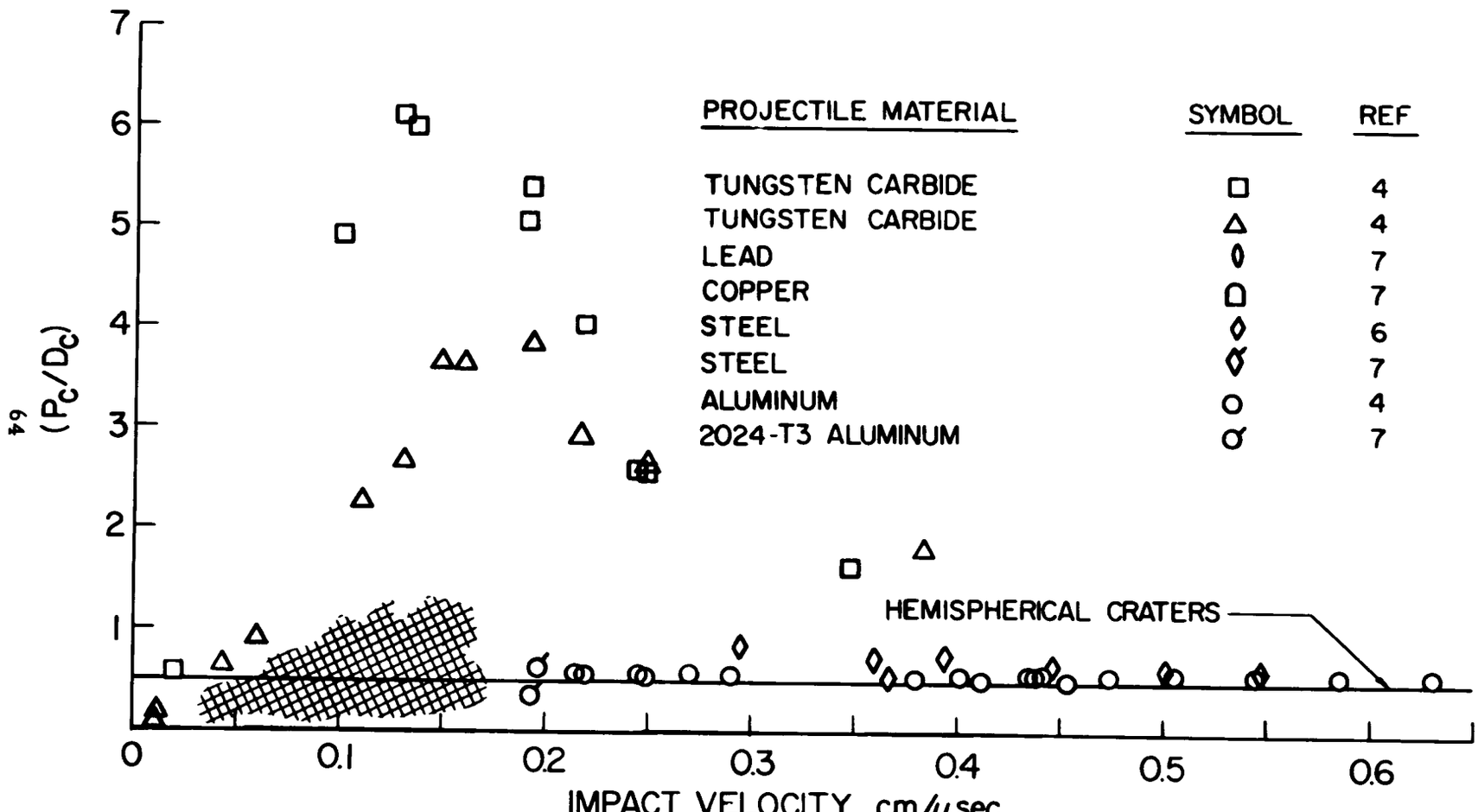

Figure 4 Crater profile vs impact velocity for aluminum target and various projectile materials.

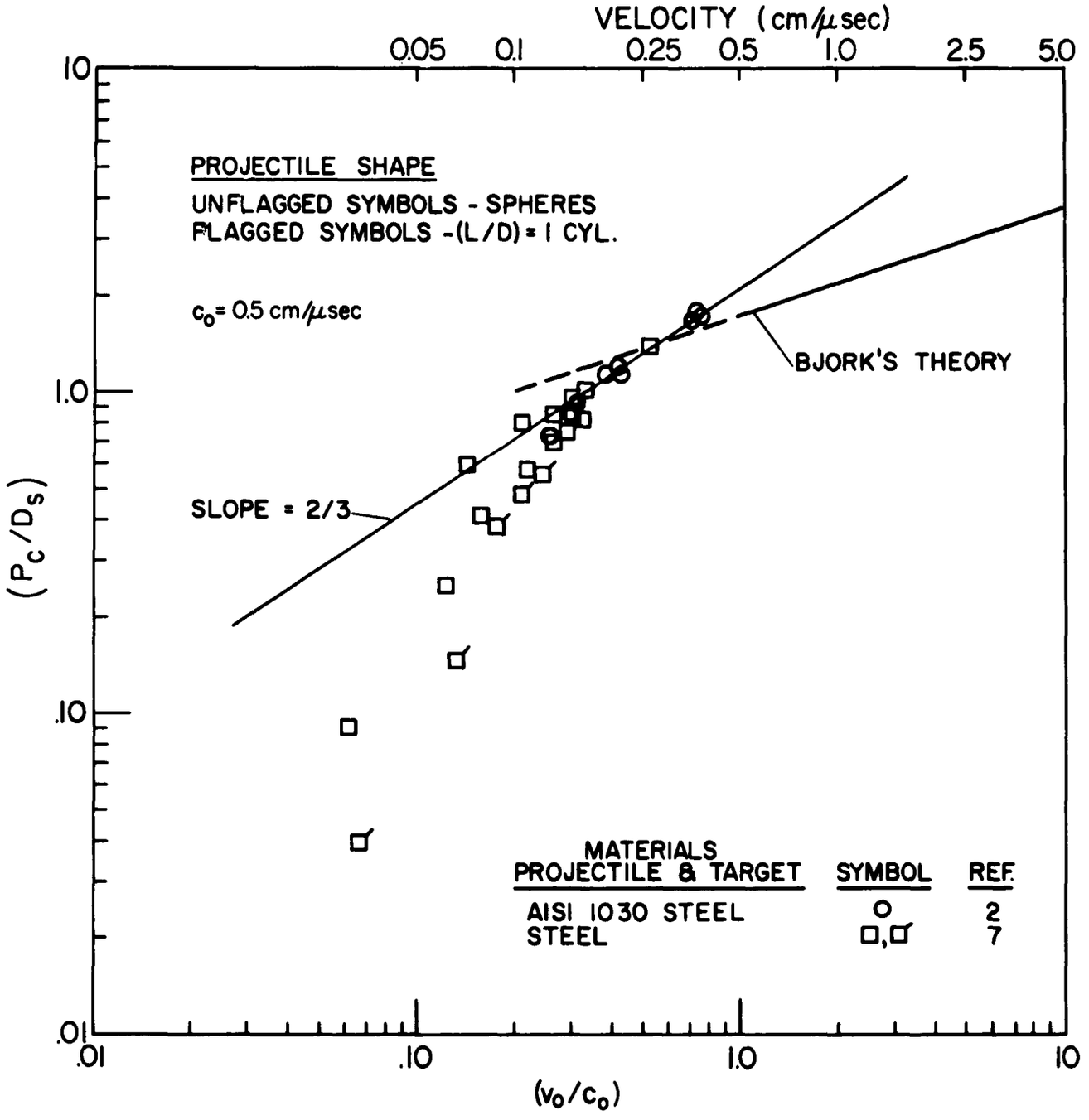

Figure 5 Penetration parameter vs impact velocity for steel target and projectile.

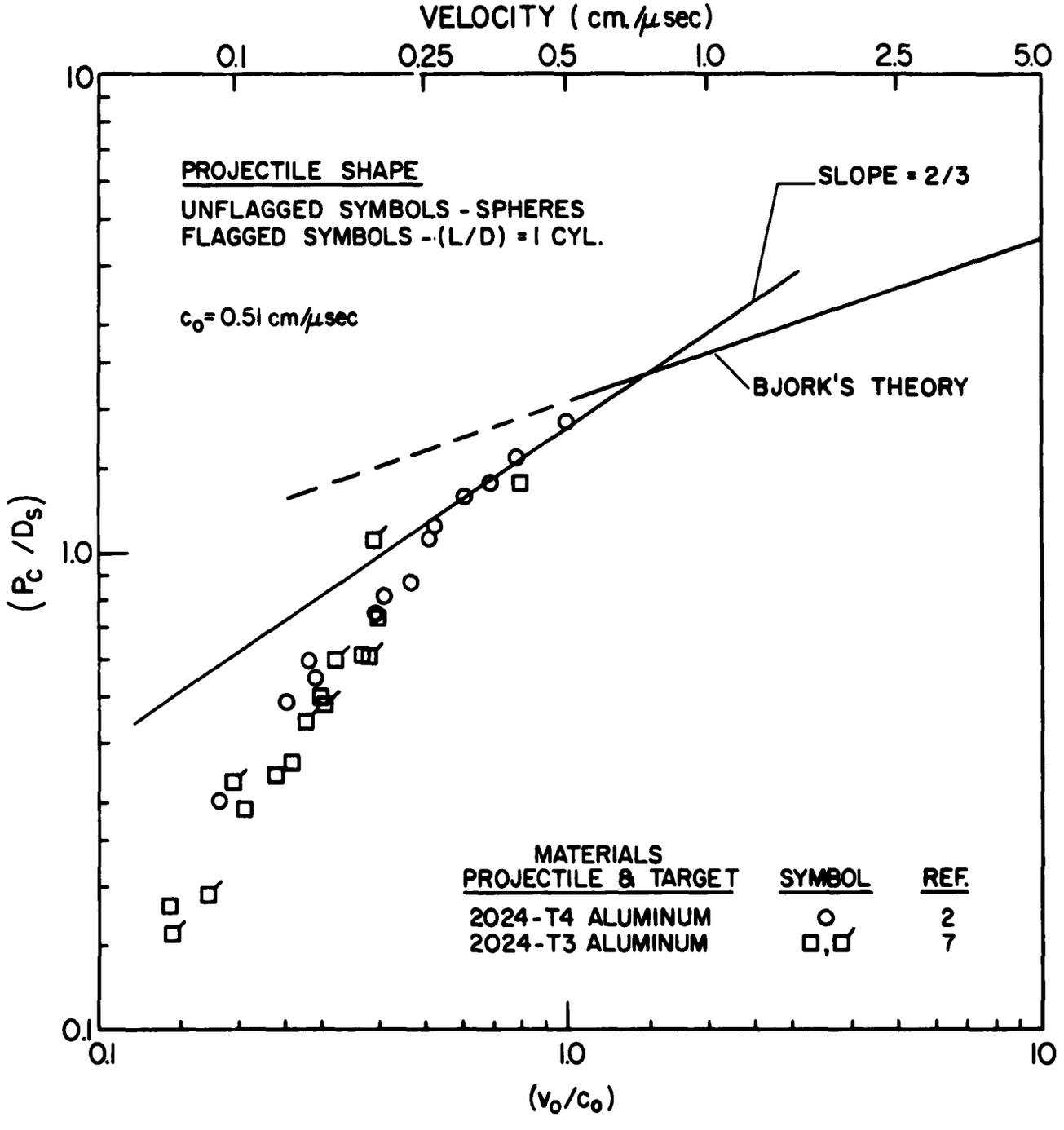

Figure 6 Penetration parameter vs impact velocity for aluminum alloy target and projectile.

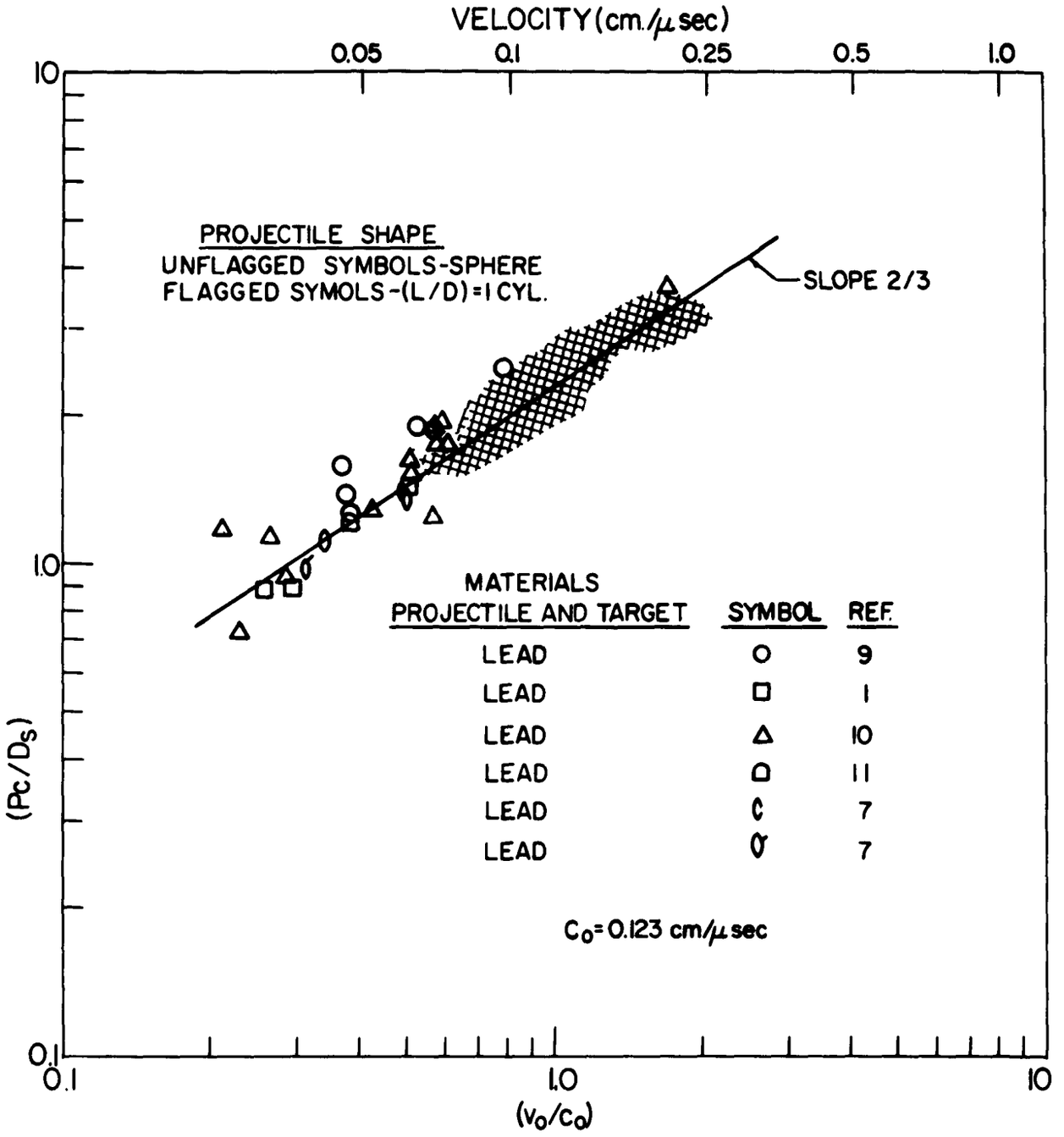

Figure 7 Penetration parameter vs impact velocity for lead target and projectile.

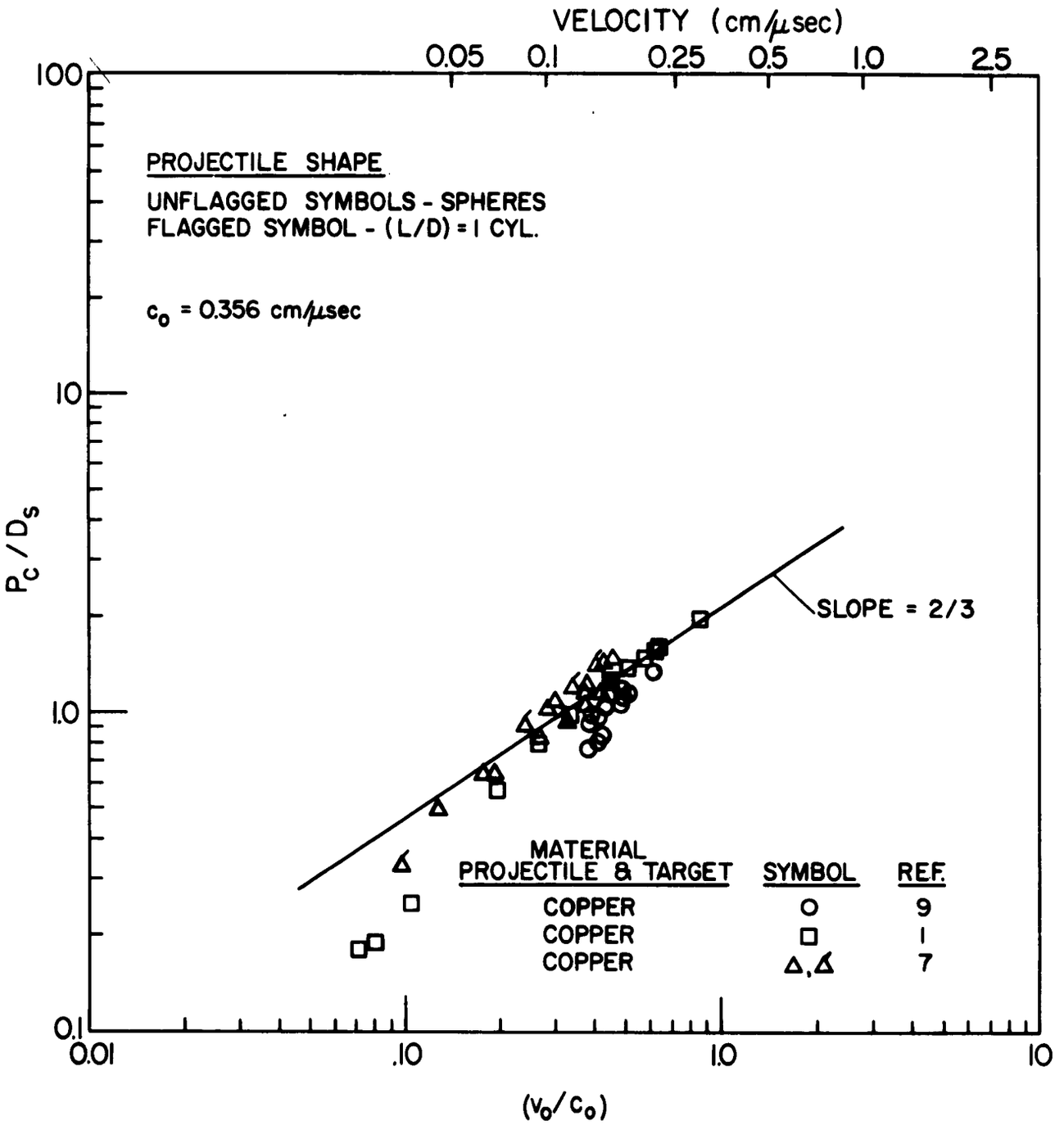

Figure 8 Penetration parameter vs impact velocity for copper target and projectile.

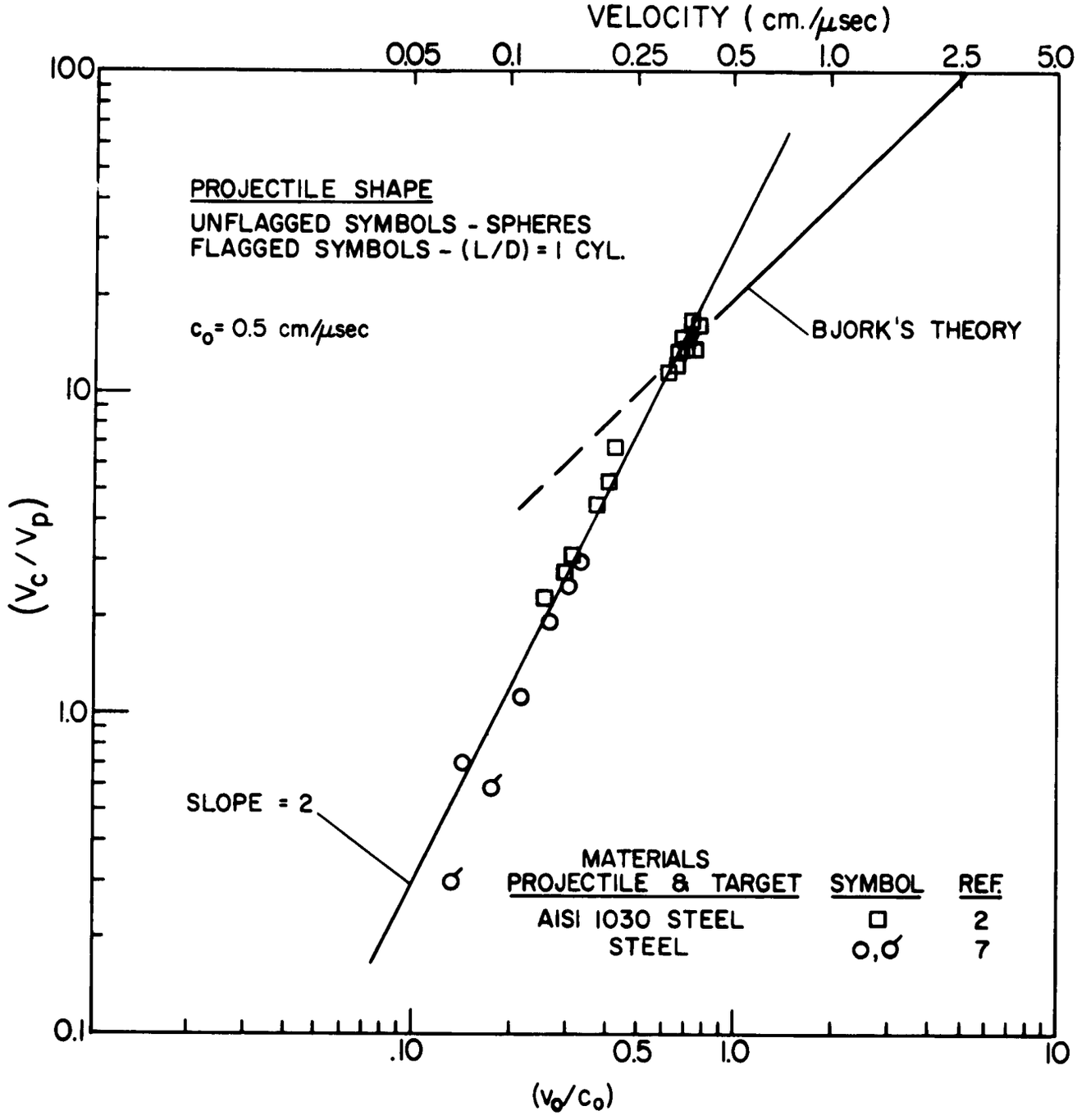

Figure 9 Crater volume parameter vs impact velocity for steel target and projectile.

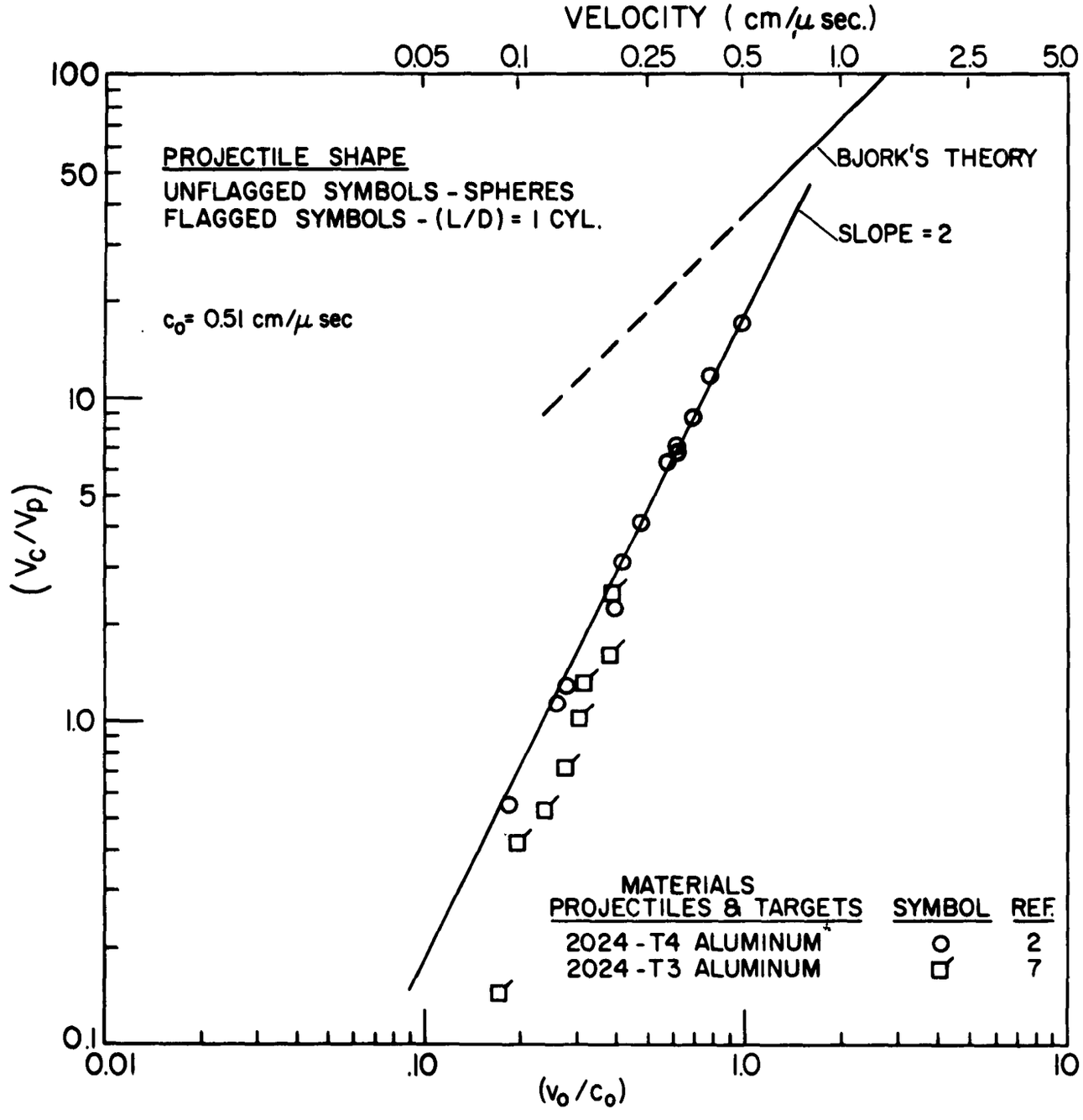

Figure 10 Crater volume parameter vs impact velocity for aluminum alloy target and projectile.

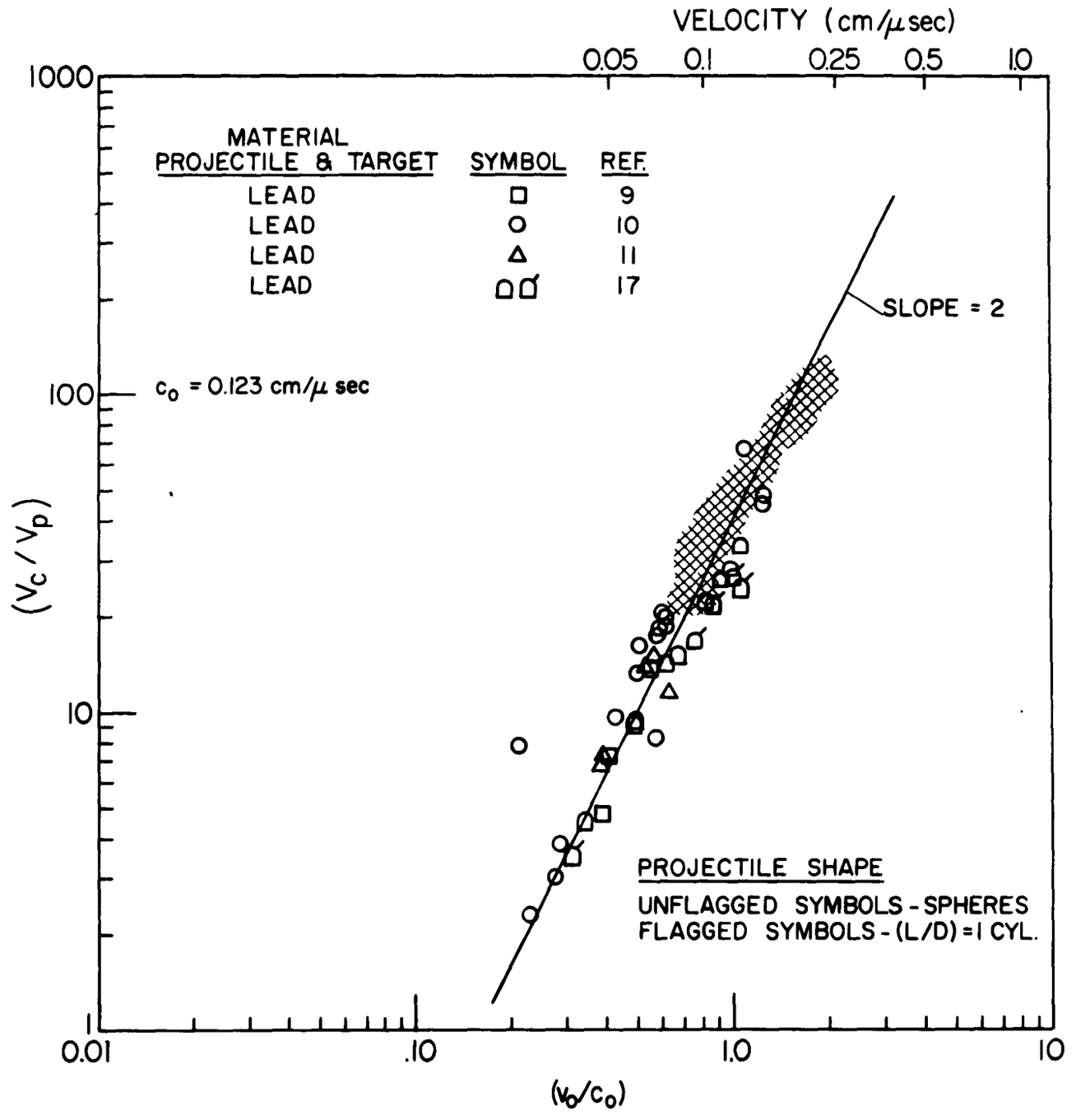

Figure 11 Crater volume parameter vs impact velocity for lead target projectile.

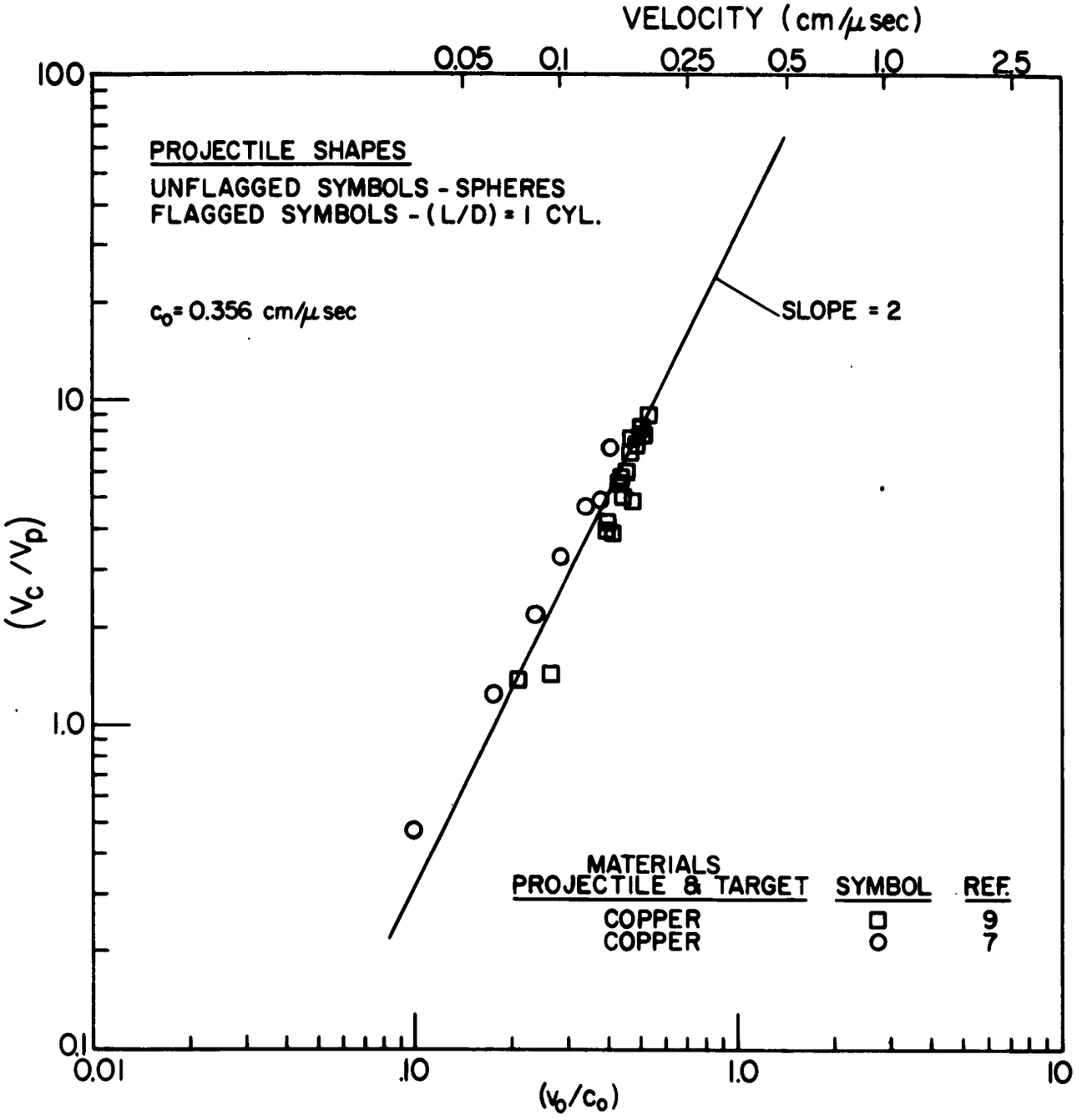

Figure 12 Crater volume parameter vs impact velocity for copper target projectile.

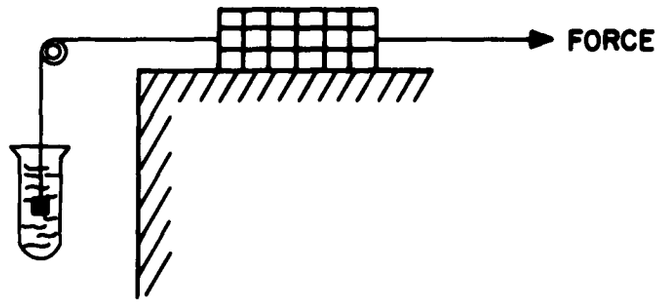

(a)

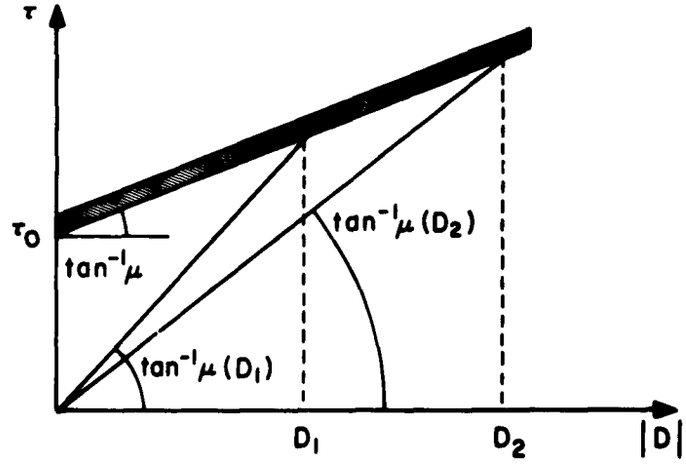

(b)

Figure 13. Schematic representations of the (a) forces in a Bingham body and (b) the dependence of the viscosity on the strain-rate.

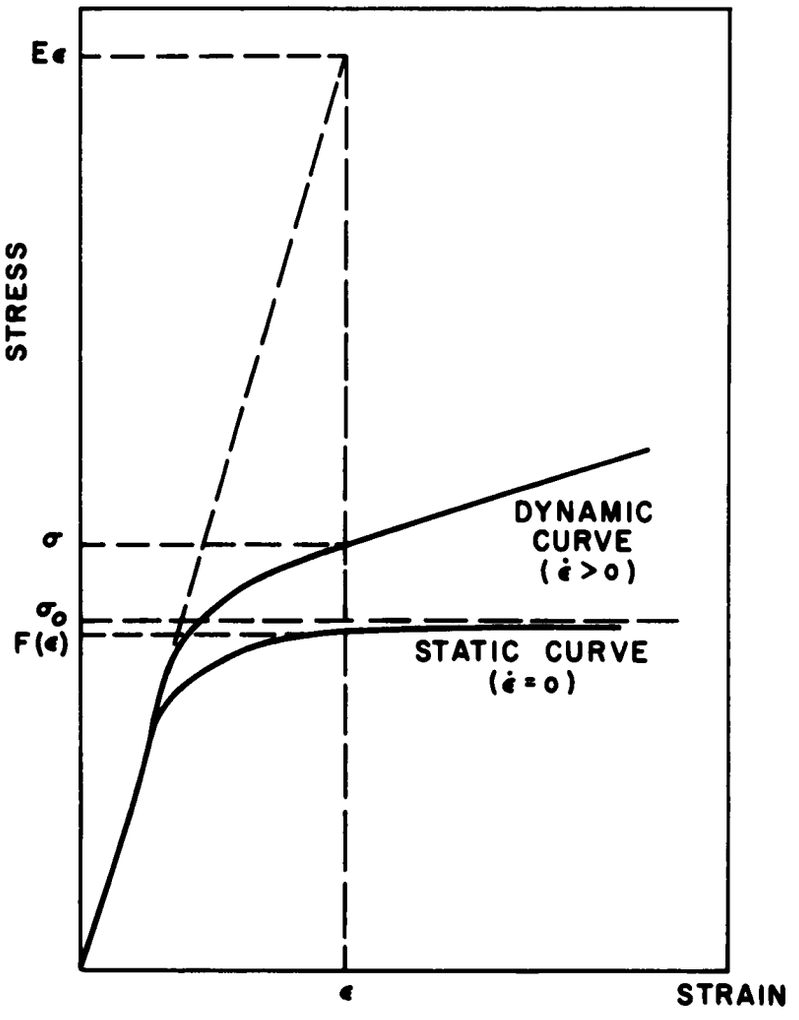

Figure 14 Illustration of the quantities in Malvern's strain-rate dependent constitutive relation.

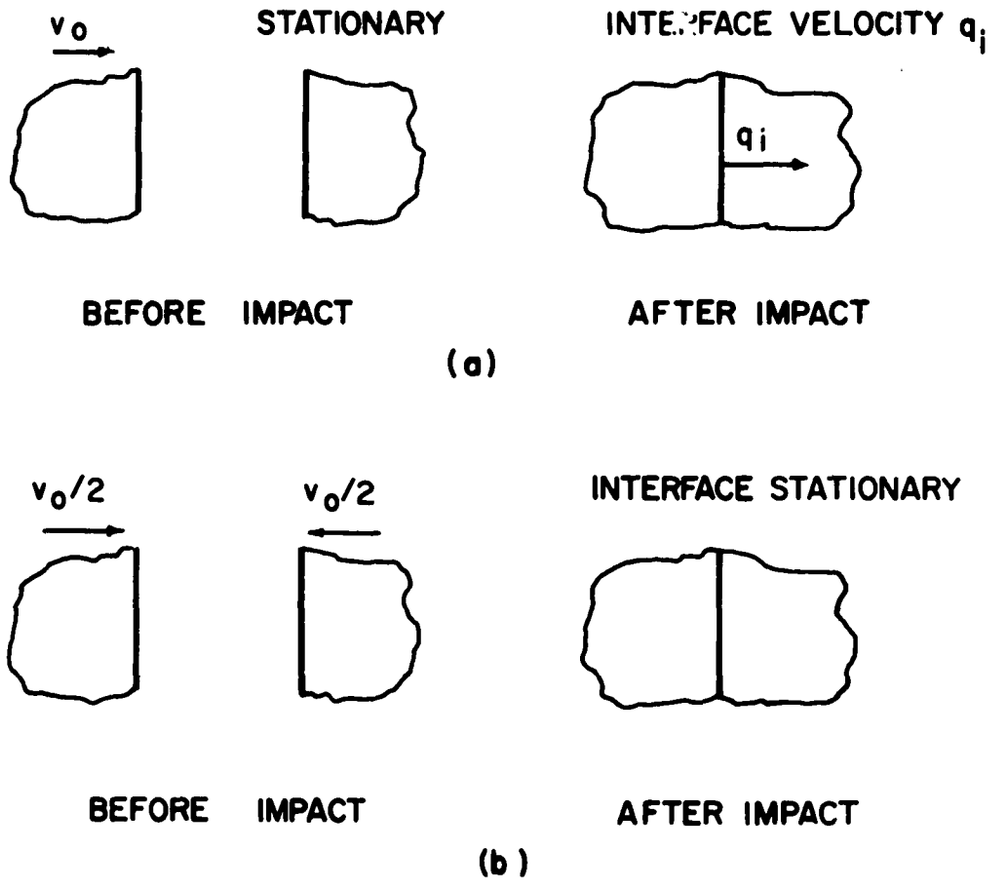

Figure 15 Illustration of impact situation in (a) laboratory coordinates and (b) center of mass coordinates.

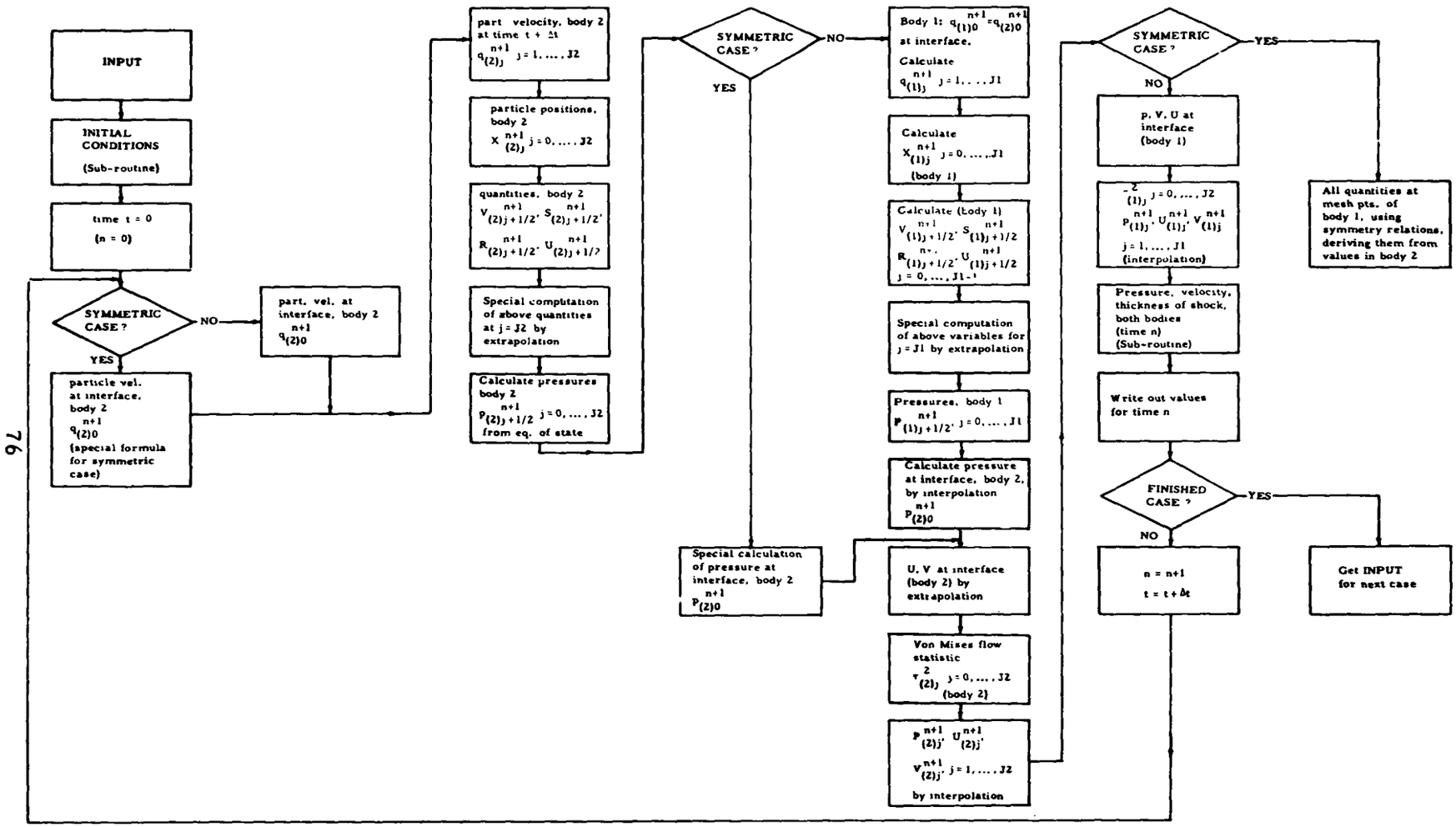

Figure 16 **Flow chart depicting the sequence of calculations in the explicit difference scheme.**

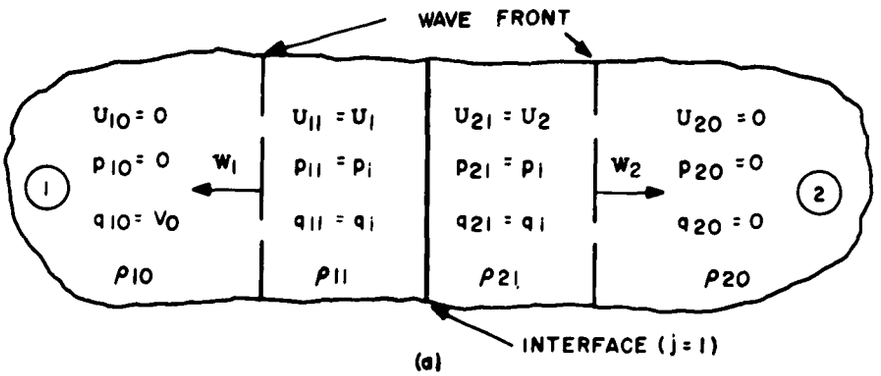

(a)

	BODY 1		BODY 2	
STATION j / QUANTITY	$-\infty$ TO -1	0	0	1 TO ∞
q	V_0	q_i	q_1	0
X	$j\Delta x$	0	0	$j\Delta x$
$V = 1/\rho$	$1/\rho_{10}$	$1/\rho_{11}$	$1/\rho_{21}$	$1/\rho_{20}$
S	0	0	0	0
Q	0	0	0	0
U	0	U_1	U_2	0
p	0	pi	pi	0

(b)

Figure 17 Display of (a) impact situation immediately after impact and (b) the nomenclature used to describe the initial and boundary data.

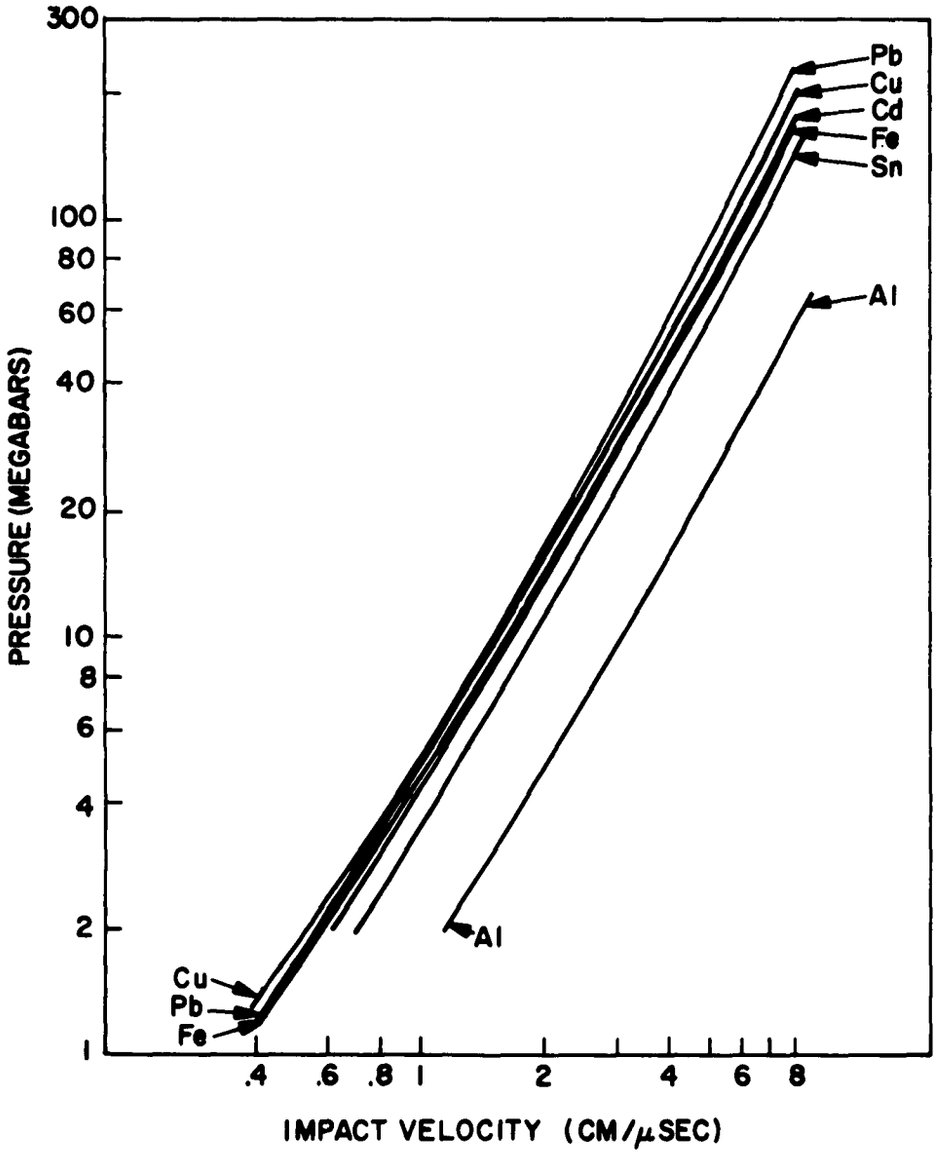

Figure 18 Rankine-Hugoniot pressures calculated for two semi-infinite bodies of indicated material impacting at velocity v_o.

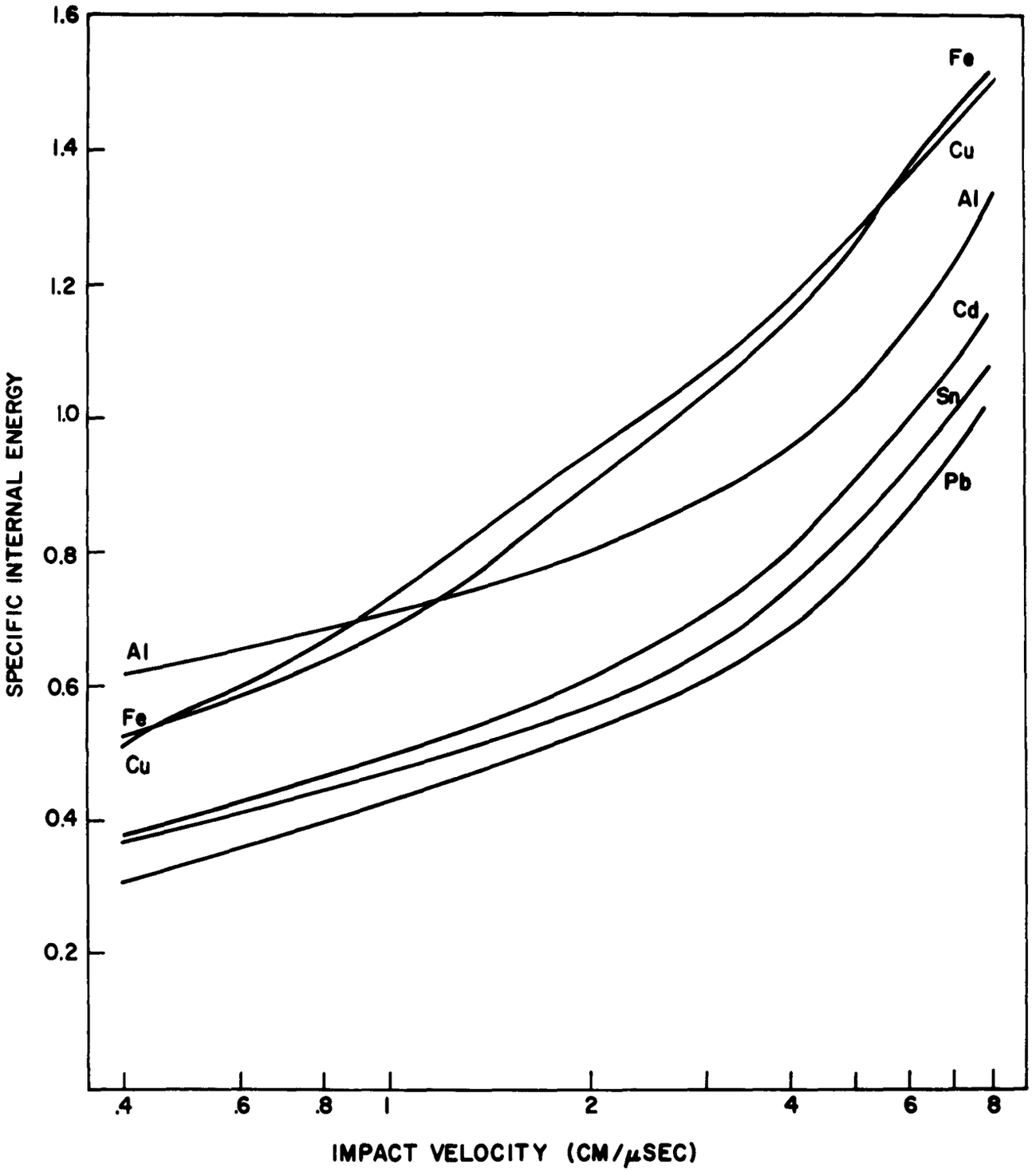

Figure 19 Rankine-Hugoniot internal energies calculated for two semi-infinite bodies of indicated material impacting at velocity v_o.

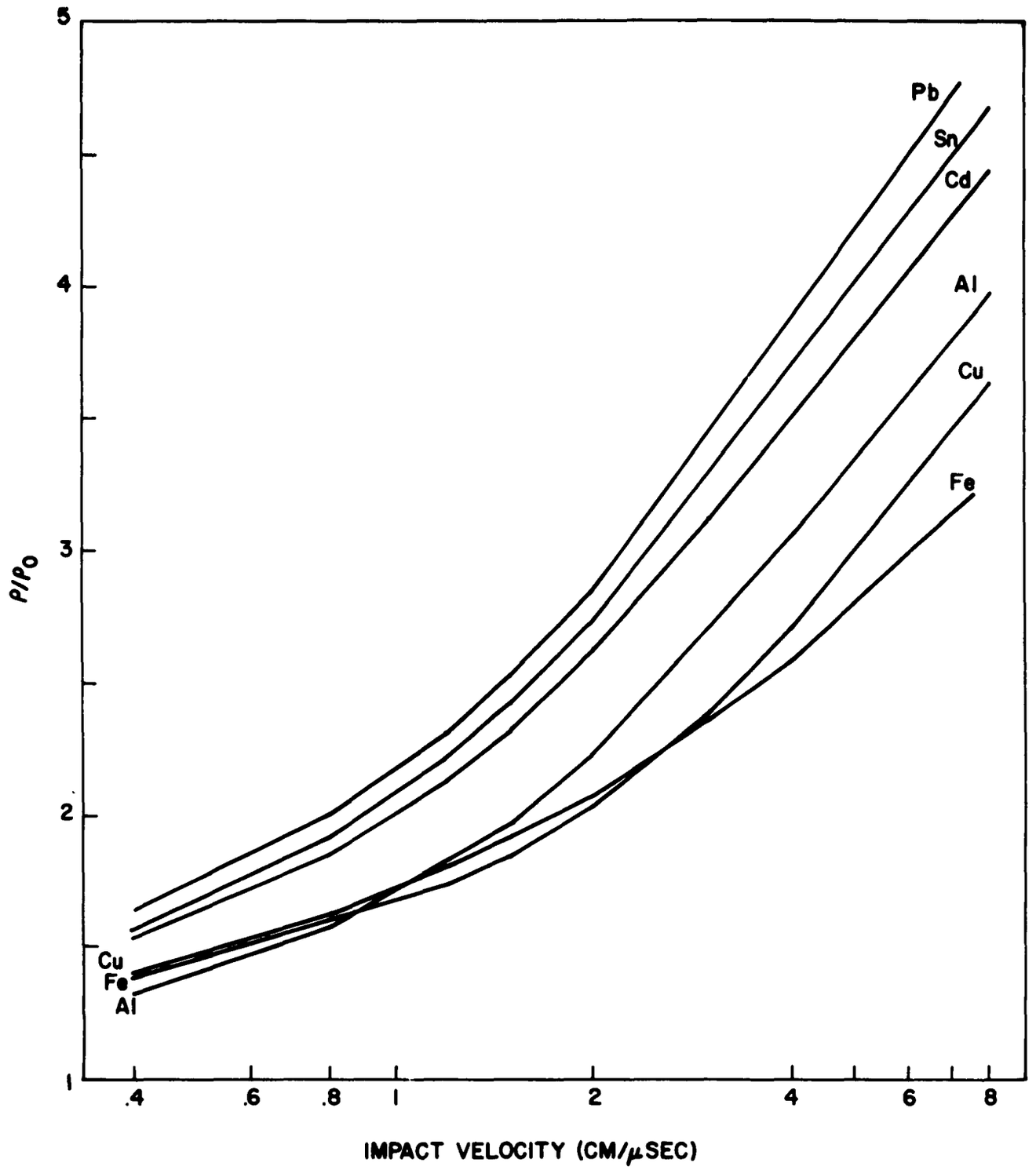

Figure 20 Rankine-Hugoniot densities calculated for two semi-infinite bodies of indicated material impacting at velocity v_o.

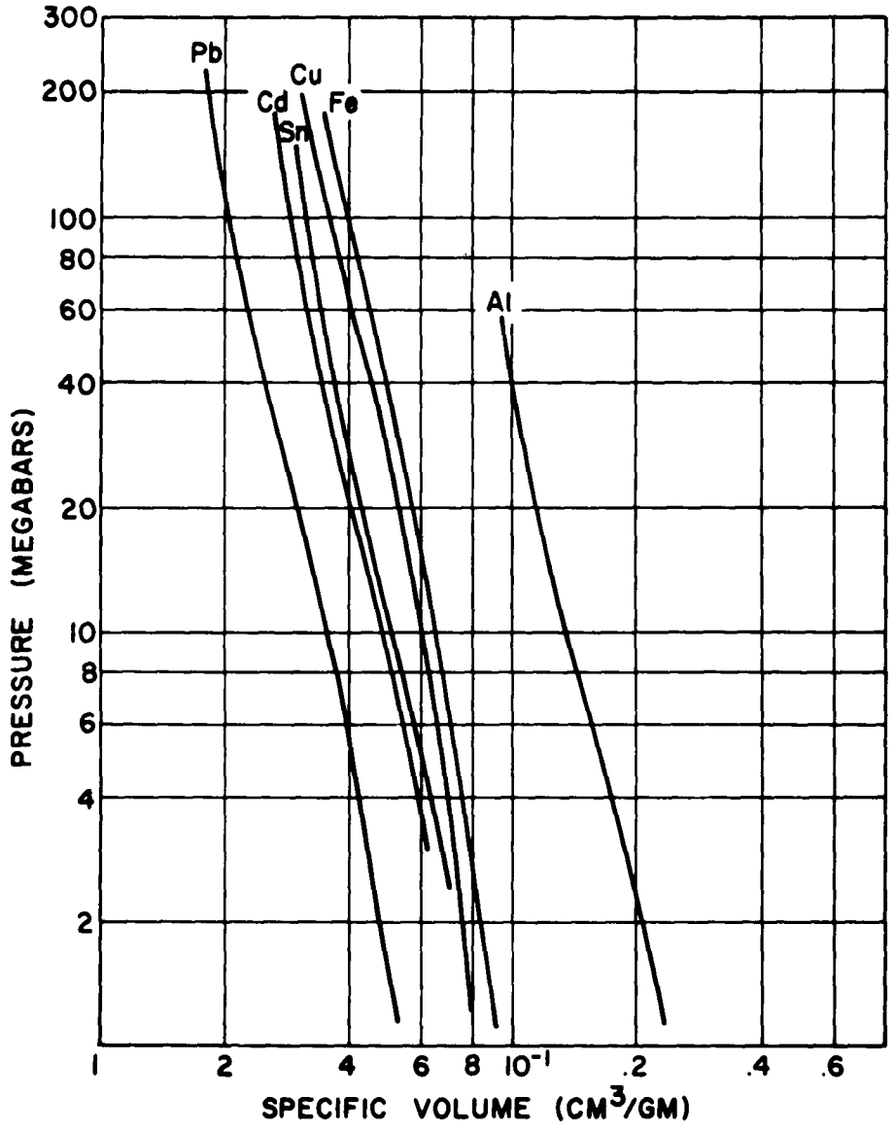

Figure 21 Hugoniot curves for indicated material.

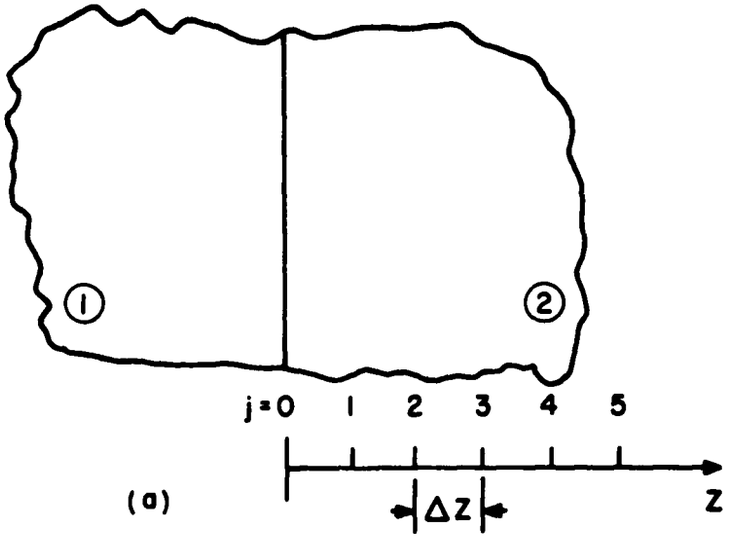

(a)

	BODY 1		BODY 2	
STATION / QUANTITY	$-\infty$ TO -1	0	0	1 TO ∞
q	$v_0/2$	0	0	$-v_0/2$
ρ	ρ_0	$\rho_0(1-\rho_0/d)^{-1}$	$\rho_0(1-\rho_0/d)^{-1}$	ρ_0
U	0	$v_0^2/8$	$v_0^2/8$	0
p	0	$v_0^2 d/4$	$v_0^2 d/4$	0

HERE d IS DETERMINED BY THE RELATION (76)

$$\frac{v_0^2}{4}\, d = f\left(\frac{\rho_0}{1-\rho_0/d}\,,\ \frac{v_0^2}{8}\right)$$

(b)

Figure 22 Display of (a) Eulerian space-mesh points and (b) initial and boundary data for the implicit difference scheme.

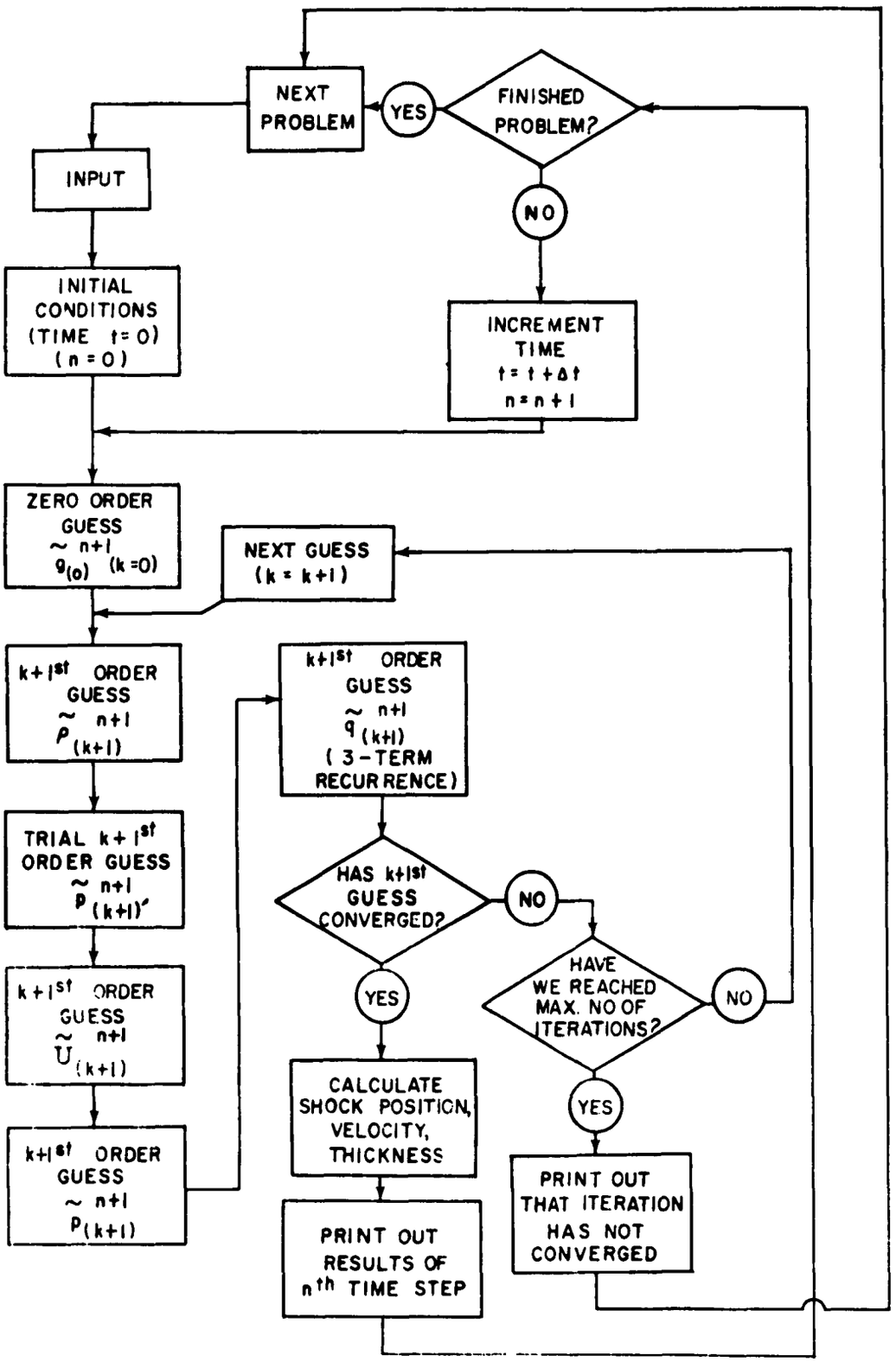

Figure 23 Flow chart depicting the sequence of calculations in the implicit difference scheme.

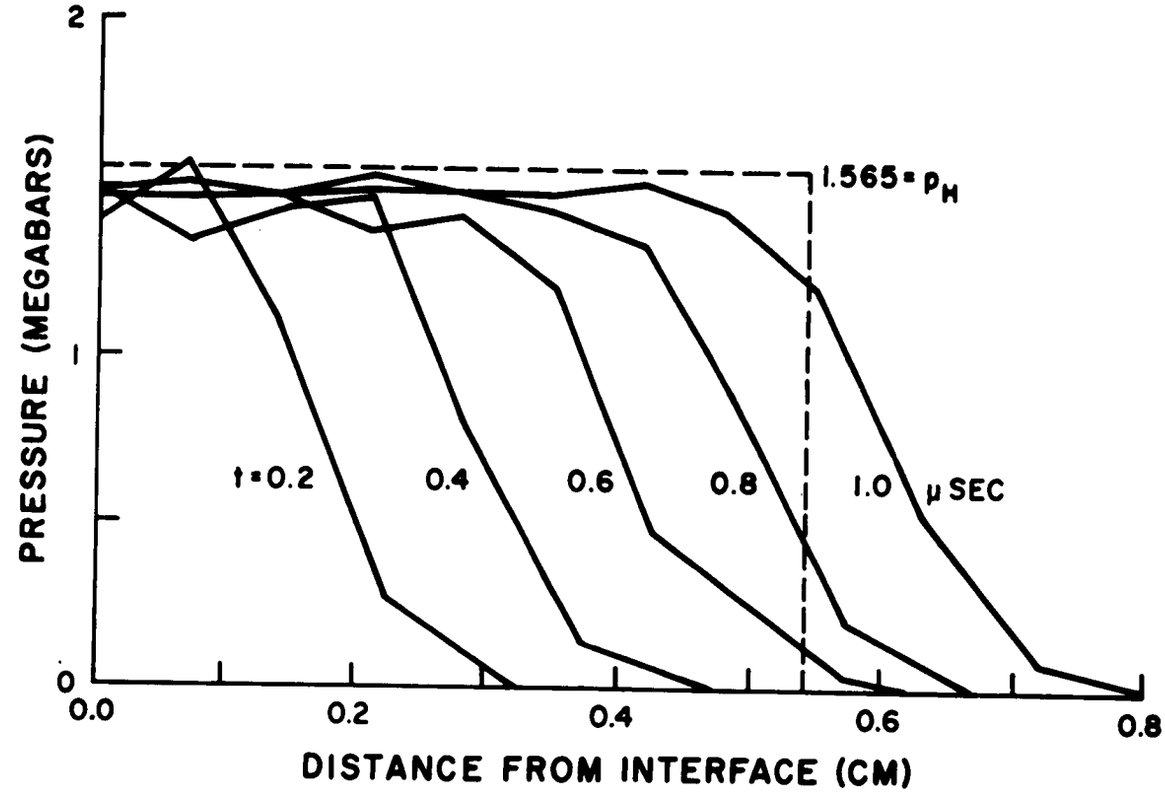

(a)

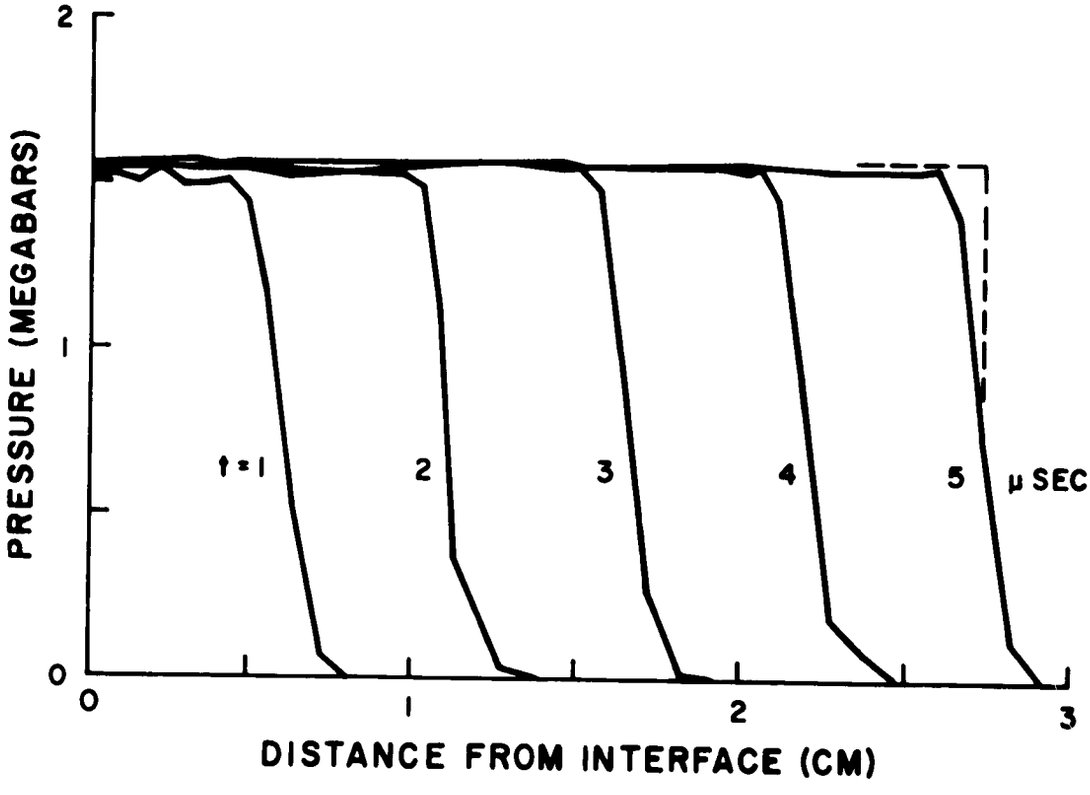

(b)

Figure 24. Calculated pressure profiles compared with the Rankine-Hugoniot solution (Case 1: $v_o = .5$, $\tau_o = \mu_o = 0$).

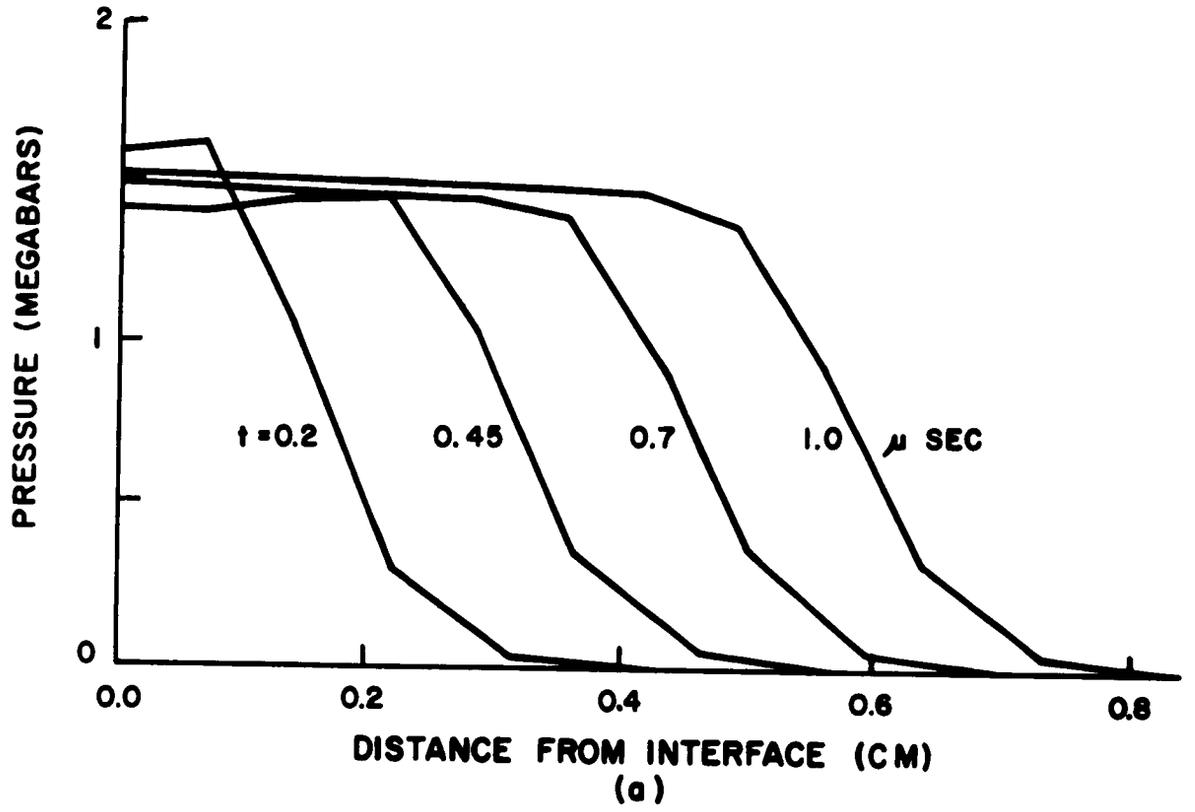

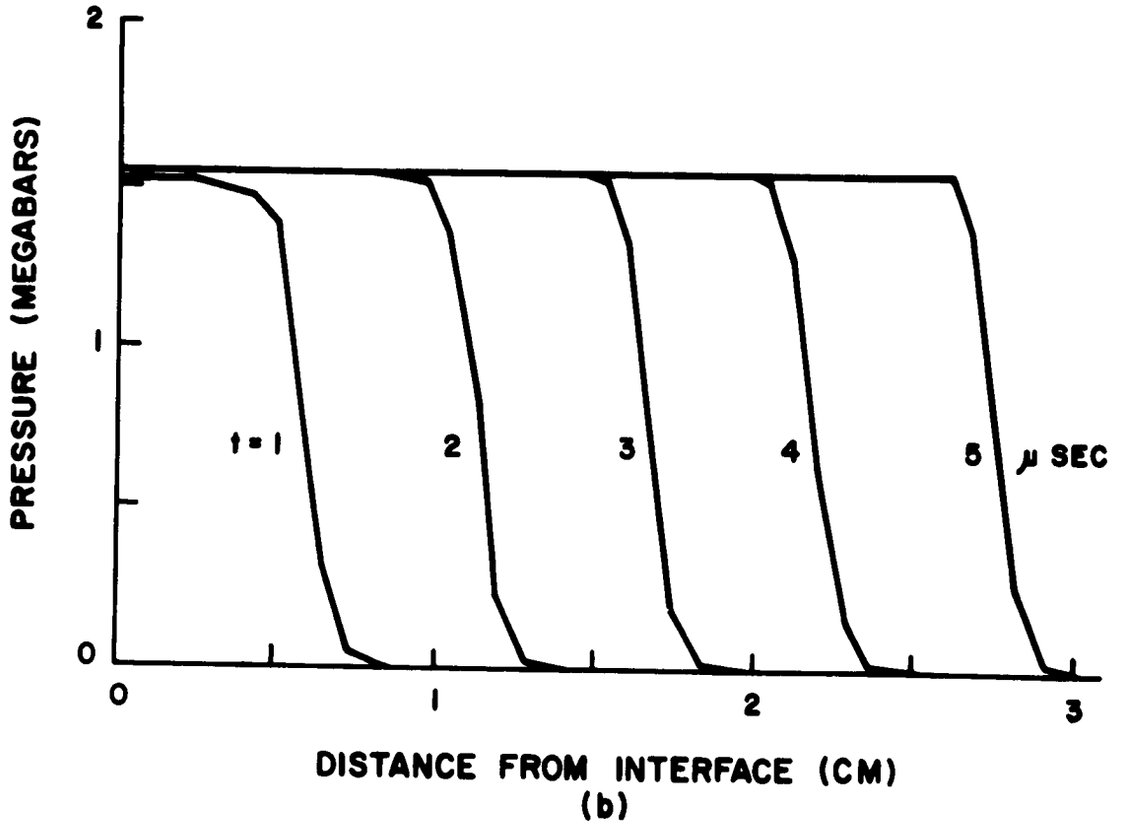

Figure 25. Pressure profiles (Case 2: $v_o = .5$, $\tau_o = 0$, $\mu_o = .08$).

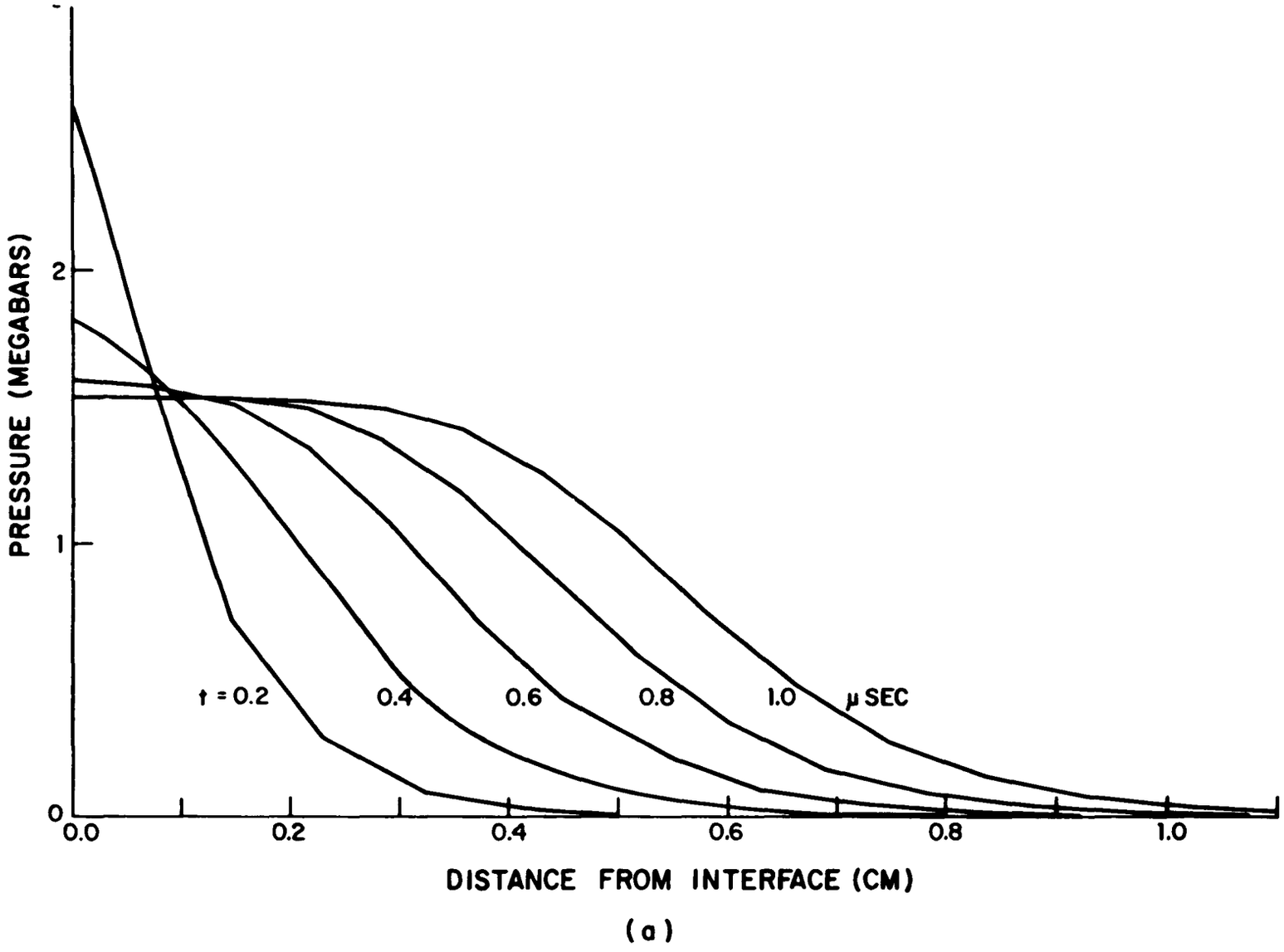

Figure 26. Pressure profiles (Case 3: $v_o = .5$, $\tau_o = 0$, $\mu_o = .8$).

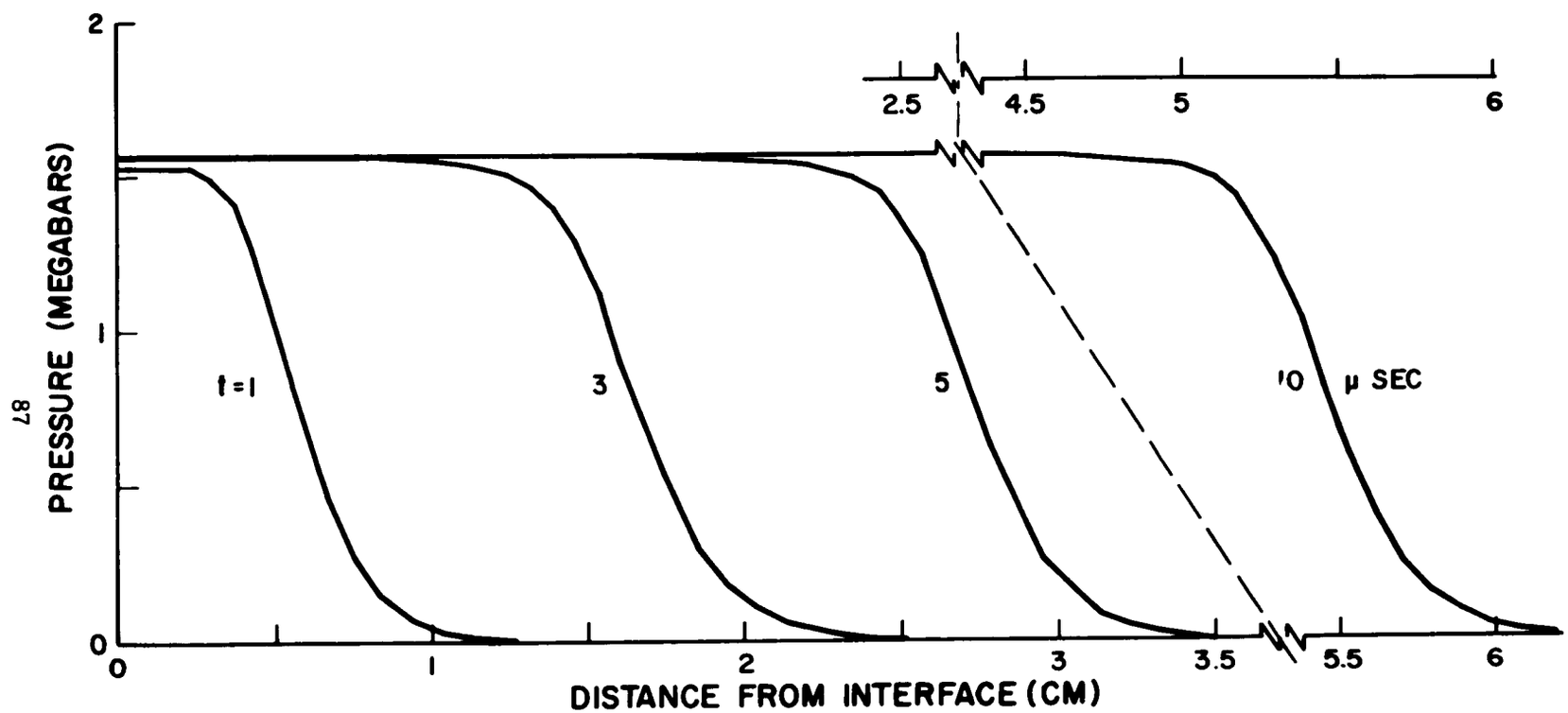

(b)

Figure 26. Pressure profiles (Case 3: $v_o = .5$, $\tau_o = 0$, $\mu_o = 8$).

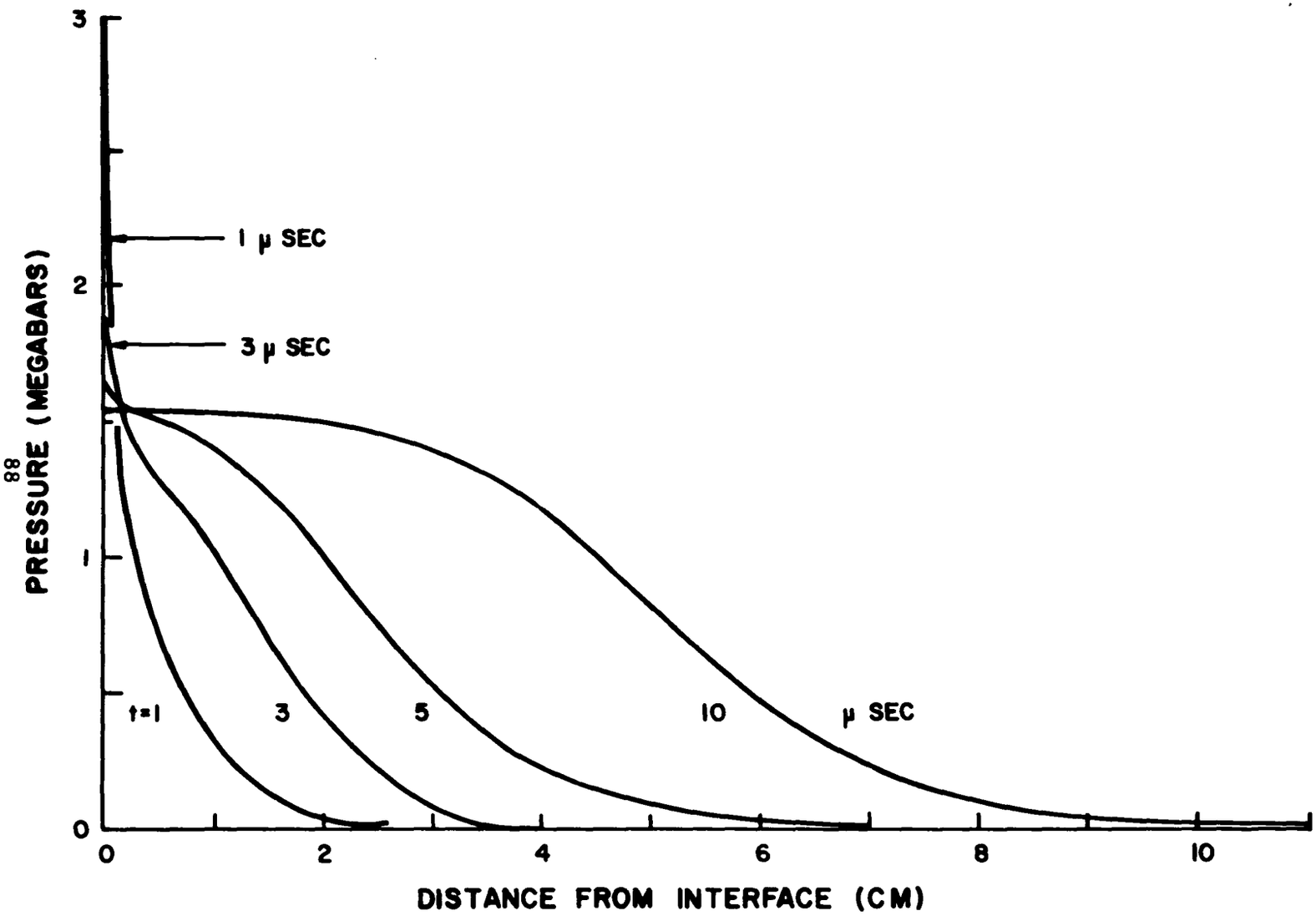

Figure 27. Pressure profiles (Case 4: $v_o = .5$, $\tau_o = 0$, $\mu_o = 8$).

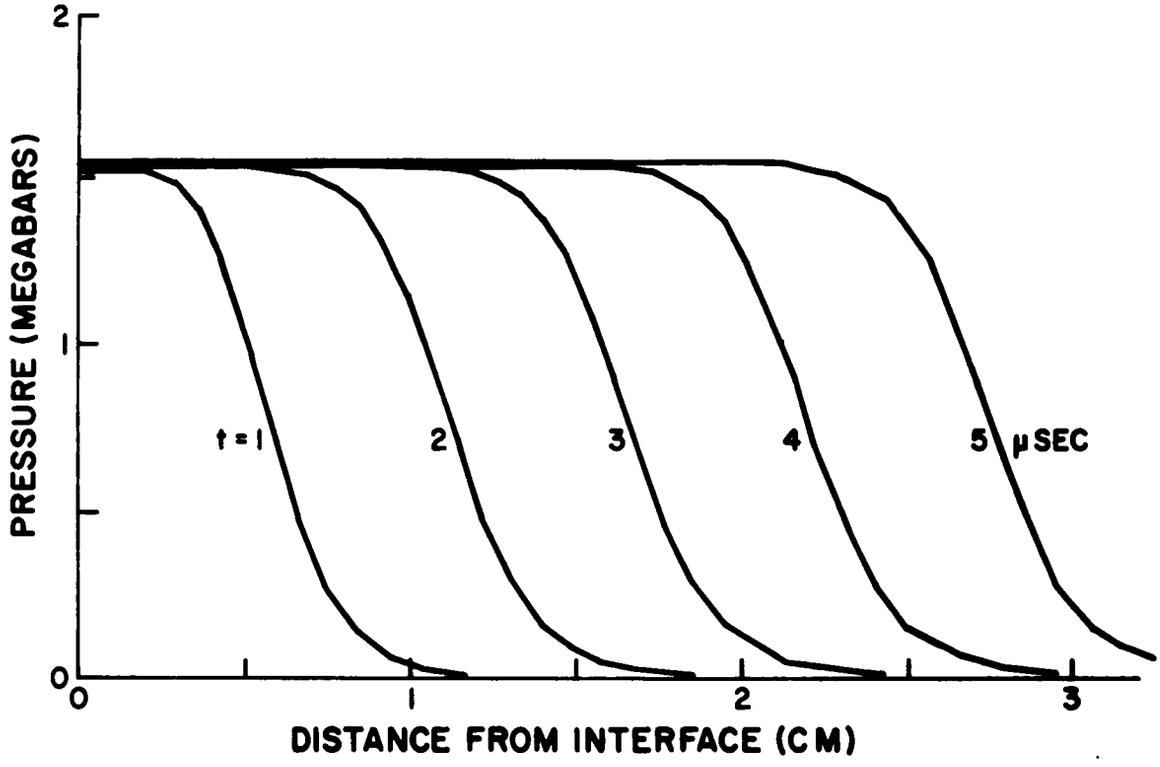

Figure 28. Pressure profiles (Case 7: $v_o = .5$, $\tau_o = .01$, $\mu_o = .8$).

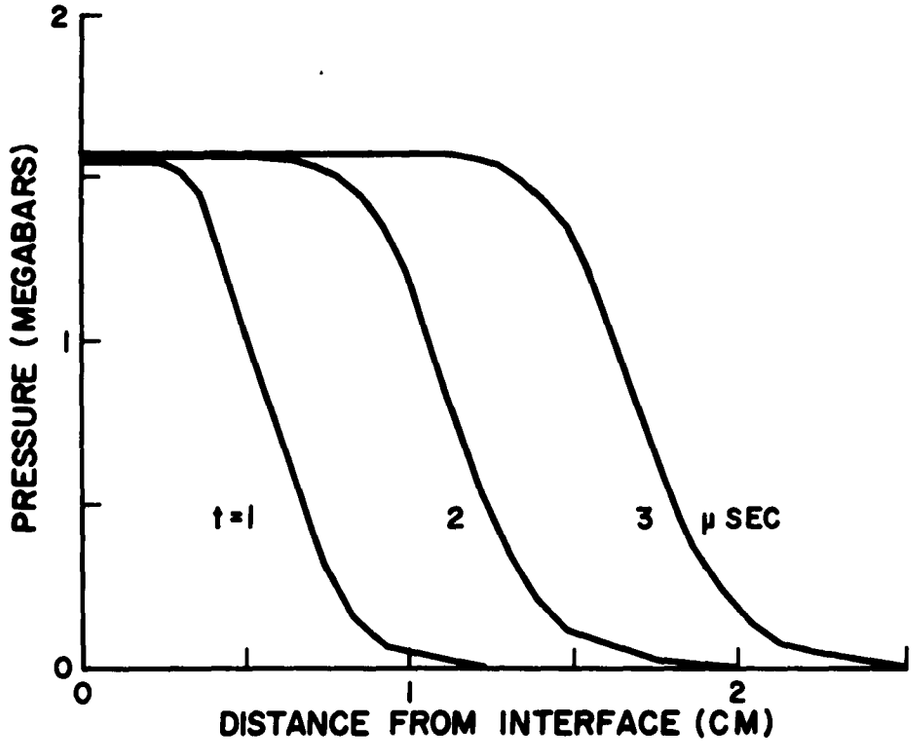

Figure 29. Pressure profiles (Case 11: $v_o = .5$, $\tau_o = .1$, $\mu_o = .8$).

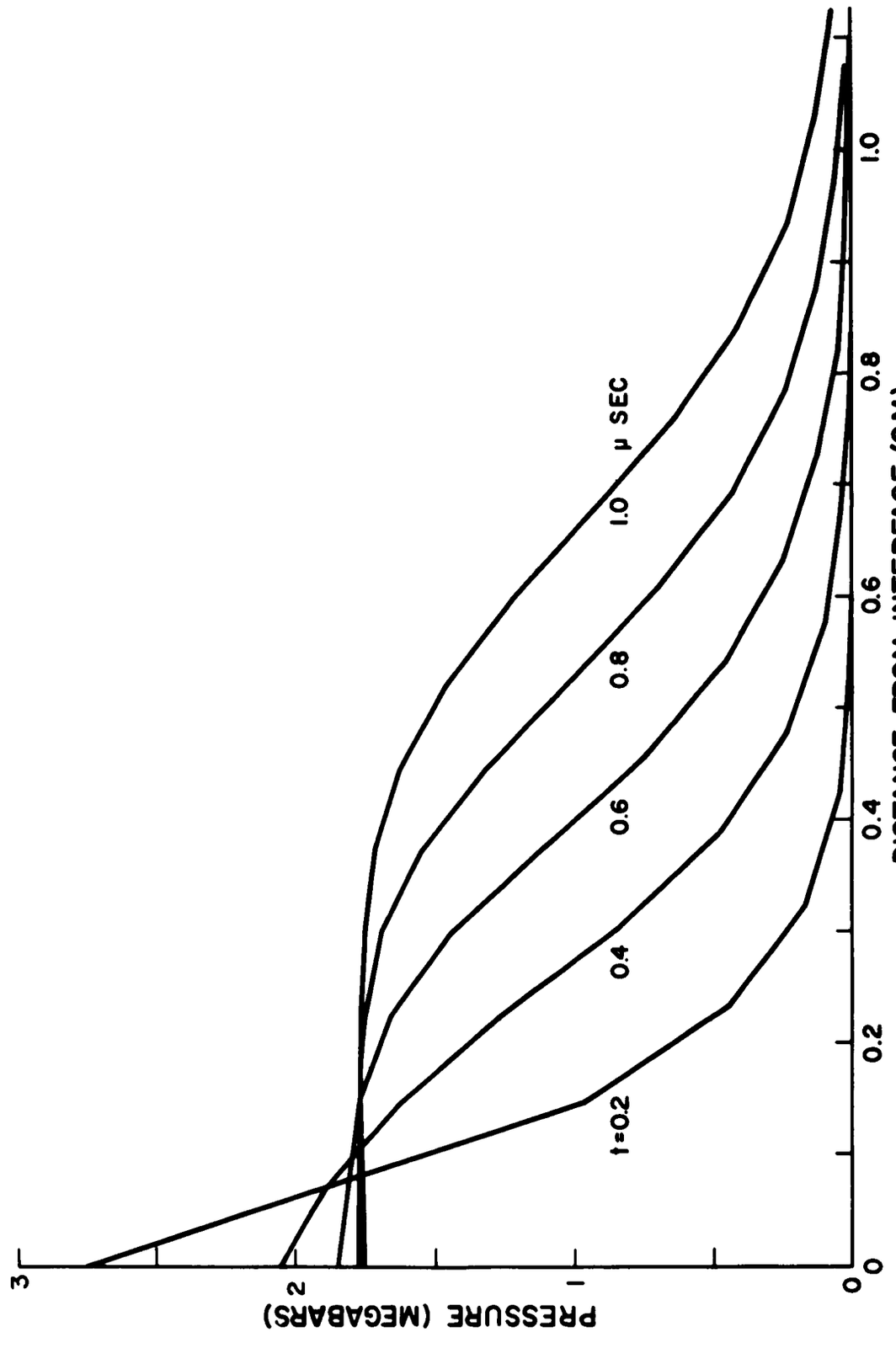

Figure 30. Pressure profiles (Case 15: $v_o = .5$, $\tau_o = 1$, $\mu_o = .8$).

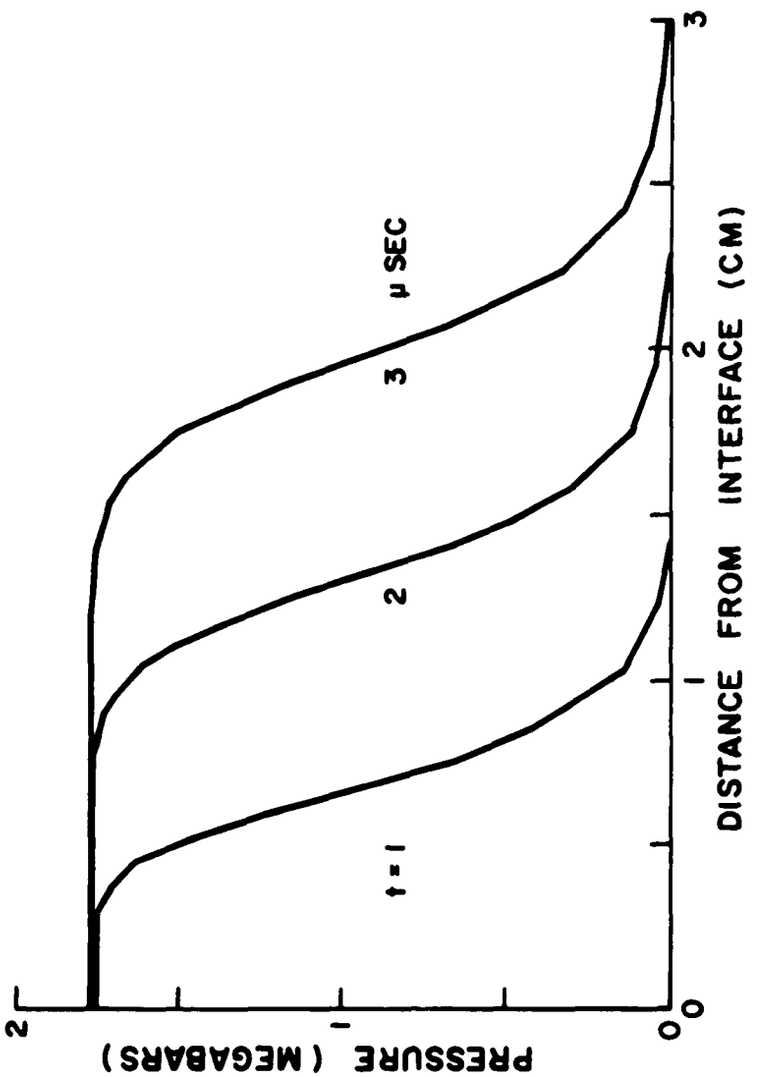

Figure 30. Pressure profiles (Case 15: $v_o = .5$, $\tau_o = 1$, $\mu_o = .8$).

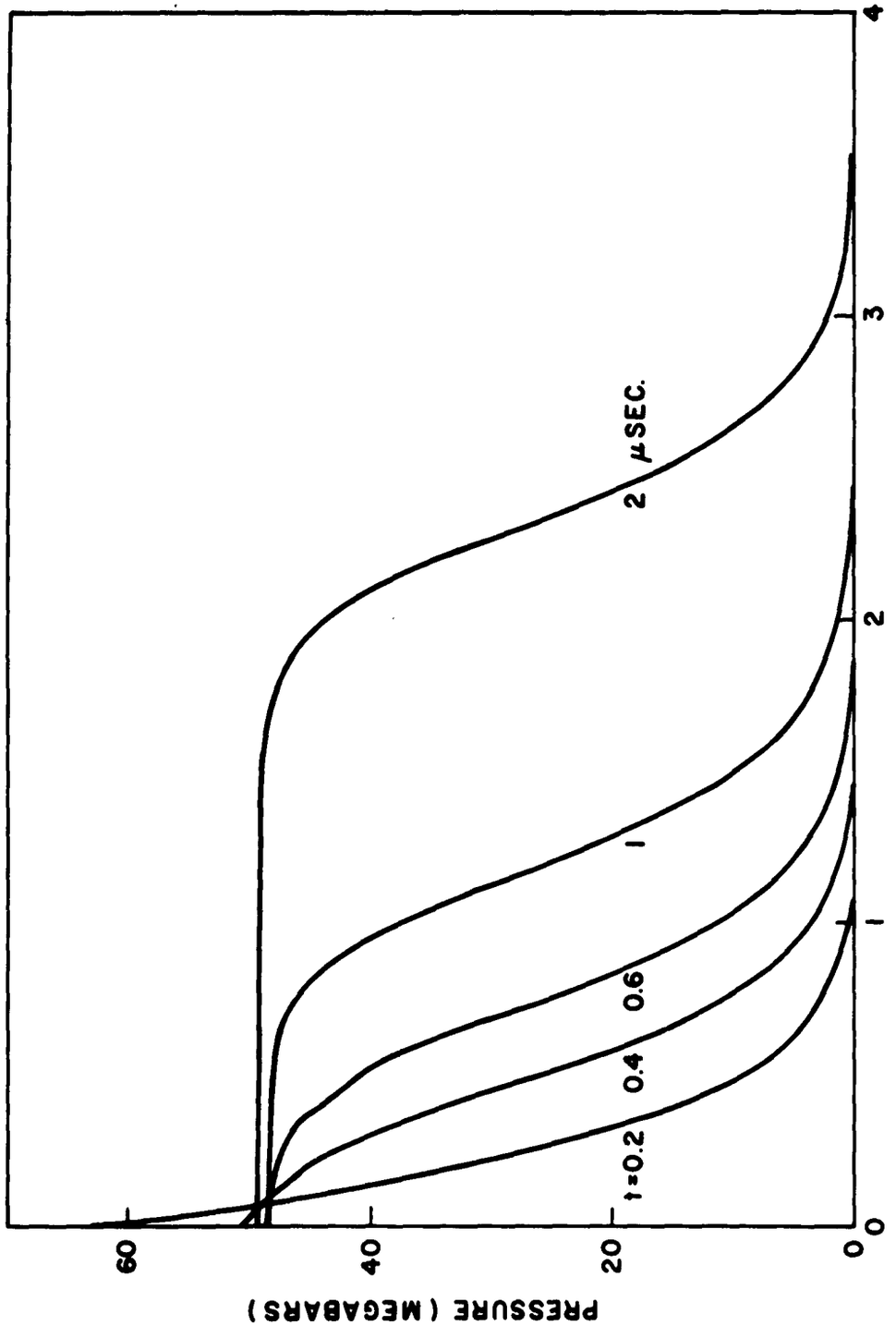

Figure 31 Pressure profiles (Case 20: $v_o = 4$, $\tau_o = 0$, $\mu_o = 8$).

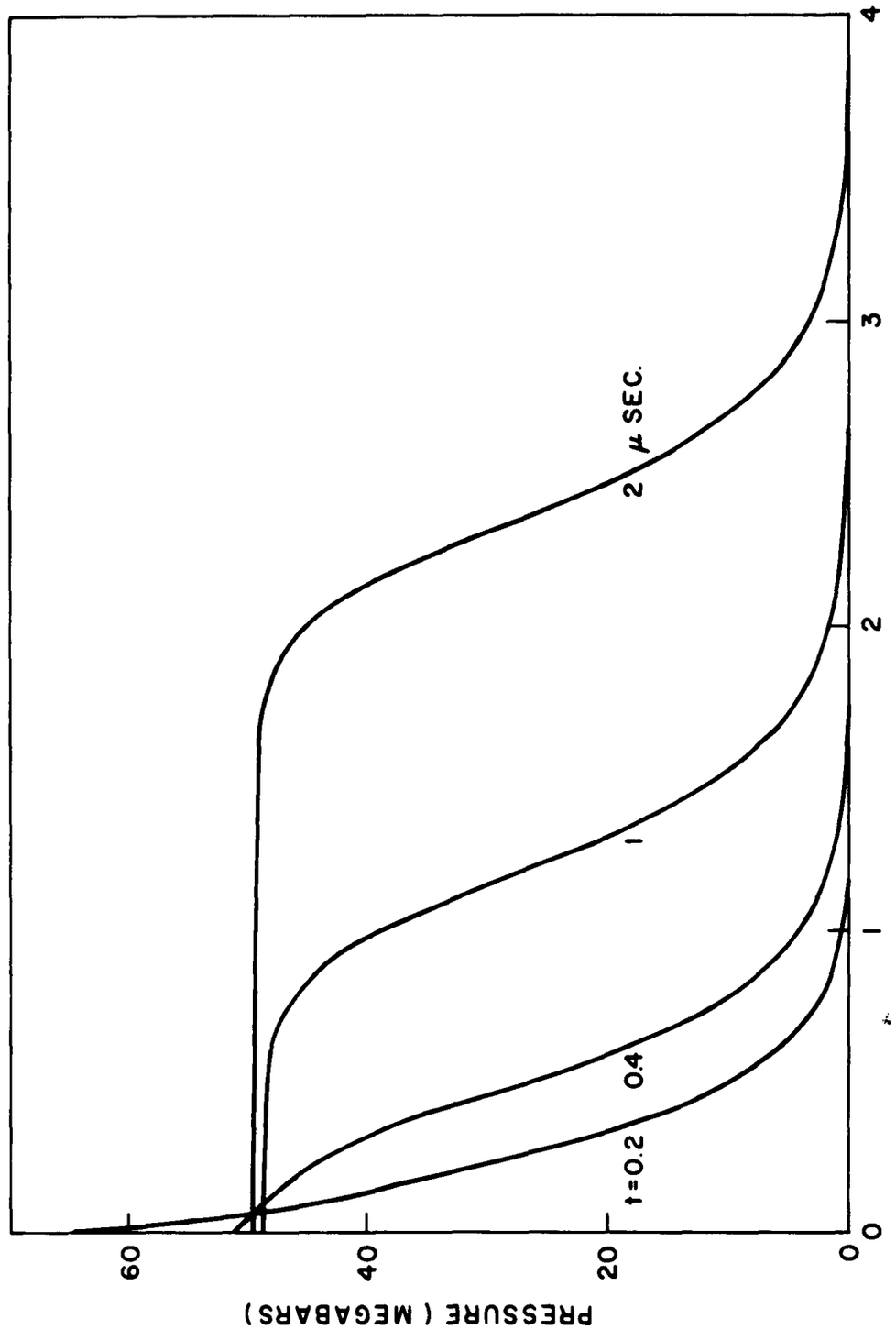

Figure 32 Pressure profiles (Case 32: $v_o = 4$, $\tau_o = 1$, $u_o = 8$).

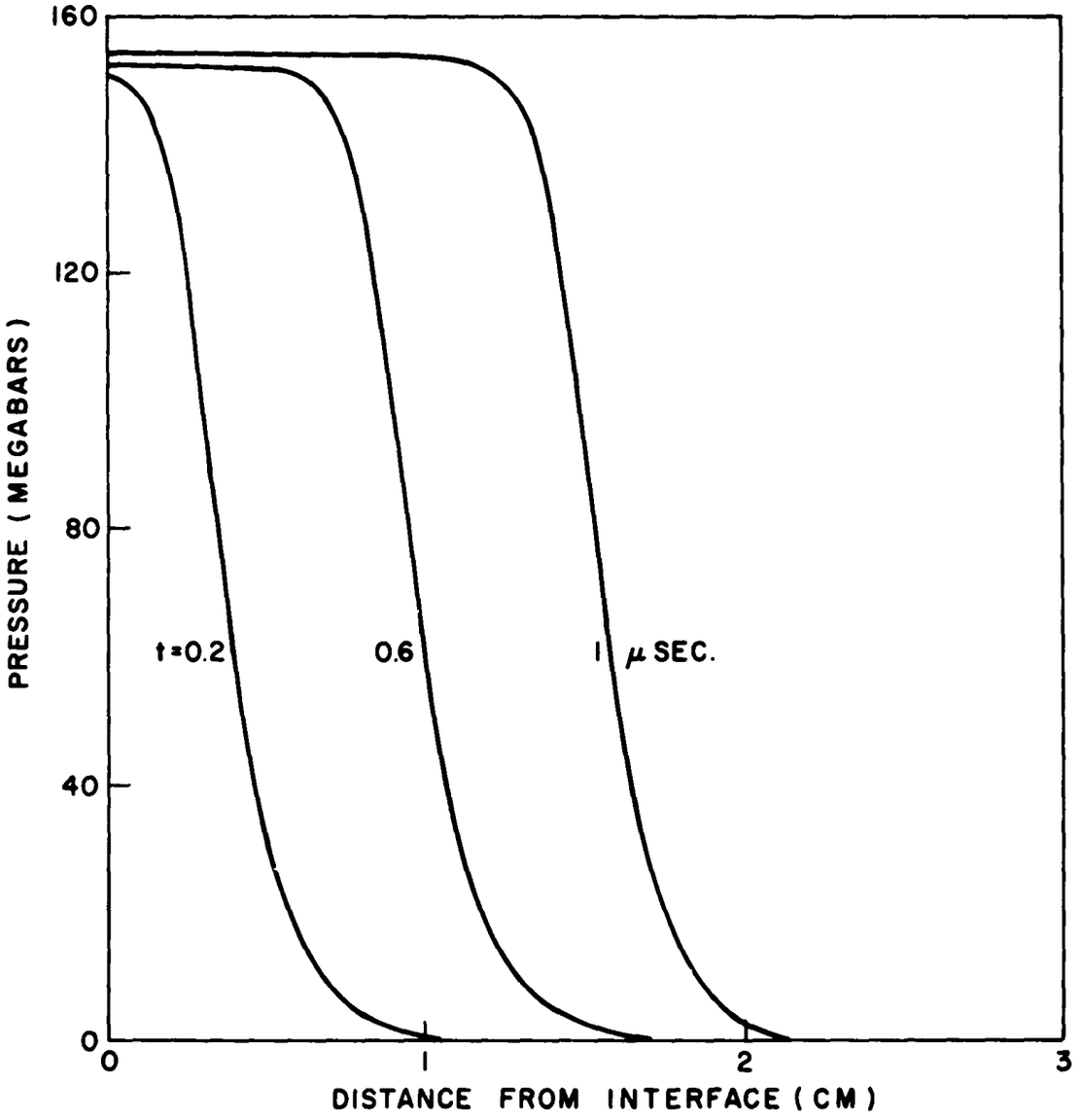

Figure 33 Pressure profiles (Case 48: $v_o = 7.5$, $\tau_o = 1$, $\mu_o = 8$).

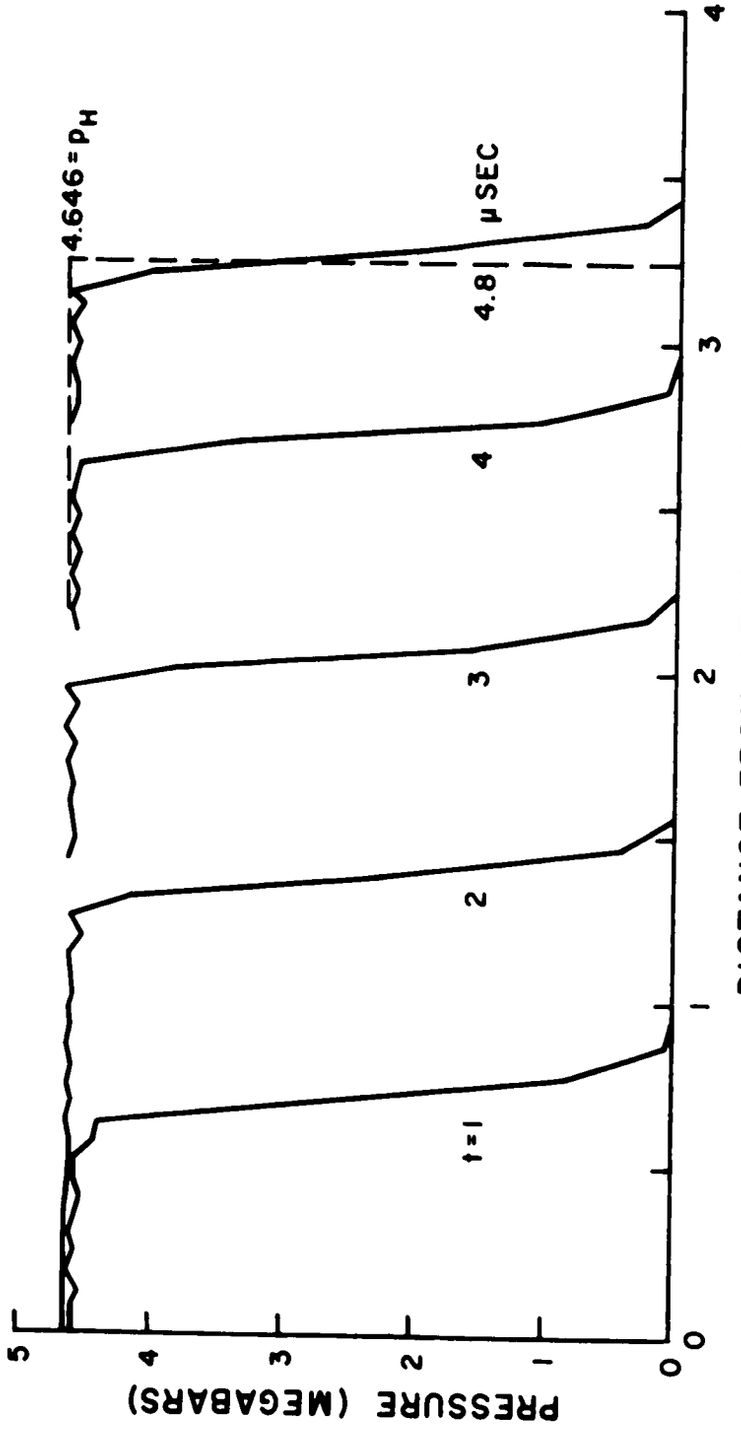

Figure 34. Pressure profiles (Case 49: $v_o = 1$, $\tau_o = 0$, $\mu_o = 0$).

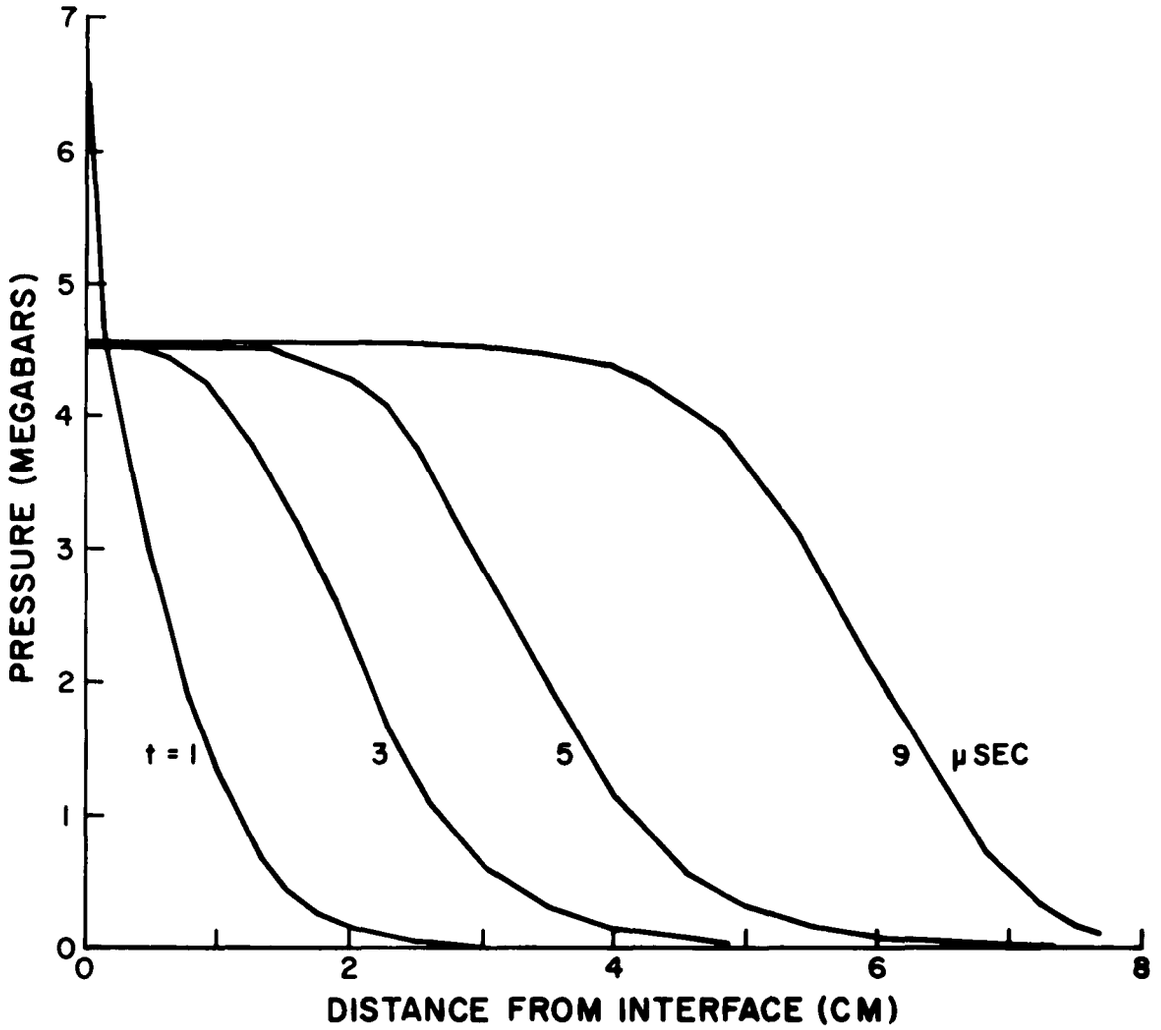

Figure 35. Pressure profiles (Case 52: $v_o = 1$, $\tau_o = 0$, $\mu_o = 8$).

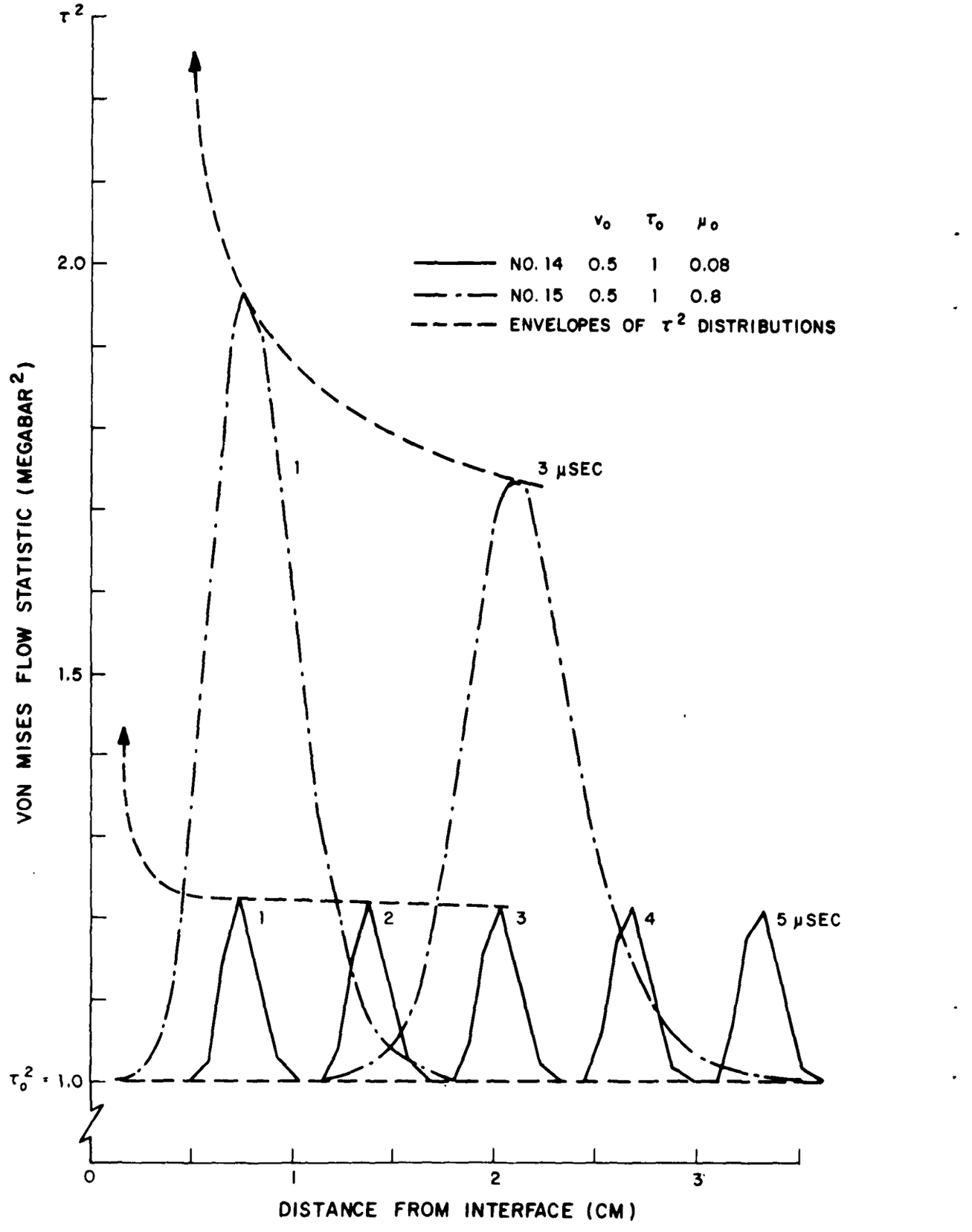

Figure 36. Von Mises flow statistic profiles and the envelopes of their maximum values.

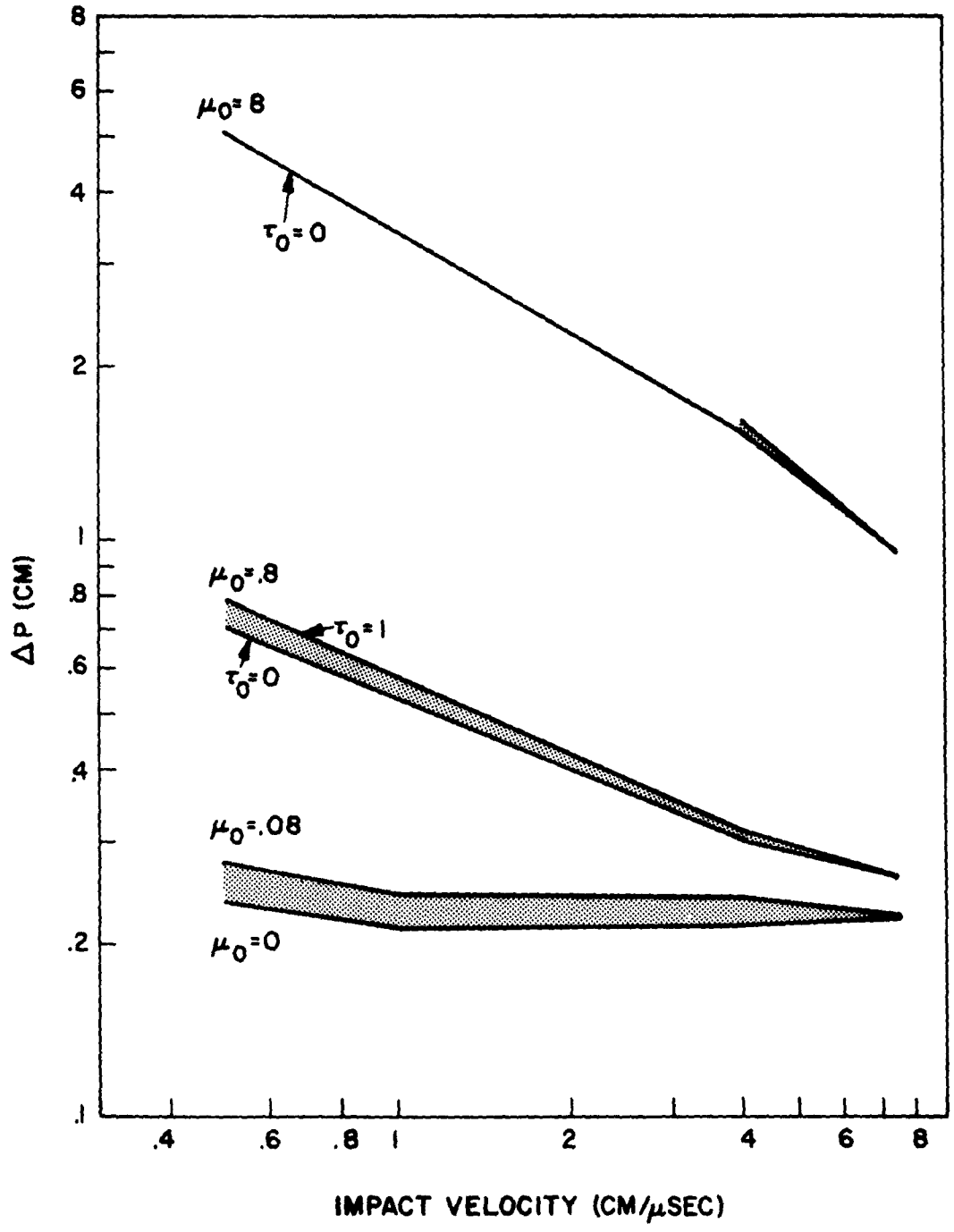

Figure 37 Thickness of the stable profile as a function of impact velocity. The effect of the strength term is much less than that of the viscosity.

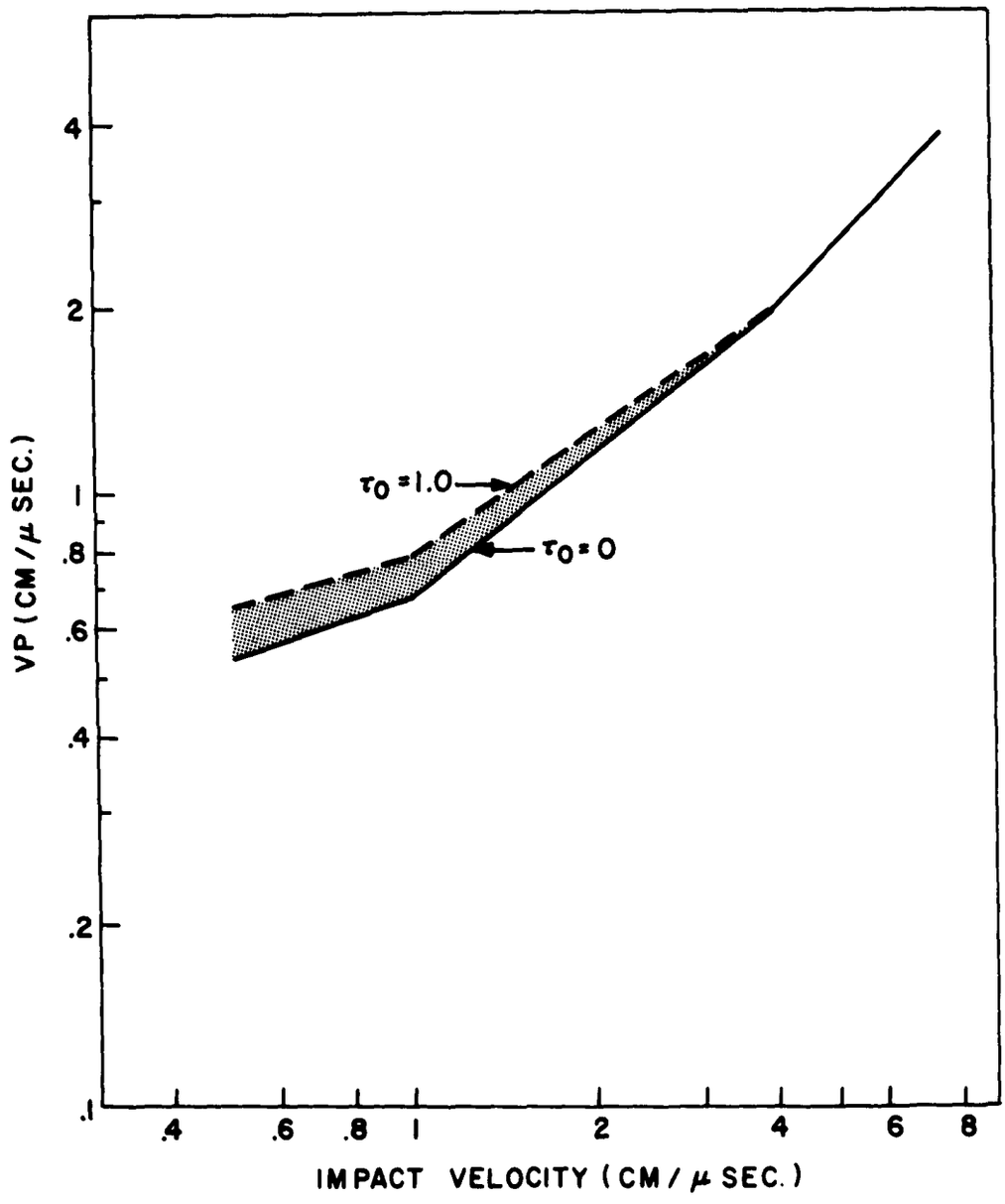

Figure 38 Velocity of the stable pressure profile as a function of the impact velocity. The viscosity has practically no effect.

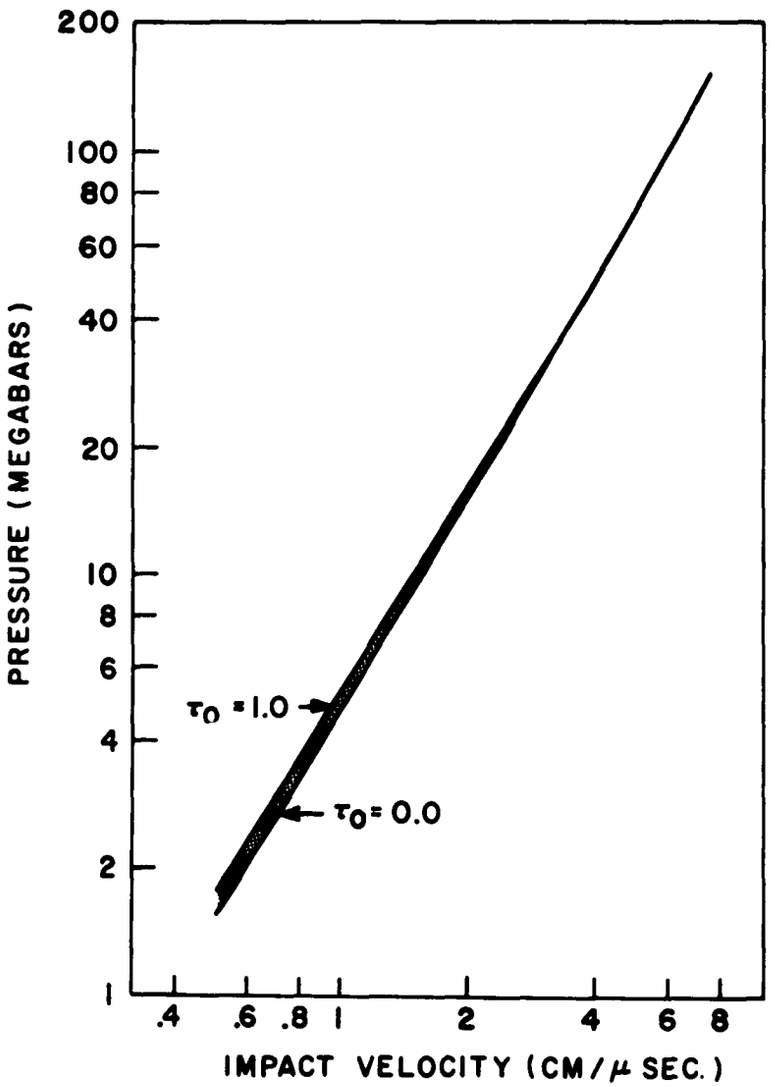

Figure 39 The pressure behind the stable pressure profile as a function of impact velocity. The viscosity has very small effect.

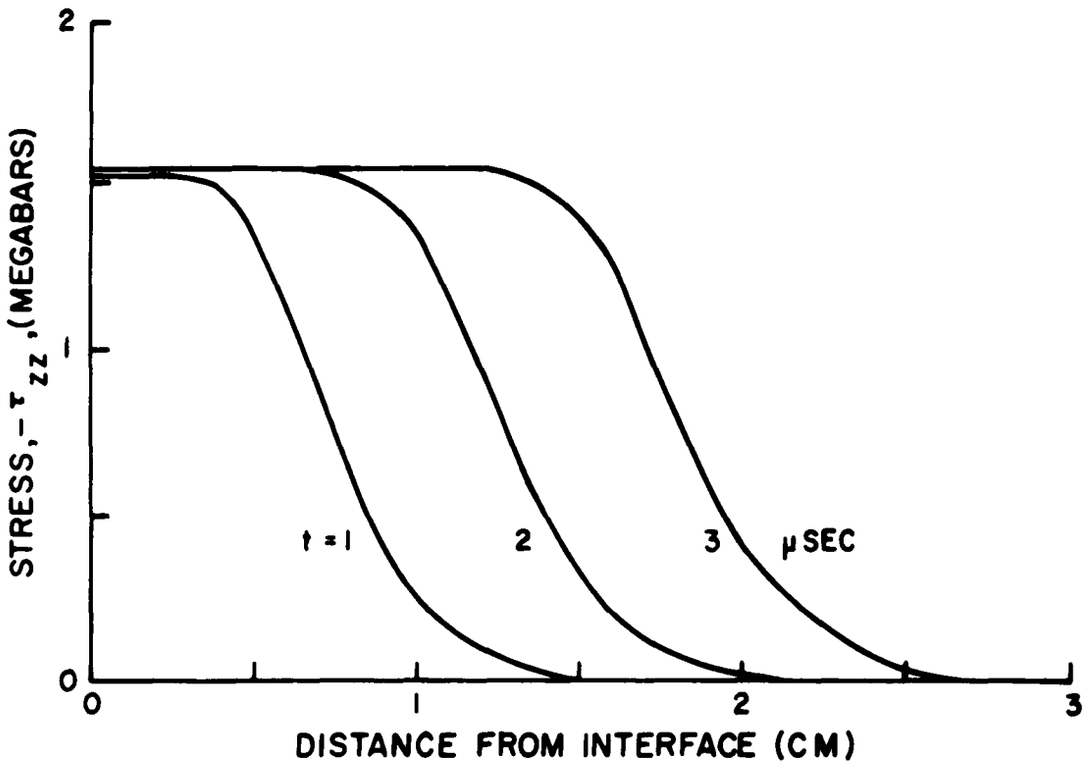

Figure 40. Profiles of stress normal to the wave front (Case 3: $v_o = .5, \tau_o = 0, \mu_o = .8$).

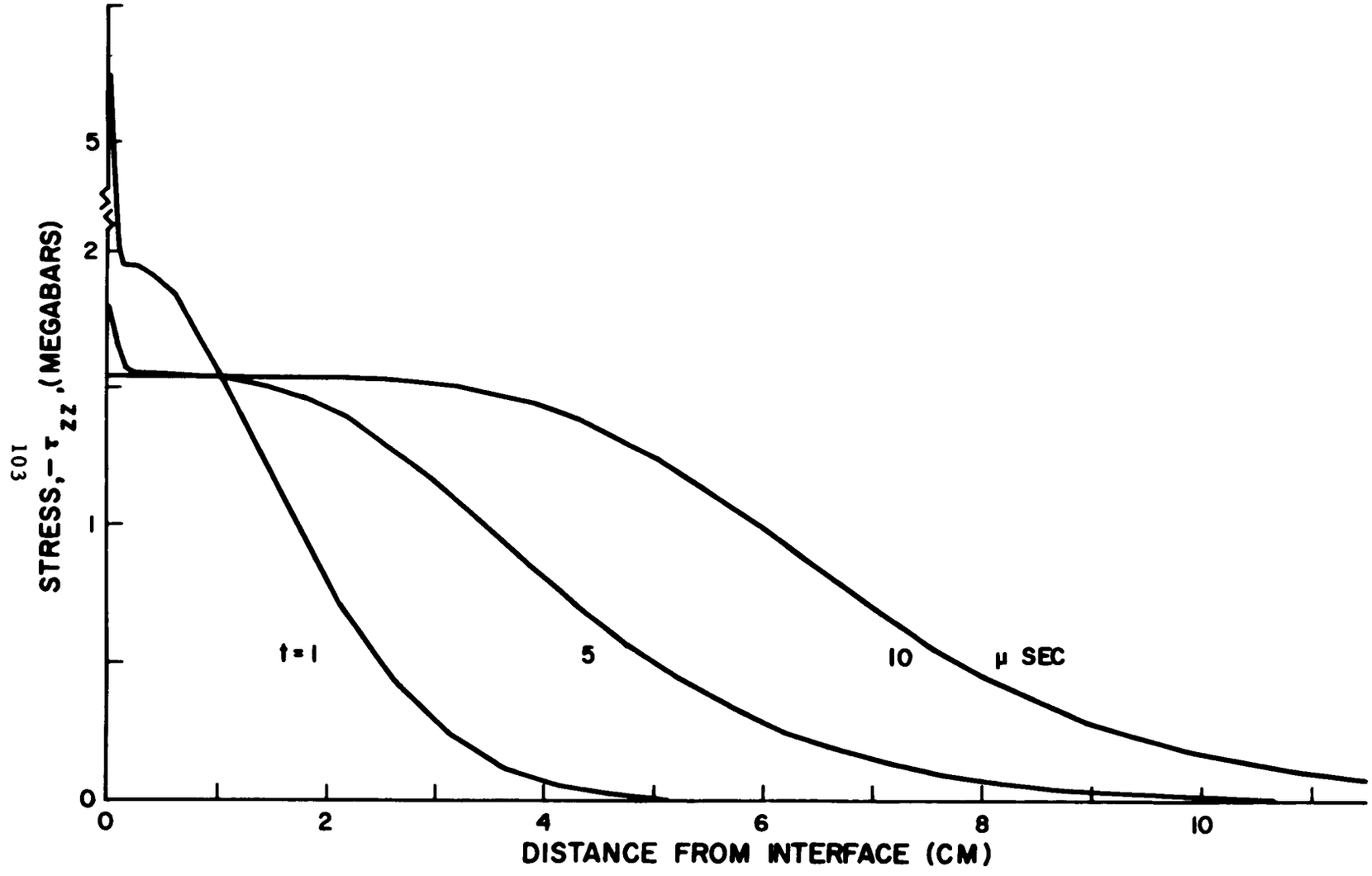

Figure 41. Profiles of stress normal to the wave front (Case 4: $v_o = .5$, $\tau_o = 0$, $\mu_o = 8$).

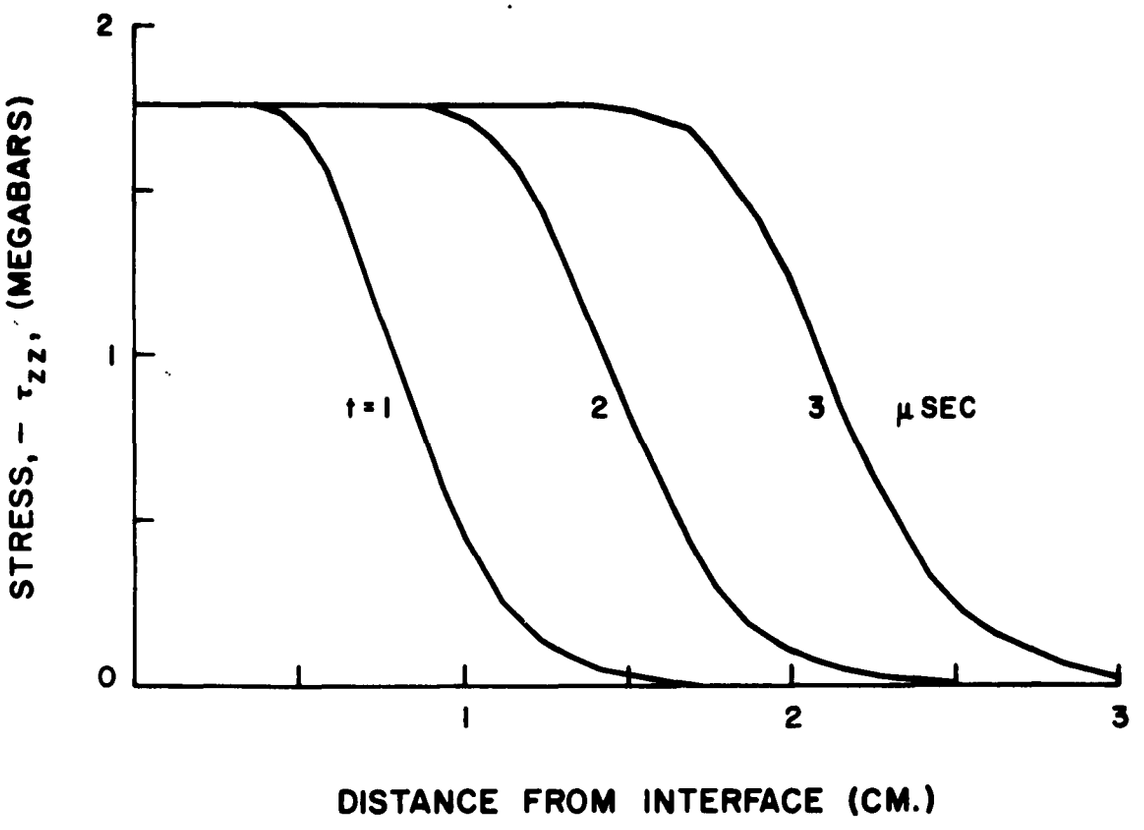

Figure 42. Profiles of stress normal to the wave front (Case 15: $v_o = .5$, $\tau_o = 1$, $\mu_o = .8$).

INITIAL DISTRIBUTION

2	Wpns Sys Eval Gp
2	Hq USAF (AFDAP/W-AD)
2	Hq USAF (AFDRD-ER-1)
2	ASD (ASRCEP-1)
2	ASD (ASRNGW)
2	AFSWC
2	OAR
2	OAR (RROSA)
2	BSD
2	SSD
1	AFCRL
2	AU
1	TAC (TPL-RQD-M)
2	Langley Rsch Ctr (Lib)
2	NASA (Code 9262)
2	Springfield Armory (R&D Div)
2	Watervliet Arsenal (ORDBR-R)
2	ARO (Scientific Info Br)
2	ABMA (ORDAB-HT)
2	Watertown Arsenal
2	Picatinny Arsenal (ORDBB-TH8)
1	CofOrd (ORDTB)
1	CofOrd (ORDTM)
1	CofOrd (ORDTS)
1	BRL (Free-Flight Aero Br)
1	BRL (Exter Ballistics Lab)
1	BRL (Tech Info Br)
1	BRL (Dev & Proff Svcs)
1	ARGMA (ORDDW-IDE)
1	Frankford Arsenal (Lib)
1	Frankford Arsenal (Pitman-Dunn Lab)
1	Rock Island Arsenal
2	NOTS (Code 5007)
2	NOTS (Tech Lib)
1	BUWEPS (R-12)
3	BUWEPS (RM)
1	BUWEPS (RM-3)
1	BUWEPS (RMGA-41)
1	BUWEPS (RT-1)(J.D.N.)
1	BUWEPS (RMMO-4)
1	NOL (Assoc Dir/Aeroballistics)
1	NOL (Aerodynamics Dept)
1	NOL (Ballistics Dept)
2	Nav Wpns Lab (Tech Lib)
2	Ames Rsch Ctr (Lib)
2	Ames Rsch Ctr (High Speed Rsch Div)
2	Lewis Rsch Ctr
2	Applied Rsch Lab (JHU)
1	Armour Rsch Foundation
1	Franklin Institute (Lib)
1	Franklin Institute
1	Jet Propulsion Lab
1	USAF Proj RAND
1	University of Chicago
30	ASTIA (TIPCR)
	APGC
2	ASQR
2	PGAPI
3	PGEH
2	PGWR
2	PGW
40	PGWRT

Air Proving Ground Center, Eglin Air Force Base, Florida
Rpt No. APGC-TDR-62-20. THEORY OF HIGH SPEED IMPACT.
Final report, Mar 62, 105p. incl. illus., tables.
Unclassified Report

Existing experimental results of hypervelocity impact tests have been gathered from various sources and the composite data are presented and discussed. The results of the calculations are related to the qualitative model of crater formations that has evolved from experimental studies in which the actual cratering process has been monitored. It is concluded that the viscous and strength effects strongly affect the cavitation process which is the essential mechanism of crater formation. Finally, experiments are suggested which would provide the necessary data to verify and extend the theory.

1. Impact shock
2. Hypervelocity projectiles
I. AFSC Project 9860
II. Contract AF 08(635)-1713
III. General Electric Co., King of Prussia, Pa.
IV. Riney, T. D.
V. In ASTIA collection

Air Proving Ground Center, Eglin Air Force Base, Florida
Rpt No. APGC-TDR-62-20. THEORY OF HIGH SPEED IMPACT.
Final report, Mar 62, 105p. incl. illus., tables.
Unclassified Report

Existing experimental results of hypervelocity impact tests have been gathered from various sources and the composite data are presented and discussed. The results of the calculations are related to the qualitative model of crater formations that has evolved from experimental studies in which the actual cratering process has been monitored. It is concluded that the viscous and strength effects strongly affect the cavitation process which is the essential mechanism of crater formation. Finally, experiments are suggested which would provide the necessary data to verify and extend the theory.

1. Impact shock
2. Hypervelocity projectiles
I. AFSC Project 9860
II. Contract AF 08(635)-1713
III. General Electric Co., King of Prussia, Pa.
IV. Riney, T. D.
V. In ASTIA collection

Air Proving Ground Center, Eglin Air Force Base, Florida
Rpt No. APGC-TDR-62-20. THEORY OF HIGH SPEED IMPACT.
Final report, Mar 62, 105p. incl. illus., tables.
Unclassified Report

Existing experimental results of hypervelocity impact tests have been gathered from various sources and the composite data are presented and discussed. The results of the calculations are related to the qualitative model of crater formations that has evolved from experimental studies in which the actual cratering process has been monitored. It is concluded that the viscous and strength effects strongly affect the cavitation process which is the essential mechanism of crater formation. Finally, experiments are suggested which would provide the necessary data to verify and extend the theory.

1. Impact shock
2. Hypervelocity projectiles
I. AFSC Project 9860
II. Contract AF 08(635)-1713
III. General Electric Co., King of Prussia, Pa.
IV. Riney, T. D.
V. In ASTIA collection

Air Proving Ground Center, Eglin Air Force Base, Florida
Rpt No. APGC-TDR-62-20. THEORY OF HIGH SPEED IMPACT.
Final report, Mar 62, 105p. incl. illus., tables.
Unclassified Report

Existing experimental results of hypervelocity impact tests have been gathered from various sources and the composite data are presented and discussed. The results of the calculations are related to the qualitative model of crater formations that has evolved from experimental studies in which the actual cratering process has been monitored. It is concluded that the viscous and strength effects strongly affect the cavitation process which is the essential mechanism of crater formation. Finally, experiments are suggested which would provide the necessary data to verify and extend the theory.

1. Impact shock
2. Hypervelocity projectiles
I. AFSC Project 9860
II. Contract AF 08(635)-1713
III. General Electric Co., King of Prussia, Pa.
IV. Riney, T. D.
V. In ASTIA collection

Air Proving Ground Center, Eglin Air Force Base, Florida
Rpt No. APGC-TDR-62-20. THEORY OF HIGH SPEED IMPACT.
Final report, Mar 62, 105p. incl. illus., tables.
Unclassified Report

Existing experimental results of hypervelocity impact tests have been gathered from various sources and the composite data are presented and discussed. The results of the calculations are related to the qualitative model of crater formations that has evolved from experimental studies in which the actual cratering process has been monitored. It is concluded that the viscous and strength effects strongly affect the cavitation process which is the essential mechanism of crater formation. Finally, experiments are suggested which would provide the necessary data to verify and extend the theory.

1. Impact shock
2. Hypervelocity projectiles
I. AFSC Project 9860
II. Contract AF 08(635)-1713
III. General Electric Co., King of Prussia, Pa.
IV. Riney, T. D.
V. In ASTIA collection

Air Proving Ground Center, Eglin Air Force Base, Florida
Rpt No. APGC-TDR-62-20. THEORY OF HIGH SPEED IMPACT.
Final report, Mar 62, 105p. incl. illus., tables.
Unclassified Report

Existing experimental results of hypervelocity impact tests have been gathered from various sources and the composite data are presented and discussed. The results of the calculations are related to the qualitative model of crater formations that has evolved from experimental studies in which the actual cratering process has been monitored. It is concluded that the viscous and strength effects strongly affect the cavitation process which is the essential mechanism of crater formation. Finally, experiments are suggested which would provide the necessary data to verify and extend the theory.

1. Impact shock
2. Hypervelocity projectiles
I. AFSC Project 9860
II. Contract AF 08(635)-1713
III. General Electric Co., King of Prussia, Pa.
IV. Riney, T. D.
V. In ASTIA collection

Air Proving Ground Center, Eglin Air Force Base, Florida
Rpt No. APGC-TDR-62-20. THEORY OF HIGH SPEED IMPACT.
Final report, Mar 62, 105p. incl. illus., tables.
Unclassified Report

Existing experimental results of hypervelocity impact tests have been gathered from various sources and the composite data are presented and discussed. The results of the calculations are related to the qualitative model of crater formations that has evolved from experimental studies in which the actual cratering process has been monitored. It is concluded that the viscous and strength effects strongly affect the cavitation process which is the essential mechanism of crater formation. Finally, experiments are suggested which would provide the necessary data to verify and extend the theory.

1. Impact shock
2. Hypervelocity projectiles
I. AFSC Project 9860
II. Contract AF 08(635)-1713
III. General Electric Co., King of Prussia, Pa.
IV. Riney, T. D.
V. In ASTIA collection

Air Proving Ground Center, Eglin Air Force Base, Florida
Rpt No. APGC-TDR-62-20. THEORY OF HIGH SPEED IMPACT.
Final report, Mar 62, 105p. incl. illus., tables.
Unclassified Report

Existing experimental results of hypervelocity impact tests have been gathered from various sources and the composite data are presented and discussed. The results of the calculations are related to the qualitative model of crater formations that has evolved from experimental studies in which the actual cratering process has been monitored. It is concluded that the viscous and strength effects strongly affect the cavitation process which is the essential mechanism of crater formation. Finally, experiments are suggested which would provide the necessary data to verify and extend the theory.

1. Impact shock
2. Hypervelocity projectiles
I. AFSC Project 9860
II. Contract AF 08(635)-1713
III. General Electric Co., King of Prussia, Pa.
IV. Riney, T. D.
V. In ASTIA collection